Young stars and circumstellar disks

Alexis Brandeker

Department of Astronomy
Stockholm Observatory
Stockholm University

2003

Cover image: Earth floating freely in space, as rendered by the planetarium software *StarStrider* (http://www.starstrider.com/), written by Markus Jönsson and Alexis Brandeker. The star β Pictoris is located slightly above the centre, close to the right edge of the front cover.

Figs. 1.1, 1.2, 1.8, 2.1, 2.2, and 3.1 are reproduced by permission of the AAS.

© Alexis Brandeker 2003
ISBN 91-7265-775-8 pp 1–72

Doctoral Dissertation 2003
Department of Astronomy
Stockholm University
SE-106 91 Stockholm
Sweden

Abstract. Theories of star and planet formation depend critically on the stellar environments found in the early stages. This thesis explores the physical conditions of the near environments of young stars.

The first part of the thesis presents high spatial resolution adaptive optics observations from the ESO 3.6 m telescope, the Keck telescope, and NACO at the VLT, probing the inner regions of nearby T Tauri stars. The discovery of several sub-arcsecond companions is reported, some that are prime targets for follow-up studies, with the possibility to determine *dynamical mass estimates* in a few years time. This allows for calibration of the ill-constrained theoretical tracks of early stellar evolution in colour-magnitude diagrams.

The second part of this thesis reports on observations of the nearby, young main-sequence star β Pictoris, known to harbour an edge-on circumstellar disk. Imaging of the thermal emission from the β Pic disk in 1.2 mm by SEST/SIMBA is presented and discussed. The thermal emission is found to be strongly asymmetric with respect to the star, but in the opposite way compared to observations of light scattered in the dust: The thermal emission is strongest from the south-western side of the disk, while the scattered emission is strongest at the north-eastern side. The interpretation is that the dust populations are different between the two sides. The dust grain sizes detected in thermal emission are inferred to be large, of typical diameter $\sim$1 mm.

The discovery of extended emission from circumstellar gas around β Pic is presented. The characterisation of the gas in this borderline disk in the transition between a thick, planet-forming disk and a mature main-sequence zodiacal disk, is particularly important for the theoretical assessment of planet formation timescales. The gas is observed by making use of long-slit high-resolution echelle spectrographs at the NTT/EMMI and the VLT/UVES. The velocity field of the gas disk is found to be consistent with Keplerian rotation. 88 lines from 13 metal ions are detected in widespread emission, extending to the limits of our observations at 323 AU radius and 80 AU height. Several of these ions are subject to a very high radiation pressure that should cause them, if not restrained, to leave the β Pic system on timescales of 100 years. Two different scenarios for braking the gas are investigated in some detail, braking by the gas drag of an invisible gas component, and braking by an imposed magnetic field. Due to the variable radiation pressure on elements, a non-cosmic composition is predicted for the gas disk.

I dedicate this work to my parents
and their parents in turn
and so on, all the way
to the first heterotroph

Preface

This thesis, studying details of the formation of stars and planets, is based upon one invited review article from a conference, and six peer-reviewed articles, reprinted in the second part of this volume:

I Brandeker, A., 2003, "*Multiple T Tauri systems*", review in proceedings from IAU Symp. 221, Star Formation at High Angular Resolution, Eds. M. G. Burton, R. Jayawardhana, & T. L. Bourke (2003)

II Brandeker, A., Liseau, R., Artymowicz, P., & Jayawardhana, R., 2001, "*Discovery of a new companion and evidence of a circumprimary disk: adaptive optics imaging of the young multiple system VW Chamaeleontis*", Astrophysical Journal, 561, L199

III Jayawardhana, R., & Brandeker, A., 2001, "*Discovery of close companions to the nearby young stars HD 199143 and HD 358623*", Astrophysical Journal, 561, L111

IV Brandeker, A., Jayawardhana, R., & Najita, J., 2003, "*Keck adaptive optics imaging of nearby young stars: detection of close multiple systems*", Astronomical Journal, 126, 2009

V Liseau, R., Brandeker, A., Fridlund, M., Olofsson, G., Takeuchi, T., & Artymowicz, P., 2003, "*The 1.2 mm image of the β Pictoris disk*", Astronomy & Astrophysics, 402, 183

VI Olofsson, G., Liseau, R., & Brandeker, A., 2001, "*Widespread atomic gas emission reveals the rotation of the β Pictoris disk*", Astrophysical Journal, 563, L77

VII Brandeker, A., Liseau, R., Olofsson, G., & Fridlund, M., 2003, "*The spatial structure of the β Pictoris gas disk*", Astronomy & Astrophysics, in press

These papers will be referred to in the text by their Roman numerals. The papers are shortly summarised in Appendix B, where I also detail explicitly what my contributions have been.

Any thesis in the natural sciences of today is highly specialised to a very narrow subject. This is a necessity imposed by the progress of science, but also makes it difficult for the non-specialist to see the significance of the work to the Big Picture. In the first part of this thesis, I have therefore tried to give an overview of the Very Big Picture, to subsequently narrow it down to my own contributions, in order to give them their proper context. More than being a summary of the papers, this first part is to be considered an introduction and an extension of the articles. In Appendix C, I list and define a few technical words used in this thesis.

Alexis Brandeker
November 2003

Contents

Appendices

Chapter 1

Introduction

Why? is an important question often overlooked, and often difficult to answer. In this introduction to this thesis, I will therefore try to give a very broad description to answer *why* we are studying young stars and their circumstellar material the way we do. I will start with the most general questions and gently turn to the more particular, more directly relevant to this thesis.

1.1 The *Very* Big Picture

Over the millennia, we have gradually come to learn a few basic facts about our place in the cosmos. We now know that we, together with every living thing we know of, live on a rocky planet (the Earth) orbiting a star (the Sun) in the outskirts of an island of stars in the universe, the galaxy we call the Milky Way. How did we come to be? Are we alone in the Universe? What does the Universe look like, in general? What laws govern it? These are questions the natural sciences, with astronomy as an important part, ultimately try to address. Although the questions may be simple to ask, they are certainly not simple to answer. To paraphrase Socrates, *The more we know, the more we know that we don't know*.

A well-known strategy to answer difficult questions in science is to divide the questions into, hopefully, simpler sub-questions. The idea is that the answers to these sub-questions together will provide the answer to the super-question. The strategy is called *Divide and conquer*, and is the main reason we have such narrow specialisations in science today.[1] An example would be the first question above, *How did we come to be?*, that can be divided into the biological part *How did life arise on Earth?* and the astronomical part *How did the planet Earth come to be?*. These sub-questions can then be divided in turn, *ad infinitum* it seems. This

[1] Some will argue that we are still in the 'dividing' part and have not reached the 'conquer' part yet, but I think that is being overly pessimistic.

thesis belongs to a part far down the astronomical side of the tree of questions, but before we go into too much detail, let us overview of how solar systems are thought to form.

1.2 Star and planet formation: the paradigm

This is a very short, descriptive review of the current paradigm of star system formation, and more precisely low mass star formation (stars of a mass comparable to our Sun). Technical reviews of star and planet formation may be found in Shu, Adams, & Lizano (1987), Lissauer (1993) and Hartmann (1998).

1.2.1 The interstellar clouds

Even if interstellar space (i.e. the space between the stars) is very empty compared to our Earthly standards, it is far from empty in an absolute sense. At sea level, we find the number of molecules per cubic centimeter to be roughly $n = 10^{19}\,\mathrm{cm}^{-3}$, to be compared with the typical interstellar density of $n = 1\,\mathrm{cm}^{-3}$. The interstellar medium is far from homogeneous, however, and densities from as low as $n = 10^{-3}\,\mathrm{cm}^{-3}$ to as high as $n = 10^{8}\,\mathrm{cm}^{-3}$ are observed. Regions where $n \gtrsim 10\,\mathrm{cm}^{-3}$ are often referred to as interstellar clouds. An example of such a cloud is seen in Fig. 1.1, showing the Chamaeleon region in the southern sky. The inhomogenity is evident, with "clumpiness" on all scales. Looking into to a sub-region of the cloud (Fig. 1.2), one can see still smaller sub-structures, and this goes on to the resolution limit of known observations. The geometry is reminiscent of a fractal, and that is the reason fractals have been suggested as geometric density models of the interstellar medium (Mandelbrot 1982; Bazell & Desert 1988; Elmegreen & Falgarone 1996; Brandeker 1998; Stutzki et al. 1998).

It is expected that star formation starts in one of the denser regions of giant molecular clouds, like the one in Fig. 1.1, by gravitational self-contraction. If one assumes that the only force opposing gravity is the thermal motions of the molecular gas, one can derive an expression for the critical mass M_J, the smallest mass that will start run-away self-contraction. This was done by Jeans (1902), who derived

$$M_\mathrm{J} = \left(\frac{5k_\mathrm{B}T}{G\mu m_\mathrm{H}}\right)^{3/2}\left(\frac{3}{4\pi\rho_0}\right)^{1/2}, \tag{1.1}$$

where $k_\mathrm{B} = 1.381 \times 10^{-23}\,\mathrm{J\,K}^{-1}$ is the Boltzmann constant, T is the local temperature of the cloud, $G = 6.673 \times 10^{-11}\,\mathrm{m}^3\,\mathrm{kg}^{-1}\,\mathrm{s}^{-2}$ is the gravitational constant, μ is a dimensionless quantity conventionally called the mean molecular weight, $m_\mathrm{H} = 1.674 \times 10^{-27}\,\mathrm{kg}$ is the mass of the hydrogen atom, and ρ_0 is the (constant) density of the cloud.

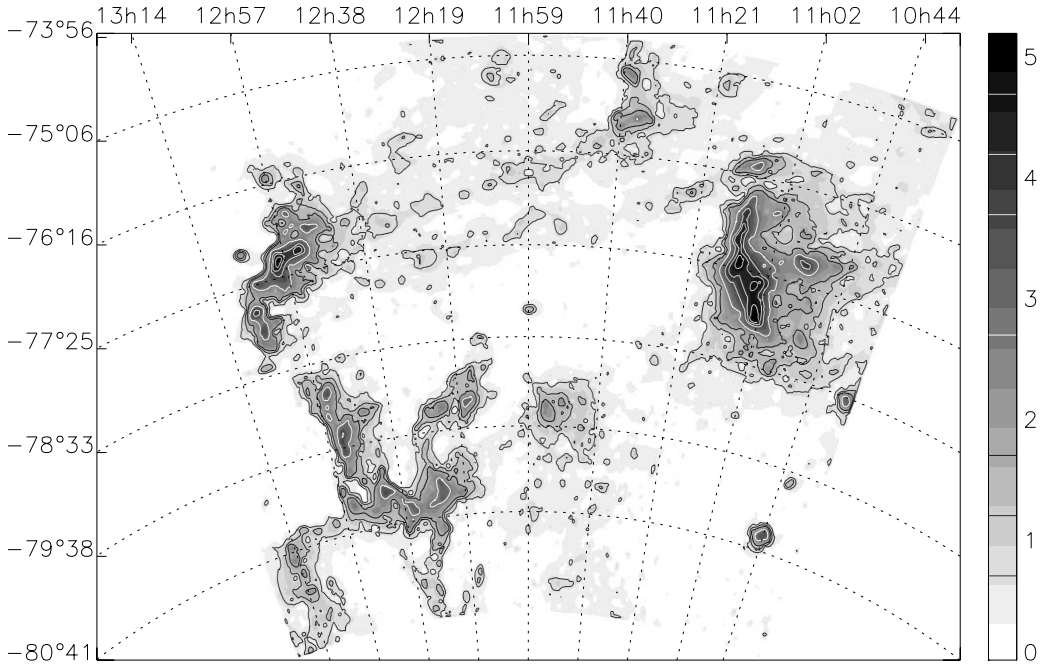

Figure 1.1: The Chamaeleon cloud complex. Extinction map derived from optical star counts (USNO *B*-band data). From Cambrésy (1999).

A cloud of the super-critical mass $M > M_{\rm J}$ should thus be gravitationally unstable and start to self-contract. Observations of the parameters M, T, ρ_0 and μ for various clouds have shown, however, that they often fulfil $M > M_{\rm J}$ without collapsing. It is as if an invisible force is holding the cloud up against its own weight. Consensus among astronomers today is that this invisible force probably is due to magnetism, supported by turbulence. I will not go into details (see Shu et al. 1987; Heitsch et al. 2001), but merely note that magnetic pressure is directional, so that if the clouds are indeed supported by magnetic pressure, they should be highly flattened along one dimension; the $M > M_{\rm J}$ magnetically supported clouds would be sheet-like in shape.

1.2.2 The collapse phase

Once a cloud becomes gravitational unstable, it starts to collapse in a run-away manner (Fig.1.3). The reason is that the more the cloud collapses, the higher the density becomes, implying smaller $M_{\rm J}$ and thus an even more super-critical state. This continues until the gravitational energy released from the infall heats up the cloud sufficiently to increase T^3 quicker than ρ_0 (from Eq. 1.1), braking the infall and starting the protostellar phase.

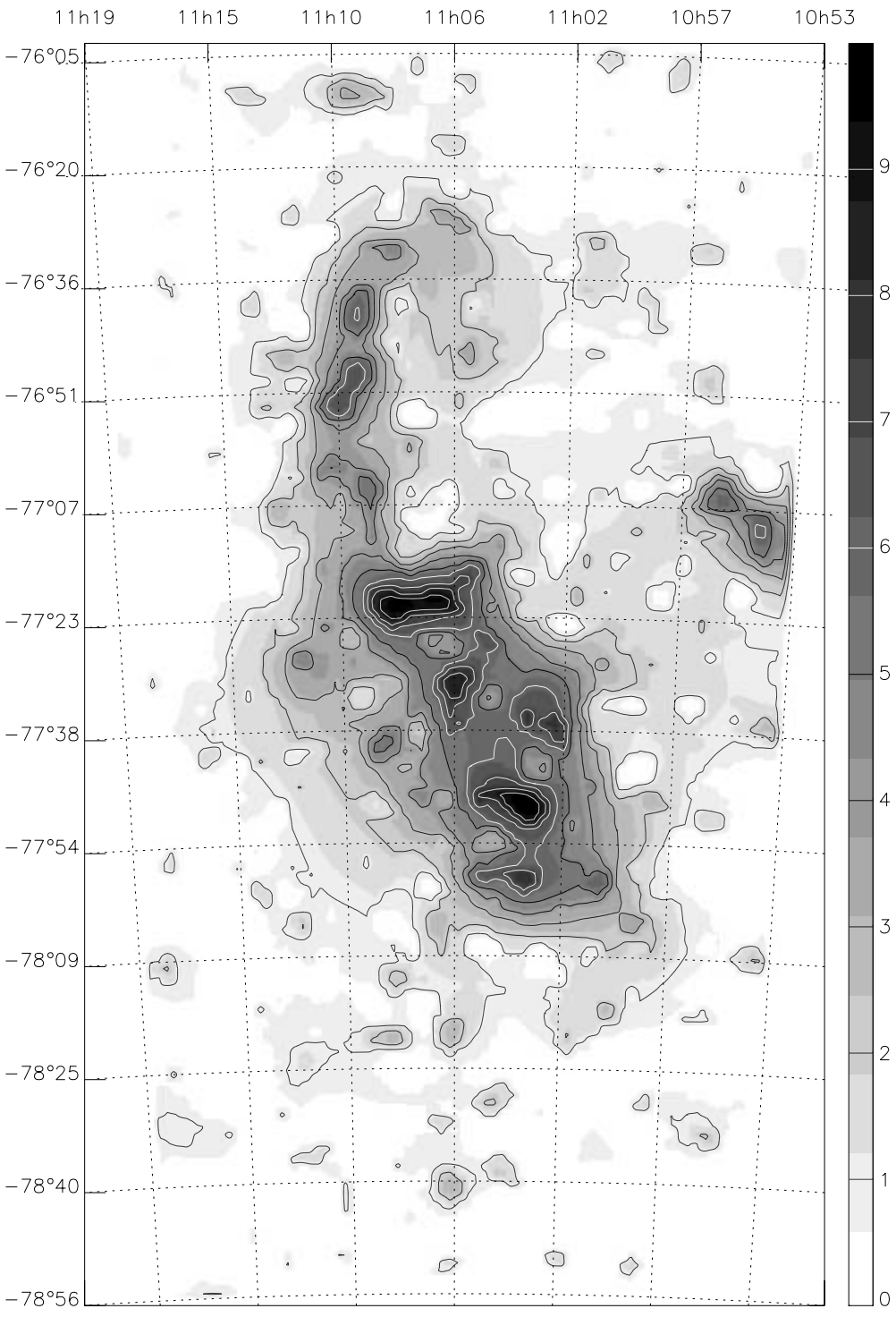

Figure 1.2: The Chamaeleon cloud complex detail. Extinction map derived from infrared star counts (DENIS *J*-band data). From Cambrésy (1999).

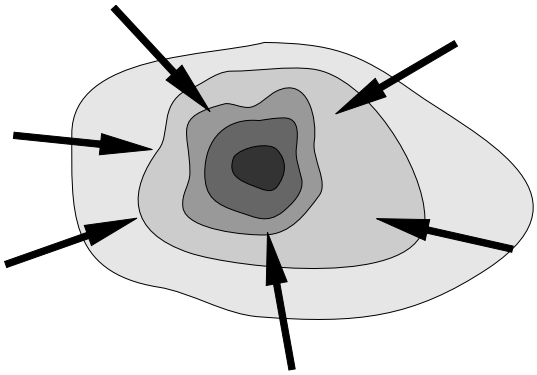

Figure 1.3: The first stage of star formation is the free fall collapse, caused by a gravitational instability. The timescale for the collapse is $t_{\rm ff} \sim 10^4 - 10^5$ years, a short moment in the life time of a solar-type star.

The collapse phase is very short in comparison to the other phases of star formation, given that it only lasts essentially the time it takes the cloud to free-fall. Let us estimate what this free-fall time scale is. For simplicity, assume a spherical cloud of initial constant density ρ_0 such that $M \gg M_{\rm J}$. As shown already by Newton, each shell of the sphere at radius R_0 will feel the gravitational force equivalent to that from a point of mass $M = 4\pi R_0^3 \rho_0/3$. Assuming that the cloud is initially at rest, this gives the equation of motion

$$\frac{{\rm d}^2 R}{{\rm d}t^2} = -\frac{GM}{R^2}, \tag{1.2}$$

where G again is the gravitational constant, and t is the time. The simple differential equation 1.2 is disturbingly difficult to solve, but one may verify that

$$\zeta + \frac{1}{2}\sin(2\zeta) = \sqrt{\frac{8\pi G\rho_0}{3}}\, t, \tag{1.3}$$

where $\cos^2(\zeta) = R/R_0$, gives an analytical (albeit implicit) solution (see, e.g., Kippenhahn & Weigert 1994). Now, if we assume that $R(t = 0) = R_0$, then the time when the shell reaches the centre, $R(t_{\rm ff}) = 0$ gives $\zeta = \pi/2$ and Eq. 1.3 gives

$$t_{\rm ff} = \sqrt{\frac{3\pi}{32 G\rho_0}}. \tag{1.4}$$

Note that Eq. 1.4 is *independent* of R_0, all shells take the same time to reach the centre, whatever initial radius. This is called a *homologous* contraction.

Using the number density $n = 10^5\,{\rm cm}^{-3}$ typical for dark molecular cloud cores, translating to the mass density $\rho = 3.3 \times 10^{-19}\,{\rm g\,cm}^{-3}$ for $\mu({\rm H}_2) = 2$, gives the typical free fall timescale $t_{\rm ff} \sim 10^5$ years.

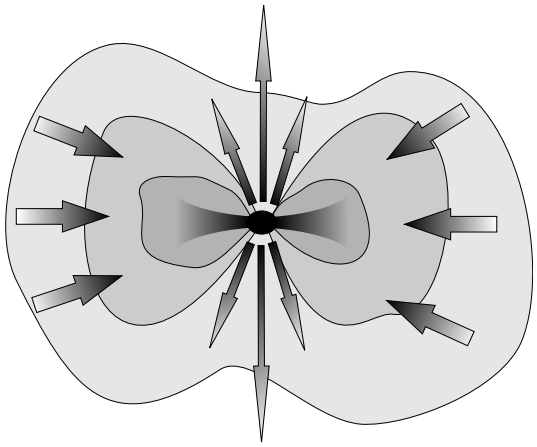

Figure 1.4: Protostars are deeply embedded in the surrounding, still collapsing, cloud. As the cloud contracts more, a flattened structure starts to develop, the circumstellar disk. Material accretes slowly in the disk, while bi-polar outflows remove angular momentum.

1.2.3 The protostellar phase

The free fall approximation breaks down when the heating from gravitational energy, released during the infall, increases the pressure of the gas sufficiently to resist further contraction. The star-to-be now enters the *protostellar phase*, a phase of slow contraction as the heated gas slowly radiates away the heat (Fig. 1.4).

It is instructive to consider the wide range of spatial scales involved in a collapse of a dark molecular core to a star. Initially, the radius of a pre-collapse dark core is $\sim 0.2\,\mathrm{pc} = 40\,000\,\mathrm{AU}$, while the final star is of radius $\sim R_\odot = 0.005\,\mathrm{AU}$. The scale thus ranges almost seven orders of magnitude.[2] This has implications for the kinematics of the protostar, in particular due to the conservation of the angular momentum. The angular momentum $\mathbf{L}$ for a system of particles (like a cloud of molecules) is

$$\mathbf{L} = \sum_n (\mathbf{r}_n \times m_n \dot{\mathbf{r}}_n)\,, \tag{1.5}$$

where $\mathbf{r}_n$ is the position vector from the cloud centre, $\mathbf{v}_n = \dot{\mathbf{r}}_n$ its time derivative (the velocity) and m_n the mass, of particle n. If $\mathbf{L}$ is to be conserved while $r_n = |\mathbf{r}_n|$ decreases significantly, we see that $v_n = |\mathbf{v}_n|$ has to increase proportionally in a direction perpendicular to both $\mathbf{L}$ and $\mathbf{r}_n$, i.e. the angular velocity has to increase. Even a very minute initial preferred direction of rotation, amounting to say $1\,\mathrm{m\,s^{-1}}$

[2] With the same concentration ratio, I would have to read 30 000 books for every single page of my thesis I write. I am very grateful that the required concentration for a Ph. D. thesis is less than stellar.

(or, about 10^{-16} rad s^{-1}) for the cloud core, would result in a final rotational speed of 10 000 km s^{-1} for the star. This is higher than the escape velocity of solar-type stars (at ∼500 km s^{-1}), and would blow the star apart. Clearly, something must happen to the collapsing cloud before it reaches this stage.

Since changes in vector components of $\mathbf{r}_n$ and $\mathbf{v}_n$ parallel to $\mathbf{L}$ in Eq. 1.5 do not change $\mathbf{L}$, infalling matter does not feel the resistance of inertial momentum along the direction of $\mathbf{L}$ and contracts freely. In contrast, matter falling in perpendicular to $\mathbf{L}$ has to transfer a high fraction of its infall velocity to a rotational velocity, consequently braking the infall. The net result is a highly flattened structure perpendicular to $\mathbf{L}$, a *disk*.

The protostellar phase starts when the free fall stops due to the build up of thermal pressure, and stops when the core gets heated enough to ignite the star by starting nuclear fusion of deuterium. In the mean time, the surrounding infalling cloud has turned from roughly spherical infall to a greatly flattened accretion disk.

Sometime during the protostellar phase, strong bipolar outflows are observed to develop, i.e. strong winds moving radially outwards from the polar regions at high speed (10–300 km s^{-1}; see Fig. 1.4). Nobody knows why these winds occur, but they provide a convenient way of removing angular momentum from the protostellar system. Granted, the angle between the outflow and $\mathbf{L}$ is supposed to be small, but this is compensated by the high outflow velocity. Outflows are most easily observed when they interact with the surrounding interstellar medium, where they produce shocks that heat the medium, often to dissociate molecules and give rise to strong line emission. These shocked objects, named Herbig-Haro, are very common in star forming regions (and then often associated with T Tauri stars). Sometimes the outflows themselves can be directly observed, in particular at radio wavelengths, where line emission from molecules escape the extinction at shorter wavelengths.

The protostars themselves are heavily obscured by the surrounding cloud, making them extremely difficult to observe directly at optical wavelengths. A progress in the far-infrared detector technology was required and enabled astronomers, using the infrared astronomical satellite IRAS, to peer into the dark cores of giant molecular clouds to find protostars (Beichman et al. 1986).

The duration of the protostellar phase depends strongly on the mass of the clump, but is typically 10^5–10^6 years for a solar-type star.

1.2.4 The T Tauri phase

Once the central (solar-type) star has ignited, it enters a more stable phase that lasts a few million years, the T Tauri phase (Fig. 1.5). Most of the collapsing cloud has either accreted onto the star, been blown away by the bi-polar outflow, or settled in the disk. The star continues to accrete gas from the disk, adding a

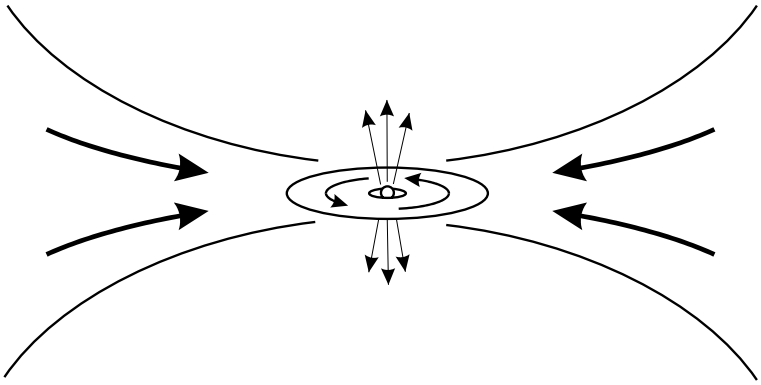

Figure 1.5: The T Tauri phase starts out with the star completely hidden by the circumstellar material. During the end of the phase, the surrounding material has cleared out by both accretion onto the star and bi-polar outflows away from it, revealing the new-born star.

luminosity to the star comparable to the energy generated from the internal fusion. T Tauri stars, named after the proto-type star T Tauri (Fig. 2.2), are more easily seen than their younger counterparts, the protostars, because of the clearing of the ambient medium. T Tauri stars show evidence for strong chromospheric magnetic activity, and often have bi-polar jets associated to them.

It is around the time of the young T Tauri stars that dust particles in the disk are expected to grow larger and stick to each other. Eventually small bodies are created from the dust particles, the planetesimal, the building blocks of planets. The "planetesimal hypothesis" states that these planetesimals build up planets by pair-wise accretion. Sufficiently massive planetary bodies in a gaseous disk will be able to accrete gas and thus create giant gas planets. The details of planet formation are not very well known, however, as the discovery of odd extra-solar planets revealed. In particular, the formation and location of gas planets is sensitively dependent on the life time of the gas disk. Unfortunately, the properties of the gaseous component of disks, such as the mass, composition, and life time, are still poorly known.

Stars in the T Tauri phase show an interesting variety of observational characteristics. In Chapt. 2 I describe T Tauri stars in more detail.

1.2.5 The debris disk phase

After most of the material in the disk around a T Tauri star has accreted/been blown away, what remains is a *debris disk* (Fig. 1.6). The star has now ceased its strong magnetic activity, and is no longer accreting any significant mass from the circumstellar disk. Any planets of a debris disk system will already have formed,

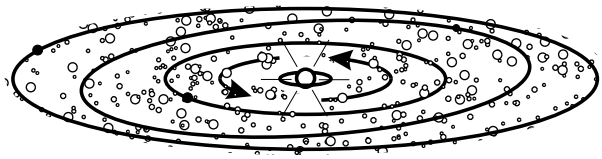

Figure 1.6: The debris disk is thought to consist of dust produced by the left-overs from the planet formation phase.

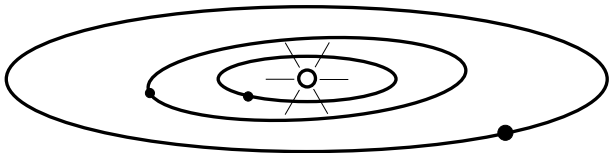

Figure 1.7: Star systems at the mature main sequence (like our solar system) contain very little circumstellar material in the form of gas and dust; most of the circumstellar mass is trapped in the planets.

as there is not enough material to form new planets. The debris disks are thought to be thin and dusty, in the sense that the total disk mass is small and mostly contained in dust. These are stars that are just entering the main sequence.

Debris disks were discovered by the aforementioned IRAS mission (Aumann et al. 1984). Astronomers were surprised to find IR excess from main-sequence stars, well-known stars such as Vega, Fomalhaut and β Pictoris. Sub-sequent observations showed these excesses to be due to circumstellar dust. In Chapt. 3 I give more details on the discovery of the debris disks and their significance to this thesis.

The debris disk phase is thought to last 10^7–10^9 years (Habing et al. 2001). The age estimates are hampered by poor statistics; we know less than fifty debris disks candidates, including β Pictoris, Vega, ε Eridani, Fomalhaut, HR 4796 A and HD 141569. This situation is expected to change, however, once the new IR satellite SIRTF, launched in August 2003, has had a closer look at the near-by IR universe.

1.2.6 The mature main-sequence phase

Over time, most of the debris of the star and planet formation phase disappears from the main sequence star (Fig. 1.7). Not completely though; even in our solar system we still have planetesimals in orbit, the asteroids, and a thin dust disk, the zodiacal dust. The dynamics of the solar system at large, however, have entered a very stable phase, thought to last 10^{10} years. This is apparently enough time to develop life on suitable planets, like plants, animals, and even astronomers. We

know nothing about life on planets in general, however, since we only have one verified example of a planet where life has emerged: the Earth. Until 1995, we did not even know if there were planets around other solar-type stars. Since then, over a hundred extra-solar planets have been discovered, all of them massive giants on par with our own giant planet, Jupiter.

The reason we discover only massive planets is not necessarily that massive planets are the most common; it is just that the surveys so far have been sensitive only to giant planets. There may very well be hoards of Earth-size planets out there, we just would not detect them with our current technology.

To understand how solar systems and terrestrial planets are formed, how common planets are around other stars, in particular potentially life-bearing planets, we need to develop our observational skills to find these terrestrial planets. It will not be easy, because terrestrial planets are *very* small in comparison to their parent stars, shining some 10^9 times fainter at optical wavelengths. In addition, the planets are always extremely close to their parent star, as seen from Earth, making it very difficult to extract the planetary signal in the glare from the star.

In spite of these difficulties, there are well-developed plans to search for extra-solar terrestrial planets. The European space agency, ESA, and the American counterpart, NASA, are planning space missions to not only find extra-solar terrestrial planets, but also to search their atmospheres for signatures of life. The strategy is to make use of infrared (IR) *nulling* interferometers. These instruments are designed to observe at IR wavelengths, where the contrast between the potential planet and the star is expected to be much lower ("only" 10^7). One major innovation is the idea to centre the star at destructive interference (hence the name "nulling" interferometer) and scan for the planet at a constructive interference, thereby increasing the contrast sensitivity to levels sufficient to detect a terrestrial planet. By taking low-resolution IR spectra of a discovered planet, the composition of its potential atmosphere can be obtained, possibly revealing the signatures of life.

ESA and NASA are now collaborating on this mission, although they still have separate technical proposals that differ in detail: the Darwin (ESA) and the Terrestrial Planet Finder (NASA). A preliminary schedule for the mission puts the launch year to 2014, but as is usual in the world of space missions, this date will probably be subject to substantial revisions.

1.3 This thesis

In the following subsections, I detail explicitly the relevance of this thesis to theories of star and planet formation.

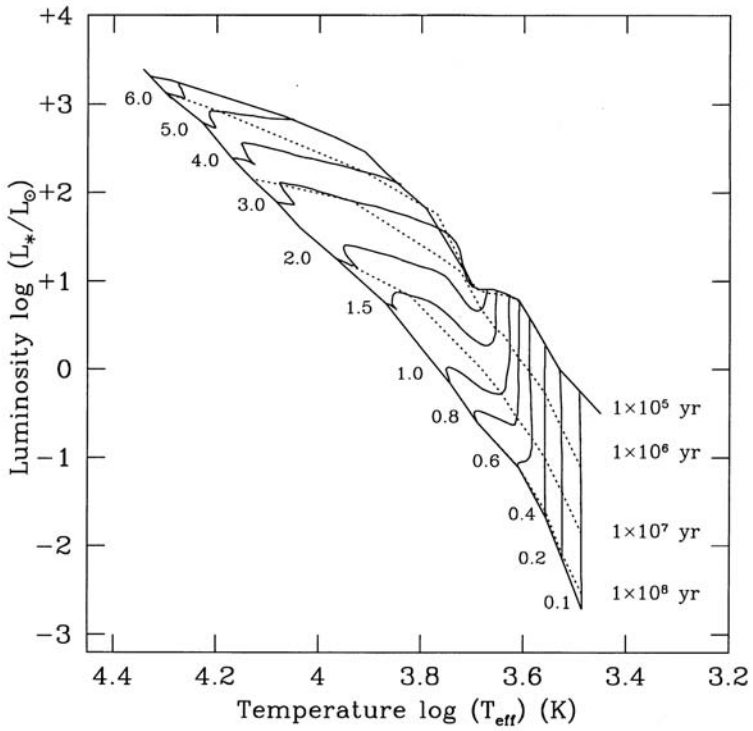

Figure 1.8: The Hertzsprung-Russel diagram with evolutionary tracks from a modern model of early evolution plotted for different stellar masses. The numbers along the diagonal are main-sequence stellar masses in units of $M_{\odot}$. From Palla & Stahler (1999).

1.3.1 Calibrating models of early stellar evolution

Our understanding of the early stages of star formation is strongly coupled to quantitative models. If young stars evolve the way we think they do, their properties should be consistent with properties derived from these models. Unfortunately there are some parameters in the models that are not well fixed by prior knowledge; opacities, for instance, are notoriously difficult to estimate yet very important to the general evolution. Fortunately, we can discriminate between most of these models by comparing their predictions to observations. In particular, models predict the stellar effective surface temperature and luminosity as a function of mass and age. By thus plotting a temperature-luminosity diagram (also known as a Hertzsprung-Russel diagram; see Fig. 1.8) for a sample of stars with observed properties, the predictions can be checked.

In practice, the luminosities L and effective surface temperatures $T_{\rm eff}$ are the most easily obtained observables. For deeply embedded objects, however, like protostars and some T Tauri stars, L and $T_{\rm eff}$ may be very difficult to impossible to

extract.

To calibrate the evolutionary tracks, L and $T_{\rm eff}$ are not sufficient; one needs the stellar mass M and/or age t as well. These are very difficult quantities to estimate independently from models of evolution, as is required if we are to calibrate them. There are a couple of strategies, one being to use tight binaries to estimate *dynamical* masses by following the orbital evolution, another to estimate an age for an ensemble of stars assumed to have been formed roughly simultaneously. Paper I to Paper IV present high resolution observations intended to support both those strategies by finding tight binaries and measuring their relative positions with great accuracy. More details are given in Chapt. 2, in particular in Sect. 2.4.

1.3.2 Setting the stage for planet formation

Paper V to Paper VII concern the debris disk phase, as outlined in Sect. 1.2.5. One question of great interest is: Are these debris disks *really* debris disks? The question may sound tautological, but simply illustrates our limited knowledge of the disks we call debris disks. These disks are called debris disks because they are thought to be produced in collisions by the leftovers from planet formation; the gas content in disks is expected to be too small for planets to gain further mass by accretion.

This view was recently challenged by observations from the infrared space observatory (ISO, Thi et al. 2001). A detected signal from the debris disk system of β Pictoris, corresponding to the substantial reservoir of 50 $M_\oplus$ (Earth masses) of molecular hydrogen, H_2, was claimed, although the signal was of low significance (3σ). A reservoir of gas this massive in a disk at the β Pic's age of $\sim 10^7$ years would have important consequences for the formation and orbital evolution of gas giants, as they would have more time to accrete mass and migrate in the disk (Lissauer 2001).

Why are we still not sure about the status of the debris disks? The reason is the difficulty we have to measure their gas contents. I postpone the discussion to Chapt. 3, where I describe the debris disks, and the attempts to characterise them, in some detail. My own contributions to the study of the debris disks have been to investigate thermal emission from the dust disk of β Pic (Paper V) and to develop and successfully apply (to β Pic) a novel method to study gas disks (Paper VI & Paper VII). The method of studying gas disks, developed together with my collaborators Göran Olofsson and René Liseau, shows great potential to put sensitive constraints on the gas content of the borderline post-T Tauri disks. The ground is set for future studies to make important contributions to the understanding of gas disk evolution and planet formation (see Sect. 4.2).

Chapter 2

T Tauri stars

The first part of this thesis, consisting of Paper I–Paper IV, concerns the earliest stellar phases of solar-type stars. Here I explain shortly what it is all about.

2.1 T Tauri stars: the definition

T Tauri stars were first observed by Joy (1945) and were then singled out due to their strong observational characteristics. These are strong emission lines, resembling the solar chromosphere, and strong photometric variability. T Tauri stars were thus early on operationally defined by their observational characteristics and not mainly for their evolutionary status in low-mass star formation (Sect. 1.2.4). Today, T Tauri stars have become synonymous with low-mass pre-main-sequence stars. With the progress of detector technology, new wavelength bands in ultraviolet (UV), infrared (IR), and X-rays, have revealed new peculiarities of T Tauri stars, such as veiling (excess emission in the UV), IR excess and strong magnetic activity.

Not all characteristics are shown by all T Tauri stars. In fact, the diversity among the T Tauri stars is large; there is even a sub-class of so-called Weak-line T Tauri stars (WTTS) that are singled out mainly by their X-ray emission. The WTTS are complemented by the classical T Tauri stars (CTTS), with the formal distinction that T Tauri stars with the equivalent width of Hα emission less than 5 Å are called WTTS, and all other T Tauri stars CTTS.

Several circumstances point towards the youth of T Tauri stars. They are often found close to large interstellar clouds; with an average relative velocity of 1–2 km s^{-1}, the small distances imply ages of $\lesssim 10^6$ years. Strong absorption of Li I λ6707 in the stellar atmosphere is an indication of youth as the strong convective mixing in these stars is transporting the lithium to hot regions, gradually destroying the metal.

2.2 Why T Tauri stars?

Studying T Tauri stars is a powerful way of constraining star formation theory, for several reasons:

- T Tauri stars represent the dynamic early stages, when the properties of the stars still trace their formation histories. This contrasts to stars at the main sequence, which can be well characterised by a few parameters (such as mass and metallicity).
- T Tauri stars are luminous in the IR, and are visible over larger distances and extinctions than their main sequence counterparts, in particular for the stars of lowest mass.
- The progress in detector technology in the IR and near-infrared (NIR) together with modern adaptive optics (AO) has made dynamical mass estimates of young stars, using binaries, feasible.

The last point is important for calibrating theoretical evolutionary tracks, which are sensitive to physical quantities (like opacities) that are less well known at the early cool stages. The expected errors of the theories at these early stages are therefore large enough that dynamical mass estimates will put significant constraints.

2.3 Circumstellar disks and their evolution

As outlined in Sect. 1.2, circumstellar disks play an important role in star as well as planet formation. There are several ways of detecting disks around T Tauri stars. Signs of disk accretion can be detected by looking for emission lines, thought to be emitted from gas heated by matter shocked during infall onto the star. Even without the additional luminosity from accretion, *passive* disks still reveal their presence by irradiating significant amounts of the stellar luminosity into the IR, causing the system to show an IR excess with respect to the photospheric emission. Important questions that may be addressed by systematically survey young stars for disks are

- How large fraction of the stars form with disks (all of them?)
- Are the properties of the circumstellar disks dependent on the stellar type, and in that case how?
- How do circumstellar disks in multiple systems evolve?

- How large fraction of the disks form planets, and what distinguishes them from the other disks?

- How does an circumstellar disk evolve in general, i.e. what does the distribution of disks look like around stars of different ages?

When looking indiscriminately for circumstellar disks, searching for IR excess using wide-field IR cameras and broadband filters proves more efficient than painstakingly obtaining spectra on an individual basis. This is an area where the detector improvements have been revolutionary during the last 20 years, with the detector sizes closely following Moore's law[1]. Space observatories like IRAS, ISO, and SIRTF have allowed increasingly sensitive measurements at higher angular resolutions of the far infrared (FIR) wavelength domain at $10\,\mu$m–$100\,\mu$m, difficult to impossible to observe from the surface of the Earth. One of the key discoveries of IRAS was the detection of protostellar sources deeply embedded in their parent molecular clouds (Beichman et al. 1986; Sect. 1.2.3), representing the pre-T Tauri phase with dusty envelopes falling in from all directions, and thus also representing a pre-disk phase. Another key discovery of the IRAS mission was the *Vega-excess phenomenon*, or, the debris disks (Aumann et al. 1984; Sect. 1.2.5; see also Chapt. 3), representing a *post*-T Tauri phase with optically thin dust disks where any planets should already have formed.

By searching young clusters and associations of stars, one can investigate the life-times of disks by assuming the stars of a cluster to be co-eval and determine the fraction of stars that show IR excess. Comparing this fraction between clusters and associations of different ages, conclusions can be drawn about the disk life-times. A recent such attempt is found in Fig. 2.1 (Haisch, Lada, & Lada 2001), where the disk life-time is estimated to 6 million years (see also Spangler et al. 2001). This estimate refers to the dust disk, however, since it is the dust of the disk that gives rise to the IR excess; the evolution of the gas disk, thought to be 10 –100 times more massive than the dust disk in the youngest stars, is poorly constrained. In Sect. 4.2 I discuss possible future projects to remedy this deficiency.

2.4 T Tauri multiple systems

Most stars, including pre-main-sequence stars, are part of multiple systems (Duchêne 1999). Fig. 2.2 shows three examples of similar multiple systems. To understand star formation in general, we thus need to understand formation of stars in

[1]Moore's law states that computer performance roughly doubles every 18 months; in our case the number of pixels of IR detectors have increased a few thousand times over the last two decades, and the sizes continue to grow.

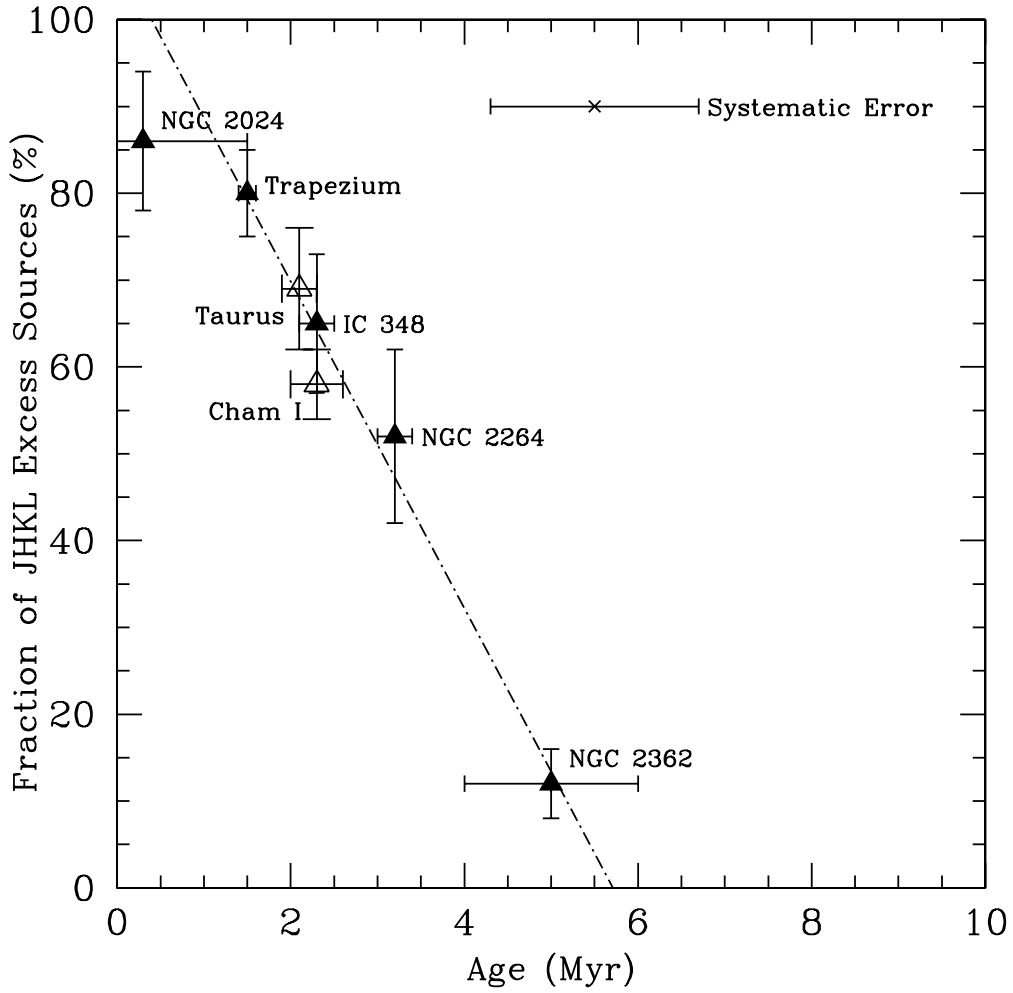

Figure 2.1: Fraction of IR-excess sources as a function of age for various young clusters and associations. Adopted from Haisch et al. (2001).

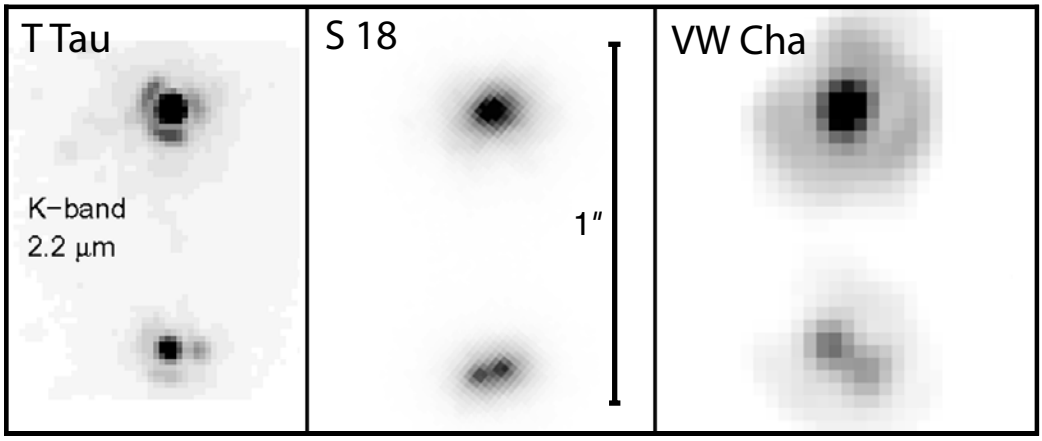

Figure 2.2: High resolution adaptive optics images of three near-by triple T Tauri stars of similar appearance: T Tauri, S 18 (in MBM 12), and VW Chamaeleontis. The three panels are on the same scale, but have different orientations in the sky. From Paper I.

multiple systems. There are several other good reasons to look for multiple systems among the T Tauri stars. As mentioned in Sect. 2.2, binary stars can be used to determine dynamical masses, and thereby calibrate models of the early stellar evolution (see also Palla & Stahler 2001). When estimating the ages of stars from colour-magnitude diagrams, unresolved binaries may yield erroneous ages. To illustrate the importance of finding binaries to age estimates, consider an unresolved binary of stars with equal luminosity and colour (and therefore estimated surface temperature). If uncorrected for binarity, the derived luminosity would be twice the real ones for the individual companions. Looking at the evolutionary tracks in the Herzsprung-Russel diagram of Fig. 1.8, we find that the difference of 0.75 in magnitude corresponds to at least a factor of 10 in age.

A third reason to look for companions, is that they may give rise to an IR excess difficult to distinguish from a circumstellar disk, in particular in the NIR, and if only few photometric bands are used. This factor contributes to the error of important diagrams like Fig. 2.1.

One way of finding close companions is by looking at their combined spectrum. Their orbit around each other will give rise to periodically moving sets of spectral lines (see, e.g., Torres et al. 2003; Steffen et al. 2001). The search for these *spectroscopic binaries* is most sensitive to very tight companions, where the radial velocities change over the course of a few days or weeks. For longer period binaries, spectroscopic searches are very time consuming, as observations of at least an entire period is usually required to confirm the existence of companions. A practical upper limit for detecting binaries spectroscopically is thus an orbit

of at most a few years, corresponding to a physical separation of a few AU for solar-mass stars.

To directly image T Tauri stars of a few AU separation, one needs very high angular resolution observations. The nearest T Tauri stars, with a few exceptions, are typically 100 pc distant. With telescopes limited by the atmospheric seeing, $\sim$0.″5 at best, the physical spatial resolution at the distance of the nearest T Tauri stars becomes $\sim$50 AU. This is at least ten times wider than the widest physical separation that spectroscopic binary surveys are sensitive to, and yields a gap between a few AU and 50 AU were companions can hide, without being detected. To estimate a dynamical mass from the orbital motion of a 50 AU orbit would take some hundreds of years, just for the stars to revolve around each other.

The development of adaptive optics, to fight the blurring effect of the atmosphere to improve the angular resolution with a factor of $\sim$10, has been revolutionary in many ways, one being the possibility to finally close the gap in sensitivity between spatial and spectroscopic surveys of T Tauri multiple systems.

In Paper I, I review the current status of high resolution imaging of T Tauri multiple systems, and give more detailed examples of its benefits. In the subsequent Paper II to Paper IV, we report our usage of adaptive optics to image and find multiple systems.

In Paper II, we report the discovery of a tight binary (0.″1 $\triangleq$ 16 AU) in orbit around a primary star, i.e. a triple system. The estimated orbital period of the tight binary is 74 years, meaning that constraints on the system mass can be put already after a few years. To get a reliable dynamical mass estimate, however, we probably have to wait at least 50 years. We also provide evidence for a circumprimary dust disk, truncated by the gravitational perturbations from the orbiting binary.

Paper III shows two associated near-by post-T Tauri stars to be binary. Later these stars were found to be associated with the β Pictoris moving group (Zuckerman et al. 2001; Kaisler et al. 2003).

Using the adaptive optics system at Keck (Paper IV), we investigated the near-by associations of young stars MBM 12 and TWA, at roughly 275 pc and 55 pc respectively. Among other things, we discovered a very tight binary – TWA 5 A – separated by only 55 mas, corresponding to the physical projected separation of 3 AU. This is a very promising candidate for accurate dynamical mass estimates in follow-up studies, as the estimated period is on the order of 5 years.

As the high-resolution imaging provided by adaptive optics became available only recently, these studies mark only the very beginning of a multi-year effort to calibrate the theory of pre-main-sequence evolution. A few future prospects of this programme are detailed in Sect. 4.1.

Chapter 3

Main sequence debris disks

In this chapter, I give an overview of the debris disks in general and β Pictoris in particular. I elaborate on my contributions in the field, and set them into a broader context. The relevant papers are Paper V, Paper VI and Paper VII.

3.1 Background

From the surface of the Earth, the infrared wavelengths between 10 μm and 100 μm are seriously shielded by molecular absorptions, and overwhelmed by the warm, terrestrial atmosphere. When the infrared astronomical satellite IRAS was launched in 1983, it therefore opened a whole new universe in the infrared (Neugebauer et al. 1984). One of the major highlights of the IRAS mission was the discovery of the "Vega-excess" phenomenon. From certain main-sequence stars, among them *the* standard photometric star Vega, a strong excess emission over the expected photospheric emission was observed (Aumann et al. 1984). One of the stars with the strongest detected infrared (IR) excess was the main-sequence star β Pictoris (Aumann 1985). Subsequent imaging of β Pic, using a coronograph to shield the bright light from the star itself, revealed a linear feature aligned in the north-east to south-west direction, interpreted as the first imaged circumstellar disk (Smith & Terrile 1984). Coronographic searches around other Vega-excess stars were unsuccessful in finding similar features (Smith et al. 1992; Kalas & Jewitt 1995a).

Since then, these stars have been subject to intense studies. Although still not detected in scattered light, the dust disks of the Vega-excess stars Vega, Fomalhaut, and ε Eridani, have recently been imaged in thermal emission at 850 μm (Holland et al. 1998) as well as by radio interferometers (Spangler et al. 2001; Wilner et al. 2002). A few new Vega-excess stars with resolved disks in scattered light have more recently been added to the β Pic disk, including HR 4796 A (Jayawardhana et al. 1998; Koerner et al. 1998; Schneider et al. 1999) and HD 141569

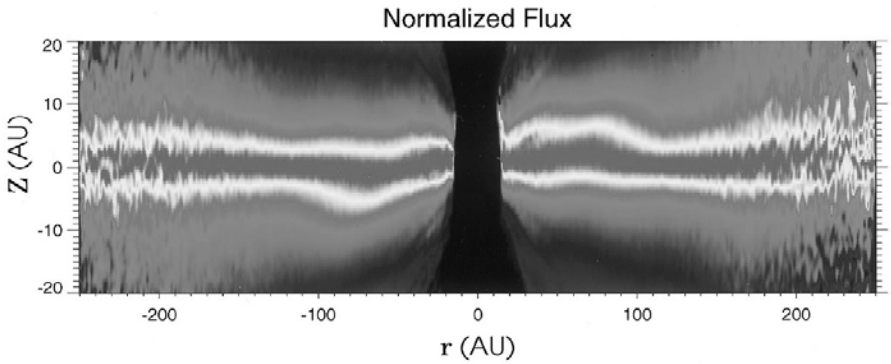

Figure 3.1: The inner dust disk of β Pictoris, as imaged by STIS/HST. Note that the vertical scale is expanded relative to the horizontal scale, to emphasize the warp inside ~100 AU. From Heap et al. (2000).

(Augereau et al. 1999; Weinberger et al. 1999; Clampin et al. 2003). An additional number of stars with IR excess, but with disks yet to be resolved, were found by ISO (Habing et al. 2001).

The evolutionary status of the debris disks, and their relation to star and planet formation, is overviewed in Sect. 1.2.5.

3.2 β Pictoris – the crowned queen of disks

The best studied debris disk by far is the disk of β Pic. There are several reasons for this: β Pic is nearby (19.3 pc, Crifo et al. 1997), has a comparatively large disk (>1000 AU in radius), and a disk orientation which is edge on. Taken together, this means that the disk can be very well resolved – two arcminutes across translates to over a thousand angular resolution elements at the resolution of, say, the Hubble Space Telescope or a modern adaptive optics system. Thanks to its edge-on orientation, the disk surface brightness, as seen from Earth, is higher than it would otherwise be.

Even at the resolution of a few AU, the appearance of the dust disk is very smooth. Several asymmetries have been identified, however, the strongest being a north-east/south-west brightness difference (Kalas & Jewitt 1995b). The south-west (SW) part of the disk appears to have a higher scale-height, while being fainter and extend to a smaller radius, than the north-eastern (NE) counterpart.

Another interesting asymmetry is found in the inner 100 AU of the disk, where there seems to be a disk component inclined ~5° with respect to the outer disk (Fig. 3.1; Heap et al. 2000). By investigating numerical models, Mouillet et al. (1997) and later Augereau et al. (2001) showed that this warp could be explained

if there was a Jupiter-mass planet at an inclined orbit with a ~10 AU major axis.

Due to the favourable edge-on orientation of the β Pic disk, circumstellar gas was discovered early on, seen in absorption against the star (Hobbs et al. 1985). The star has actually been known to harbour circumstellar gas since the seventies (Slettebak 1975), although its association with a disk was unknown at the time.

A serendipitous discovery was the time variable absorption lines, observed to vary most strongly in the Ca II H & K lines (Ferlet et al. 1987; Lagrange-Henri et al. 1992; Crawford et al. 1994). These variable absorption lines were later interpreted as being due to *Falling Evaporating Bodies* (FEBs, Ferlet et al. 1987; Beust et al. 1990; Thébault et al. 2003), thought to be the first examples of extra-solar comets.

3.3 The dust disk of β Pictoris

The β Pic disk contains considerable amounts of dust, on the order of $0.5\,M_\oplus$ (Artymowicz 1997). The dust visible in observations, ranging from optical to radio wavelengths, have a size distribution ranging from $\sim 1\,\mu$m to ~ 1 mm (Artymowicz et al. 1989, Paper V). There probably exist larger grains, but they are unfortunately difficult to observe. The main reason is that the reflecting/thermally emitting area to mass ratio is much greater for small particles than for larger ones, since area scales with the particle radius as $A \propto r^2$, while volume scales as $V \propto r^3$.

Small dust grains do not survive for long in the β Pic environment, as they are blown away from the star by the radiation pressure (as the gas is, see Sect. 3.5 below). Larger grains, on the other hand, are subject to gas drag, due to a different orbital velocity from the gas, and/or the Poynting-Robertson drag (Robertson 1937), effectively reducing the orbital radii of these particles until they are evaporised by the star. Since the time scale for this dust destruction is much shorter ($\sim 10^4$ years, Takeuchi & Artymowicz 2001) than the estimated age of the system (12^{+8}_{-5} Myr, Zuckerman et al. 2001), the dust must somehow be replenished. Suggested mechanisms include evaporation of comets (Li & Greenberg 1998) and collisional erosion by kilometer-sized planetesimals (e.g., Artymowicz 1997; Thébault et al. 2003, and references therein). The total mass contained in planetesimals producing the dust might be around $140\,M_\oplus$ (Artymowicz 1997), although this estimate is due to extrapolation of a mass distribution law, and consequently highly uncertain.

The dust disk in scattered light is very smooth and symmetrical (Heap et al. 2000), although a few asymmetries have been observed (Kalas & Jewitt 1995b). One is the slight brightness differences of the north-east (NE) and south-west (SW) parts of the disk, another is the slight inclination of the inner disk with respect to the outer (Fig. 3.1). More recently, similar asymmetries were found

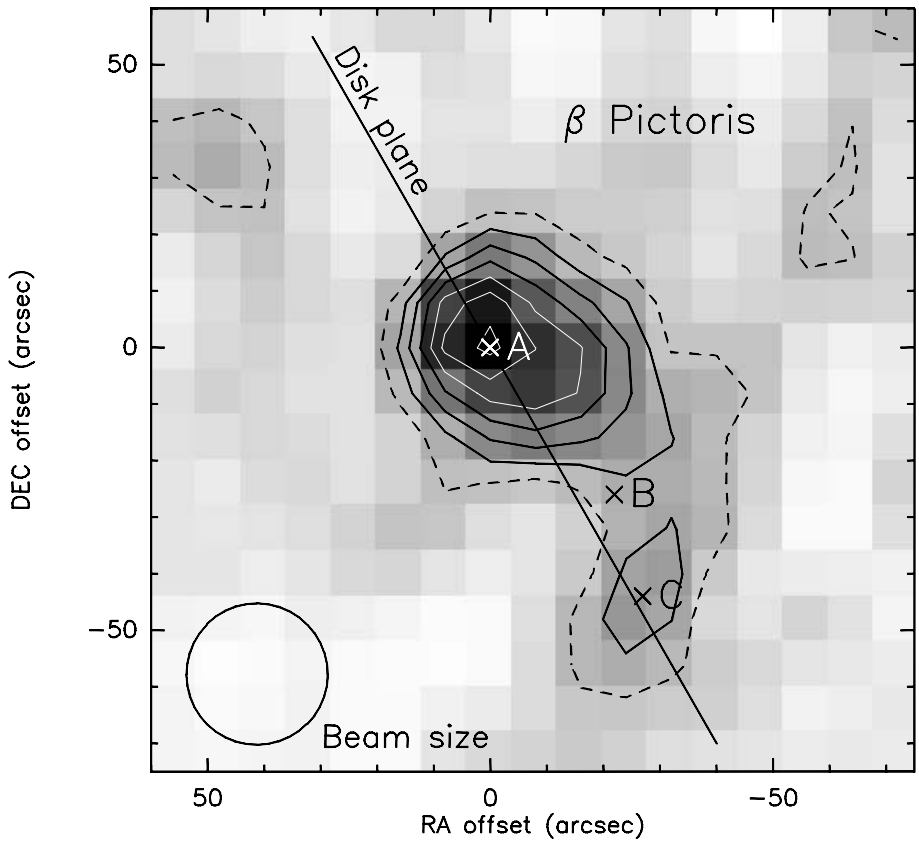

Figure 3.2: The 1.2 mm image of β Pictoris. The letters A, B and C denote the positions of the star, the SCUBA-blob, and the SIMBA-blob, respectively. From Paper V.

in the infrared (Pantin et al. 1997; Wahhaj et al. 2003), and in the sub-mm/mm (Holland et al. 1998, Paper V), which trace the thermal emission from the dust rather than scattered light from the star. The thermal emission shows interesting differences to the scattered light. While the NE part is brightest in the scattered light, the reverse is true for the thermal emission (Paper V). This is probably due to a difference in the dust properties between the NE and SW. For instance, if the NE side consisted mainly of small, bright grains, and the SW side of large, dark grains, then the NE would be most easily seen in scattered light and the SW in thermal emission (Paper V).

The imaging of β Pic in 850 μm by JCMT/SCUBA on Hawaii (Holland et al. 1998), revealed an interesting emission feature at the projected distance of 650 AU from β Pic (position B, Fig. 3.2). The detection significance of this "SCUBA-blob" was only 5σ, but later we found a similar feature when imaging β Pic in 1.2 mm with SEST/SIMBA at ESO, Chile, but at a slightly different position (Pa-

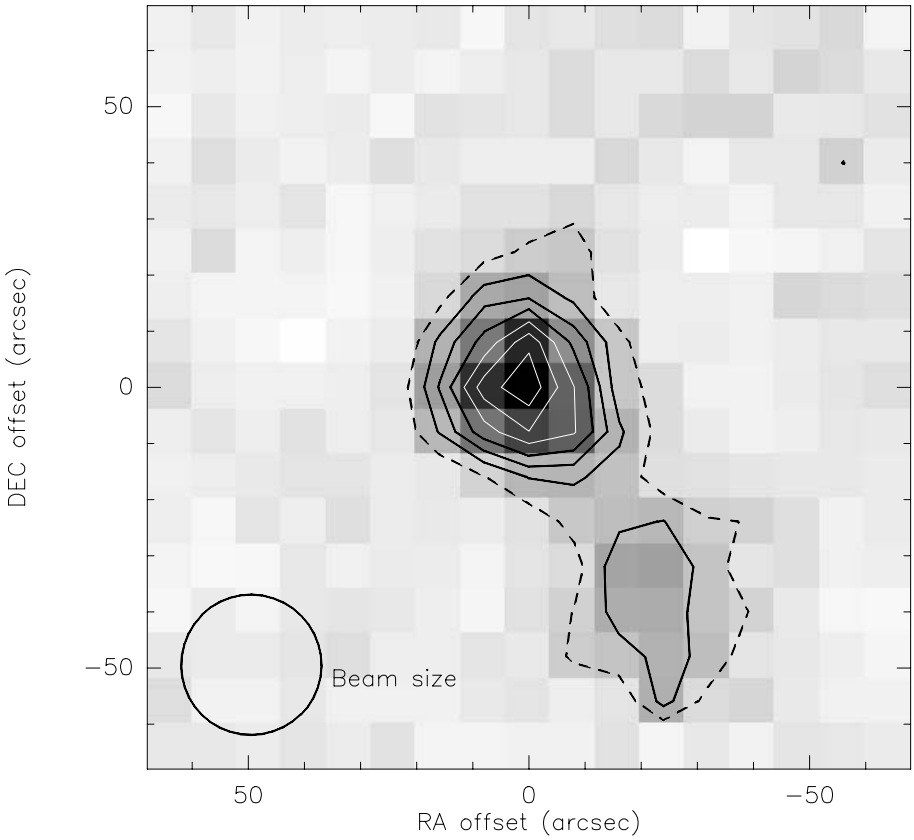

Figure 3.3: A simulated 1.2 mm image of the β Pictoris system, including three point sources (the star, the SCUBA-blob and the SIMBA-blob) put at their observed positions and relative flux. This image is consistent with the real, observed image of Fig. 3.2.

per V, position C in Fig. 3.2). The significance of this "SIMBA-blob" is even less, 3σ. It is interesting, however, that they are that close to each other. Could it be the same blob? The projected distance between the blobs is 370 AU, and the epoch difference between the observations is 4 years. Assuming that the blobs are the same requires it to have moved at an average velocity of at least 420 km s^{-1} with respect to β Pic. This super-sonic velocity is much higher than the motion of β Pic itself in the galaxy (of order 200 km s^{-1}). The β Pic velocity relative to our Sun is even less, corresponding to $0\farcs4$ during the time between the two observations. The blob-velocity is actually similar to the escape velocity of the star (630 km s^{-1}). Assuming the blob to be some sort of ejection from the star, end extrapolating the blob position linearly back in time, puts the ejection event to the year 1990.

Could the SCUBA- and SIMBA-blobs both be real, but different? The SIMBA-blob position is outside the figure of Holland et al. (1998), so it may possibly be

in their data. To test if the SCUBA-blob is consistent with the SIMBA observations, we produced artificial observations by putting point sources at the locations A, B and C of Fig. 3.2 at their measured relative strength, convolved with the SEST-beam, and added noise. The result, shown in Fig. 3.3, is consistent with the SIMBA observations. We thus cannot exclude that the SCUBA-blob still is were it was when it was observed by SCUBA. However, future observations will probably settle the nature of the blobs (Sect. 4.3).

3.4 The gas disk of β Pictoris

Since the main focus during my thesis-work has been on the gas disk of β Pictoris, the following sections are the most extended. I review why we are interested in the gas disk, what kind of problems there are related to the gas disk, and how they have been approached.

3.4.1 Why gas?

There are several reasons as to why it is highly desirable to detect gas in circumstellar disks:

- Gas emission carries important information not readily available from dust observations, such as the composition, temperatures and ionisation structures of the disk.

- Because gas emission is narrow compared to the broad features of dust emission, high velocity resolution along the line of sight can be obtained. Spatially resolved gas emission may thus be used to study the dynamical state of the disk.

- Planet formation theory predicts a strong dependence of the planet formation efficiency on the gas content and gas evolution in the disk (e.g. Pollack et al. 1996). Ultimately we would like to understand where and when planets form in the disks.

The disk of β Pic is interesting in many ways. The star is nearby, only 19.3 pc away, opening up for detailed studies of its inner disk – making it easier to find signatures of any potential planets. The disk is a borderline case between the massive disks of the T Tauri stars and the thin zodiacal disks of older main-sequence stars. The question of whether or not β Pic has a massive gas disk is therefore particularly important for the timescale of gas-giant formation (Lissauer 2001).

3.4.2 The quest for the gas

The metallic gas lines detected in absorption against the star did not directly reveal the gas mass of the disk. The most abundant element in the universe is hydrogen, so it is reasonable to expect this to be true in the disk as well. Early estimates, obtained by scaling the observed metallic amounts with solar abundances (Hobbs et al. 1985), gave a column density of $N(\mathrm{H}) = 10^{18}$–$4 \times 10^{20}\,\mathrm{cm}^{-2}$ and a characteristic density of $n_{\mathrm{H}} = 10^5\,\mathrm{cm}^{-3}$, with the total gas mass $M \approx 1.5\,M_\oplus$.

To observe cold hydrogen directly is unfortunately very difficult. Atomic hydrogen, H I, can be observed in the famous 21 cm radio line. The problems with trying to detect 21 cm emission is two-fold: the line is intrinsically very weak, and radio telescopes have an inherent low angular resolution. If the debris disk of the star is aligned edge-on, like in the case of β Pic, one can try to detect the gas in absorption against the star. Unfortunately, the transitions from the ground state of H I (where most of the electrons are expected to reside) are all in the far-ultraviolet (FUV), where the flux from the star is suppressed to extremely low levels. For H_2, the situation is similar: molecular transitions of low energy can be found in the IR, where the detection is very difficult from the surface of Earth – or they can be observed in absorption of electronic transitions in the FUV.

Despite these difficulties, attempts have been made to detect hydrogen. Freudling et al. (1995) used an array of six 22 m radio telescopes to observe the 21 cm line from β Pic for a total of 20 hours integration. No signal was detected, but the upper limit of the column density was estimated to $N(\mathrm{H\,I}) \lesssim$ a few times $10^{19}\,\mathrm{cm}^{-2}$. Thi et al. (2001) used the IR satellite observatory ISO to observe two rotational transitions of the H_2 molecule, at wavelengths 17 μm and 28 μm. They detect a signal that, if real (the signal was only 3σ), would require large amounts of warm H_2, 50 $M_\oplus$ at 100 K. Smeared out over the beam of ISO, this implies a column density of $N(\mathrm{H_2}) = 3 \times 10^{21}\,\mathrm{cm}^{-2}$.

Although the photospheric UV emission from β Pic is very low, there exist a few *chromospheric* emission lines (Bouret et al. 2002). Using the UV satellite observatory FUSE, Lecavelier des Etangs et al. (2001) tried to find absorption lines from electronic transitions in H_2, against the background of a O IV doublet from the β Pic chromosphere. The electronic transitions of H_2 are easily excited, so a very small quantity of H_2 along the line of sight would be detectable, but none was found. The sensitive upper limits on the column density were given as $N(\mathrm{H_2}) < 3 \times 10^{18}\,\mathrm{cm}^{-2}$ (3σ confidence), *three orders of magnitude* smaller than the beam averaged ISO detection. This tells us that the H_2 detected by ISO is unlikely to reside in the disk, at least anywhere near the line of sight to β Pic.

Normally, CO is a good tracer of H_2. Therefore, several studies have been dedicated to detect CO from the disk of β Pic in microwave emission (Liseau & Artymowicz 1998, and references therein). Only sensitive upper limits for CO

were obtained ($N(\mathrm{CO}) < 10^{15}\,\mathrm{cm}^{-2}$ at $T \sim 45\,\mathrm{K}$). In absorption, however, against the star, CO was detected by the UV satellite IUE, and later confirmed by both the UV spectrograph GHRS at the Hubble space telescope (Vidal-Madjar et al. 1994; Jolly et al. 1998), and its successor STIS, with higher spectral resolution (Roberge et al. 2000). The CO column density was found to be $N(\mathrm{CO}) = 6.3\times10^{14}\,\mathrm{cm}^{-2}$ and the *excitation* temperature to be low, $T = 20-25\,\mathrm{K}$, indicating that it is located in the outer regions of the disk.

The situation for CO thus appears reversed to H_2; it is detected in absorption but not in emission. For CO this is easily explained, as the beam-dilution is very uncertain (i.e. the unresolved CO source could be smaller than expected). The lack of H_2 absorption is not as easily explained, however. In addition to the constraint that the H_2 cannot be located in the disk, we now also know that it cannot be mixed with CO – since CO, in contrast to H_2, *is* detected along the line of sight.

The amount of CO seen in absorption is very small. Scaled with an abundance ratio typical of solar comets (Jolly et al. 1998), the column density of hydrogen would be $N(\mathrm{H}) \approx 10^{16}\,\mathrm{cm}^{-2}$. There is reason, however, to believe that CO could be destroyed on a short timescale (10^3 years, Jolly et al. 1998), dissociated by UV radiation from the star and the ambient interstellar radiation field. In addition, with low enough temperatures, there is a possibility that CO "freezes out" on the surface of cold dust grains, effectively becoming invisible (Kamp & Bertoldi 2000, with references therein). Thus the H density could in principle be very much higher than implied from the CO observations and a cosmic $n(\mathrm{CO})$ / $n(\mathrm{H})$ ratio.

In 2001, we discovered widespread atomic gas in emission from the gas disk (Paper VI). The spatially resolved long-slit spectra of Na I D_2 & D_1, showed a large gas disk in Keplerian rotation. Follow-up observations in 2002 revealed a geometrically thick disk of a scale-height greater than theoretical expectations, and 88 spectral lines from 9 different metallic ions (Paper VII). A strong asymmetry between the two sides of the gas disk was observed, much stronger than the corresponding asymmetry in the dust disk (Sect. 3.3). We have only started to mine this huge data set, which contains many interesting, yet unexplained features. Hopefully, careful modeling will help us gain new insights of the β Pic gas disk, and possibly gas disks in general (see also Sect. 4.3).

3.5 The radiation pressure

The detection of metallic gas seen in absorption against β Pic (Hobbs et al. 1985), early posed a problem. The "stable" components of the observed lines, not associated with the transient features attributed to falling evaporated bodies, were found to be at relative rest to β Pic, within a few $\mathrm{km\,s}^{-1}$. Yet, the radiation pressure on these metallic ions is appreciable (see Table 3.1), often far exceeding the gravi-

tational force. This means that the absorbing elements would rapidly accelerate out of the β Pic system at high velocities – clearly in contradiction with the in absorption observed low relative radial velocities. Lagrange et al. (1998) proposed a solution to this problem by postulating a dense ring of H I (n(H I) $\approx 10^6\,\mathrm{cm}^{-3}$) located at a distance 0.5 AU from the star. By assuming that the metallic gas was produced inside this ring and pushed outwards by the radiation pressure, they could show that the slow-down of the metals, due to collisions with H I atoms in the ring, would build up a high density of slowly moving gas particles dominating the radial absorption profile. This would result in an observed "stable" component with the fast-moving particles outside of the H I ring invisible due to their small densities and high velocities. Because of the small volume occupied by H I, the obtained column density, $N(\mathrm{H\,I}) = 8 \times 10^{18}\,\mathrm{cm}^{-2}$, was found consistent with the upper limit by Freudling et al. (1995), $N(\mathrm{H\,I}) \lesssim$ a few times $10^{19}\,\mathrm{cm}^{-2}$.

However, as our observations reported in Paper VI and Paper VII show, the stable gas is not limited to a small region at ~1 AU, but extended to at least 320 AU. This was not known to Lagrange et al. (1998), but likewise calls for a new explanation.

3.5.1 The effects of radiation pressure in empty space

Let us investigate what the effects of radiation pressure on ions released in an empty space environment close to the star would be. In Appendix A the expressions used here are derived in more detail.

The radiation pressure from the star, like gravity, is a central force $\propto r^{-2}$, where r is the distance to the star. One may therefore introduce a convenient distance independent parameter

$$\beta = \frac{F_{\mathrm{rad}}}{|F_{\mathrm{grav}}|} \tag{3.1}$$

to quantify the relative strength of the force exerted by the radiation pressure, F_{rad}, to the force of gravity, F_{grav}. In Appendix A an expression for β_i, β for a given transition $j \rightarrow k$ in an ion, is derived (Eq. A.8):

$$\beta_i = \frac{A_{jk}\lambda^4 R_\star^2 F_\lambda(R_\star)}{8\pi c^2 G M_\star m}\frac{g_j}{g_k}, \tag{3.2}$$

where A_{jk} is the spontaneous emission probability (Einstein A coefficient) for the transition from level j to k, g_j and g_k are the statistical weights of the levels, λ is the wavelength of the transition, $R_\star$ is the radius of the star and $M_\star$ its mass, c is the velocity of light, G is the gravitational constant, $F_\lambda(R_\star)$ the flux density at the stellar surface, and m is the mass of the particle.

Table 3.1 shows the radiation pressure calculated for a number of elements using several transitions. The estimated β is sensitive to the emitted flux from the star, which is the reason both minimum and maximum values are given for β; the maximum value refers to the emitted flux in the stellar continuum, while the minimum refers to the continuum minus the *photospheric* absorption line caused by the element. The model atmosphere is calculated for a star without rotation, while β Pic is rotating with $v \sin i = 140\,\mathrm{km\,s^{-1}}$ (Hoffleit & Warren 1995). The photospheric absorption lines of the model are therefore narrower and deeper than the lines of the real rotating star. The β_{min} of Table 3.1 thus underestimates the real β, while β_{max} overestimates it, and $\beta \in [\beta_{\mathrm{min}}, \beta_{\mathrm{max}}]$.

If left alone, a particle with high β would rapidly accelerate radially away from the star. How rapidly? Assuming the particle is released at rest with respect to the star, we have the radial equation of motion

$$\ddot{r} \equiv \frac{\mathrm{d}^2 r}{\mathrm{d}t^2} = (\beta - 1)\frac{GM}{r^2}. \tag{3.3}$$

This differential equation ignores a few facts of reality:

- The released particle is probably not at rest relative to the star, but in orbit (see Sect. A.3).
- The particle will in general not be able to ascend freely, due to other forces like magnetism or collisions with other particles of different β.
- Light from the star may be blocked by particles closer to the star, i.e. the particles may be self-shielded, effectively changing β with radius.
- As the particle accelerates, β changes due to the wavelength dependence of flux at the photospheric absorption lines. I.e., a particle with a transition at a spectral absorption line of the photosphere will have its β increased as the line gets Doppler-shifted. β will therefore be a function of velocity.
- The particle may change between different ionisation states and thus change its β radically. As an example, in the disk of β Pic, Na is mostly ionised, n(Na I) / n(Na) $\sim 10^{-3}$ (Paper VII). While Na I has a β of several hundred, Na II feels almost no radiation pressure at all (Table 3.1).

Despite these shortcomings of Eq. 3.3, it is still useful to study its implications. If $\beta \gg 1$, any orbital motion of the released particle can be safely ignored (see Sect. A.3). By solving Eq. 3.3 numerically, a β varying with velocity and ionisation can be taken into account.

Table 3.1: Radiation pressure on ions close to β Pic

Ion	β^{a}_{min}	β^{a}_{max}	$-v^{b}_{\infty,min}$ [km s^{-1}]	$-v^{b}_{\infty,max}$ [km s^{-1}]	Δv^{c}_{obs} [km s^{-1}]
Ca I	74	570	−120	−340	···
Ca II	6.6	280	−34	−240	−0.3±2.1
Cr I	30	150	−77	−180	···
Cr II	0	0	0	0	2.2±3
Fe I	7.9	68	−38	−120	−0.0±0.3
Fe II	1.3	34	−7.9	−83	···
H I	0	0	0	0	···
Na I	510	540	−320	−330	−1.2±0.3
Na II	0	0	0	0	···
Ni I	1.1	43	−4.5	−93	0.4±0.4
Ni II	0.1	0.4	0	0	2.8±3
S I[d]	1.5	1.5	10	10	···
Ti I	30	164	−77	−180	···
Ti II	8.3	40	−39	−90	0.2±0.8

[a] These numbers are computed for a number of ground state transitions. β_{min} refers to the flux at the center of the (unrotated) model photospheric line, while β_{max} the continuum level. From Liseau (2003), except that $\log g = 4.20$ has been used instead of $\log g = 4.5$ (see Sect. A.1).

[b] Asymptotic velocity (according to Eq. 3.4) if released at 15 AU, without braking medium.

[c] Measured radial velocity in absorption relative β Pic. From Paper VII.

[d] From Lagrange et al. (1998).

A particle accelerated by the radiation pressure asymptotically approach a velocity given by Eq. A.12,

$$v_\infty = \sqrt{2(\beta - 1)\frac{GM}{r_0}}, \tag{3.4}$$

where r_0 is the release point radius. In absorption against the star, the line profile would be rectangular of width v_∞ (Eq. A.18 and Fig. A.4). *This is not observed.* The line profiles of metals seen in absorption are unresolved in observations with $R \sim 120\,000$ (Paper VI; Paper VII), meaning the lines are narrower than $3\,\mathrm{km\,s^{-1}}$. Using the ultra-high-resolution facility (UHRF) at the Anglo-Australian telescope, with a spectral resolution of $R \gtrsim 900\,000$, Crawford et al. (1994) resolved the Ca II K line and found the line width of the "stable" component to be $\sim 2\,\mathrm{km\,s^{-1}}$, much less than the predicted 34–240 $\mathrm{km\,s^{-1}}$ of Table 3.1. In addition, the measured radial velocities relative to the star of the metal absorptions are very small, less than a few $\mathrm{km\,s^{-1}}$ (Table 3.1).

The conclusion is that either the particles "disappear" before they reach high velocities, or there must be a braking force. Let us first consider the possibility that particles "disappear". This was first suggested in Paper VI to explain why the Na I atoms have such low velocities. Most of the Na is namely ionised in the disk, and Na II experiences almost no radiation pressure at all (Table 3.1). The Na I atom is thus ionised before it reaches any appreciable velocity, and therefore effectively "disappears".

The purported explanation works well for Na because its ionised species experiences little radiation pressure. This is not the case for Fe; both Fe I and Fe II are strongly influenced by the radiation pressure, and would reach radial velocities of 8–120 $\mathrm{km\,s^{-1}}$. Since Fe II has an ionisation potential of 16.2 eV, very little of the Fe is expected to be Fe III in the disk of β Pic. Fe I is observed through-out the disk, from radii of 13 AU to at least 323 AU (Paper VII).

3.5.2 Magnetic braking

Iron forces us to conclude that something must indeed brake the particles. Could it be a global magnetic field? A magnetic field would only brake the ionised particles, but on the other hand, the metals we see are estimated to mostly be in a singly ionised state in the disk. Maybe the short periods of neutral state in a nucleus's life is not enough to accelerate the particle appreciably.

What field strengths would be required to cancel the radiation pressure at, say, $r = 100$ AU, where most of the gas is located (Paper VII)? The magnetic Lorentz force is

$$\mathbf{F} = q\mathbf{v} \times \mathbf{B}, \tag{3.5}$$

where q is the charge of the ion, $\mathbf{v}$ is the velocity, and $\mathbf{B}$ is the magnetic field strength. To match gravity, the magnetic flux density would have to be

$$B \equiv \|\mathbf{B}\| = \frac{m}{q}\sqrt{\frac{GM}{r^3}}. \tag{3.6}$$

For Fe II, with $m = 9.27 \times 10^{-26}$ kg, $q = 4.80 \times 10^{-19}$ C, and $\beta \sim 10$, at 100 AU from β Pic, this gives $B = 5.1 \times 10^{-16}$ T $= 5.1 \times 10^{-12}$ G, a very small field strength. If we assume the field to be dipolar and emerging from the star, however, the corresponding field strength at the stellar surface would be substantial, $B = 9.8 \times 10^{-4}$ T $= 9.8$ G, since the field strength is $\propto r^{-3}$.

There are several problems with this magnetic picture. The magnetic field required to balance radiation pressure scales as $r^{-3/2}$, while a dipolar magnetic field is $\propto r^{-3}$. A magnetic force tuned to counter the radiation pressure at a particular distance would fail to do so at every other distance. Different ions have different β and different m/q; most ions would thus feel a force either too strong, resulting in super-Keplerian speeds, or too weak, granting the ion permission to leave the system. A strong dipolar field by itself can thus not be responsible for the braking of particles. An external uniform field would not help either, for the same reasons.

One could imagine a strong *toroidal* magnetic field. Ionised particles would be locked in their orbits, unable to move radially but free to move azimuthally in Keplerian orbits. The field would not have to be tuned, since just a minimum field strength would be required to hold the particles in orbit. For the ions to show a radial velocity of less than a couple of km s^{-1}, the ion should be accelerated by the radiation pressure to $v_{\max}$ = a few km s^{-1} in less time than it takes the magnetic field to reverse the direction of velocity for the ion, i.e. the time it takes the ion to travel half the gyration orbit (Fig. 3.4). With the gyration period being

$$t_{\rm g} = \frac{m}{q}\frac{2\pi}{B}, \tag{3.7}$$

and the acceleration due to radiation pressure described by 3.3, we derive the required magnetic field strength to be

$$B = \frac{m}{q}\frac{\pi G M_\star}{v_{\max} r^2}(\beta - 1). \tag{3.8}$$

For the Fe II ion at 100 AU with $v_{\max} = 1$ km s^{-1} and $\beta \approx 10$, this implies a field strength of $B \approx 2 \times 10^{-13}$ T $= 2 \times 10^{-9}$ G. For a Ca II ion at 10 AU with the same $v_{\max}$ but $\beta = 240$, the required field would be $B \sim 10^{-10}$ T $= 10^{-6}$ G. At 100 AU, the gyration time and radius would be 1 month and 10^{-2} AU respectively, and at 10 AU, 1 *hour* and 10^{-5} AU. The mean-free paths for the solar-composition model

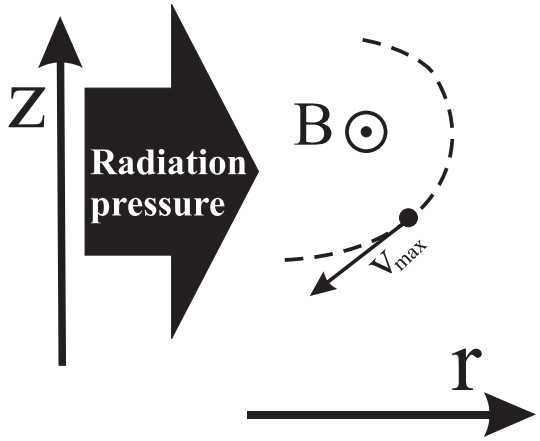

Figure 3.4: Magnetic braking by a toroidal magnetic field. Radius increases to the right, height over the disk upwards, and the magnetic field lines are coming out of the graph. If the magnetic field is strong enough, out moving ions will turn around before reaching high velocities.

of Paper VII, with $n_{\rm H}(10\,{\rm AU}) = 2 \times 10^3\,{\rm cm}^{-3}$ and $n_{\rm H}(100\,{\rm AU}) = 4 \times 10^4\,{\rm cm}^{-3}$, are $l(10\,{\rm AU}) = 0.02\,{\rm AU}$ and $l(100\,{\rm AU}) = 0.4\,{\rm AU}$.

Due to the macroscopic Ampère's law,

$$\oint_C \mathbf{B}\cdot{\rm d}\mathbf{l} = \mu_0 I, \tag{3.9}$$

where C is a path enclosing a surface, d$\mathbf{l}$ is a line element along the path, $\mu_0 = 4\pi \times 10^{-7}\,{\rm V\,s\,A^{-1}\,m^{-1}}$ is the *magnetic permeability*, and I is the total current through the surface, a toroidal magnetic field would imply a net charge transfer orthogonal to the disk. Using the numbers for B above, we get the corresponding net currents $I = 2 \times 10^7$ A and $I = 8 \times 10^8$ A. These are not terribly large figures; they correspond roughly to the sustained current of 2 000 and 80 000 lightnings on Earth, respectively. That corresponds to a net charge transfer of at most 1 000 kg of protons per year in a wind/jet perpendicular to the disk.

This ad-hoc toroidal field is thus, as far as I know, consistent with observations. The required magnetic field strengths are very small – yet have important dynamical implications. One problem is that we do not understand the origin of such a field. *Why* should there be a minuscule, yet non-zero magnetic toroidal field in the disk? In Sect. A.4, it is shown that a magnetic field this weak would be unstable to the current driven by the radiation pressure. For the magnetic field to be stable, Eq. A.46 has to be fulfilled, translating to a magnetic field strength of at least $B > 1$ mG, a factor of a 1 000 stronger than required by the observed radial velocities of ions.

Fortunately, there is a direct way to test this idea of magnetic braking. The magnetic braking applies only to charged particles, ions (and to a lesser degree charged dust particles). That neutral particles observed along the line of sight do not show appreciable radial motion was motivated above with the fact that the neutral population is a very small fraction of the total population of the species, and that most particles are singly ionised. Any given particle is neutral only for a very short while. However, any atom with a sufficiently high ionisation potential would stay neutral in the β Pic environment. If, in addition, these atoms were sensitive to the radiation pressure with $\beta > 1$, then we would expect them to be strongly depleted in the disk – no magnetic force would hold them back, and they would leave in the free-ascend mode described in Appendix A.

To summarise, *if* a high-β neutral atom is found at normal abundances at rest relative to the ions in the absorption spectrum, then that is good evidence that something else than magnetic forces must be responsible for the braking. On the other hand, if high-β neutral atoms are strongly depleted in the absorption spectrum, this could be interpreted as evidence for a magnetic braking force at work.

Unfortunately, not many elements fulfil the requirement of simultaneously having $\beta > 1$ and being predominantly neutral. H, He, C, N, O, Ne and Ar all have high ionisation potentials and are expected to be neutral in the disk, but they lack strong transitions from the ground state at suitable wavelengths for the β Pic stellar energy distribution, so the radiation pressure on them are negligible. Sulphur may be a borderline case; the radiation pressure is modest, $\beta \approx 1.5$ (Lagrange et al. 1998), and according to our modeling (in Paper VII) only 80 % is ionised, meaning the S particle is neutral 20 % of its time, free to accelerate.

S I was infact observed in absorption against β Pic, in the UV $\lambda_{\rm vac}$1807 line by the GHRS spectrograph at the Hubble space telescope (Vidal-Madjar et al. 1994; Lagrange et al. 1998). It was not found to be particularly depleted in comparison to the other metals, nor did its radial velocity depart significantly from relative rest to β Pic (Lagrange et al. 1998). This could be an indication that something else than magnetic forces must brake S I, since we would expect a significant relative depletion if only magnetic forces were at work (Table 3.2 and Sect. 3.5.4).

3.5.3 Braking by a medium

If the gas disk is dense enough, the gas drag will prevent particles from reaching high velocities. Assuming the braking gas to be at rest with respect to the moving particles at velocity v, the drag force may be written

$$F_{\rm fric}(v) = -m_{\rm m} C(v) v \tag{3.10}$$

where m_m is the mass of the moving particles and $C(v)$ dependends on the kind of interaction. For neutral particles colliding with a neutral gas,

$$C_\mathrm{nn}(v) = \frac{2\pi a_0^2 n_0 m_0}{m_0 + m_\mathrm{m}} \sqrt{v_\mathrm{T}^2 + v^2}, \tag{3.11}$$

where m_0 is the mass of gas particles in the braking medium, a_0 is the geometric radius of the atom, n_0 is the number density of the braking gas,

$$v_\mathrm{T} = \frac{3}{4}\sqrt{\frac{3k_\mathrm{B}T}{m_0}}, \tag{3.12}$$

and $k_\mathrm{B} = 1.38 \times 10^{-23}\,\mathrm{J\,K^{-1}}$ is the Boltzmann constant (see Kwok 1975, for a derivation of C_nn). For ions colliding with a neutral gas, one must take into account the induced-dipolar effect (Beust et al. 1989),

$$C_\mathrm{in}(v) = \frac{2n_0 q}{m_0 + m_\mathrm{m}} \sqrt{\frac{\pi\alpha_0 m_0}{\varepsilon_0}}, \tag{3.13}$$

where α_0 is the *polarisability* of the braking gas, and $\varepsilon_0 = 8.85\times10^{-12}\,\mathrm{A\,s\,V^{-1}\,m^{-1}}$ is the *electric permittivity*.

The equation of motion 3.3 can now be modified to include gas drag:

$$\dot{v} = (\beta - 1)\frac{GM}{r^2} - C(v)v, \tag{3.14}$$

where we have used $\dot{v} \equiv \ddot{r}$. We see that Eq. 3.14 has a stationary solution for $\dot{v} = 0$,

$$v_* = \frac{(\beta - 1)GM}{C(v_*)r^2}. \tag{3.15}$$

This is a stable and attractive solution, since we have from Eq. 3.14 that $v < v_* \Rightarrow \dot{v} > 0$ and $v > v_* \Rightarrow \dot{v} < 0$. How quickly is v_* approached? Assuming

$$\frac{r(t_x) - r_0}{r_0} \ll 1, \tag{3.16}$$

where t_x is the time it takes to reach $v_x = xv_*$ for $x \in [0, 1]$, and r_0 is the initial radius, we can treat the acceleration of Eq. 3.14 as a constant a. We see from Eq. 3.11 that $v \gg v_\mathrm{T} \Rightarrow C_\mathrm{nn}(v) \propto v$ while $v \lesssim v_\mathrm{T} \Rightarrow C_\mathrm{nn}(v) =$ constant. For typical conditions in the disk, $v_\mathrm{T} \sim 1\,\mathrm{km\,s^{-1}}$, the same order as the observed radial velocities. To simplify Eq. 3.14 further, we thus assume that we have $v \lesssim v_\mathrm{T}$ and that $C_\mathrm{nn}(v) =$ constant. For ions, $C_\mathrm{in}(v)$ is already constant for all velocities, and we need not assume $v \lesssim v_\mathrm{T}$. We get the simplified equation

$$\dot{v} = a - Cv, \tag{3.17}$$

which is readily solved to

$$v(t) = v_* + (v_0 - v_*)e^{-Ct}, \tag{3.18}$$

where v_0 is the initial velocity at $t = 0$, and $v_* = a/C$ (as in Eq. 3.15). This equation can be integrated once more to yield the time evolution of the distance r,

$$r(t) = v_* t + \frac{(v_0 - v_*)}{C}\left(1 - e^{-Ct}\right) + r_0. \tag{3.19}$$

We may now evaluate the condition 3.16. Assuming we start from rest at radius r_0, the time it takes to reach $v_x = xv_*$ is $t_x = -\ln x/C$. Inserted into 3.19 and 3.16, we have

$$\frac{r(t_x) - r_0}{r_0} = -\frac{v_*}{Cr_0}\left[x + \ln(1-x)\right] \ll 1$$

$$\Rightarrow r_0 \gg \sqrt[3]{\frac{(\beta - 1)GM}{C^2}}, \tag{3.20}$$

$$\text{for } \ln(1-x) + x = -1 \iff x = 0.84140566... \approx 84\,\%. \tag{3.21}$$

Given condition 3.20, we thus have an exponential increase in (Eq. 3.18) velocity on the timescale of $t \sim C^{-1}$. For the example of Fe II ions colliding with H I, we have that the critical density where Eq. 3.20 shows equality at 100 AU is $n_{\mathrm{H\,I}}(100\,\mathrm{AU}) \sim 10\,\mathrm{cm}^{-3}$, where we have used that the polarisability of H I is $\alpha_H = 10^{-31}\,\mathrm{m}^3$ (Beust et al. 1989). From Eq. 3.20 we see that this critical density scales as $n(r) \propto r^{-3/2}$. The implications from Eq. 3.18 and Eq. 3.20 is that the velocity of ions diffusing out of the disk probably stays close to v_* of Eq. 3.15.

Following Liseau (2003) and Paper VII, we estimate the required braking gas density to have $v_*(100\,\mathrm{AU}) = 1\,\mathrm{km\,s}^{-1}$ for Na I. Again assuming the braking medium to be H I, this gives $n_{\mathrm{H\,I}}(100\,\mathrm{AU}) = 6 \times 10^5\,\mathrm{cm}^{-3}$, where we have used $\beta = 530$, the Bohr radius $a_0 = 0.529 \times 10^{-10}\,\mathrm{m}$, $T = 36\,\mathrm{K}$ (Paper VII) giving $v_\mathrm{T} = 0.71\,\mathrm{km\,s}^{-1}$, and that $\mathrm{m_{Na}} \approx 23\,\mathrm{m_H}$. If the braking gas consisted mainly of oxygen atoms at the same temperature, then a number density of $n_{\mathrm{O\,I}}(100\,\mathrm{AU}) = 7.4 \times 10^4\,\mathrm{cm}^{-3}$ would be sufficient, due to the more massive atoms ($\mathrm{m_O} \approx 16\,\mathrm{m_H}$) absorbing more inertia.

3.5.4 Derived abundances

So far we have investigated three different scenarios from the radiation pressure point of view: free ascend (i.e. no braking), magnetic braking, and gas drag. These different scenarios affect the particles differently, and have consequences for the over-all abundance of material in the disk. Even though we may assume that the gas content was originally of cosmic abundance, or possibly replenished at cosmic

abundance, the radiation pressure drives preferentially high-β particles away from the system, strongly depleting them in comparison to the low-β particles. Magnetic forces and gas drag restrain this outward flow, but do not completely prevent it. The consequence is that the three different scenarios will deplete elements to a varying degree. By calculating the expected relative depletion for a number of elements, one may differentiate between the three scenarios by comparing the predictions to observations of abundances in the disk. If, e.g., S is predicted to have a high abundance in the gas-drag disk relative to Fe (since the radiation pressure on S I/II is much smaller than on Fe I/II), but at the same time S is predicted to have a very low abundance in the magnetically braking disk relative to Fe (because Fe is more ionised than S and more effectively magnetically braked), then observations of the S/Fe abundance ratio has the potential to discriminate between these scenarios.

A detailed calculation of expected abundance ratios requires numerical studies since the ionisation structure of the disk is an important parameter. Nevertheless, to get qualitative understanding of the processes, we develop some simple analytical models.

In the case of free ascend, the radial distribution is derived in Appendix A (Eq. A.14):

$$n(r) = \dot{\mathcal{N}} \left[2(\beta - 1)GM \left(\frac{r}{r_0} - 1 \right) r^3 \right]^{-1/2}, \text{ with } r \geq r_0, \tag{3.22}$$

where $\dot{\mathcal{N}}$ is the particle production rate per solid angle. Assuming the release point r_0 to be the same for all particles, we see that the relative density of particles of two different species trough the disk is

$$\frac{n_0(r)}{n_1(r)} = \frac{\dot{\mathcal{N}}_0}{\dot{\mathcal{N}}_1} \sqrt{\frac{\beta_1 - 1}{\beta_0 - 1}} \tag{3.23}$$

where 0 and 1 denotes two different species. The relative ratio is thus altered by the square-root factor. Things are more complicated as each species normally are divided among a few ionisation states, each with different β. E.g., Na I has a radiation pressure β of several hundred, while Na II feels no pressure at all. Assuming all species to be either neutral or singly ionised, with the same ionisation ratio ζ = ionised / (ionised + neutral), we define an "effective β",

$$\beta_{\text{eff}} = \beta^{\text{I}}(1 - \zeta) + \beta^{\text{II}}\zeta, \tag{3.24}$$

where the Roman numerals denote the ionisation state. For elements that have an ionised state with $\beta^{\text{I}} < 1$, the effective β becomes $\beta_{\text{eff}} = \beta^{\text{I}}(1 - \zeta) + \zeta$. For $\beta^{\text{II}} < 1$, $\beta_{\text{eff}} = \beta^{\text{II}}\zeta + (1 - \zeta)$.

The usage of $\beta_{\rm eff}$ in Eq. 3.23 assumes that the ionisations states are effectively coupled, or that a single particle switches between the states with a high enough frequency. It also assumes that there are no other forces than gravity and radiation pressure. These assumptions need not always be valid, as we suggested in Paper VI. Long periods in an ionised state for Na (with $\beta^{\rm II} = 0$) could potentially provide time enough to brake any motion caused by the short period in a neutral state (with $\beta^{\rm I} = 530$).

For magnetic braking we have a similar situation, with the distinction that *all* ionised particles are effectively braked (not only those with low β during long periods). A model of this behaviour could be to let a particle travel freely for a while, in accordance with Eq. 3.22, and then reset the release point r_0 periodically as the particle switches to an ionised state and back to neutral. Since the fraction of ionising photons to radiation pressure photons is distance independent, the same velocity is reached on average before a neutral particle becomes ionised, independent of the release radius r_0. Thus the averaged velocity reached for a neutral particle before becoming ionised is $v^{\rm I} \propto \sqrt{\beta-1}(\int F_\lambda(R_*)\lambda a_\lambda \,{\rm d}\lambda)^{-1}$, where $F_\lambda(R_*)$ is the flux at the stellar surface and wavelength λ, and a_λ is the photo-ionisation cross-section. With the velocity $v^{\rm II} \approx 0$ for the ionised elements, the *mean* velocity $v = v^{\rm I}(1-\zeta) + v^{\rm II}\zeta \approx v^{\rm I}(1-\zeta)$. Using the continuity equation A.13, we find that, in the case of magnetic braking,

$$n \propto \frac{1}{v} \propto \frac{\int F_\lambda(R_*)\lambda a_\lambda \,{\rm d}\lambda}{(1-\zeta)\sqrt{\beta-1}} \propto \frac{\alpha\zeta}{(1-\zeta)^2\sqrt{\beta-1}}, \tag{3.25}$$

where α is the recombination coefficient, and we have used

$$n_{\rm I}\int F_\lambda(R_*)\lambda a_\lambda \,{\rm d}\lambda \propto n_{\rm II}\alpha. \tag{3.26}$$

Consequently,

$$\frac{n_0(r)}{n_1(r)} = \frac{\dot{\mathcal{N}}_0}{\dot{\mathcal{N}}_1}\frac{\zeta_0\alpha_0(1-\zeta_1)^2}{\zeta_1\alpha_1(1-\zeta_0)^2}\sqrt{\frac{\beta_1-1}{\beta_0-1}}. \tag{3.27}$$

Particles braked by a gas medium quickly reach the stationary solution v_* of Eq. 3.15, as long as the condition of Eq. 3.20 is honoured (Sect. 3.5.3). From the continuity equation (A.13) we have that

$$n(r) = \frac{\dot{\mathcal{N}}}{v_* r^2} = \frac{\dot{\mathcal{N}}C}{(\beta-1)GM}. \tag{3.28}$$

Since $C \propto n_{\rm BR}(r)$, where $n_{\rm BR}(r)$ is the number density of the braking gas, we have that $n(r) \propto n_{\rm BR}(r)$, so the number densities of gases should approximately follow

Table 3.2: Depletion ratios from radiation pressure

Scenario	d(Na) / d(Fe)[a]	d(S) / d(Fe)[a]
Free ascend	8.1	20
Magnetic brakes	0.7	0.0006
Gas drag	0.65	2.8

[a] These numbers are sensitive to the disk ionisation structure and β values assumed, and should be regarded as order of magnitude estimates only.

each other radially. Eq. 3.28 gives

$$\frac{n_0(r)}{n_1(r)} = \frac{\dot{\mathcal{N}}_0 C_0(\beta_1 - 1)}{\dot{\mathcal{N}}_1 C_1(\beta_0 - 1)}. \tag{3.29}$$

Allowing for two ionisation states gives

$$\frac{n_0(r)}{n_1(r)} = \frac{\dot{\mathcal{N}}_0}{\dot{\mathcal{N}}_1}\left(\frac{C_1^{\mathrm{I},-1}(\beta_1^{\mathrm{I}} - 1)(1 - \zeta_1) + C_1^{\mathrm{II},-1}(\beta_1^{\mathrm{II}} - 1)\zeta_1}{C_0^{\mathrm{I},-1}(\beta_0^{\mathrm{I}} - 1)(1 - \zeta_0) + C_0^{\mathrm{II},-1}(\beta_0^{\mathrm{II}} - 1)\zeta_0}\right), \tag{3.30}$$

where the "-1" index indicates the inverse, i.e. $C^{-1} = 1/C$.

In Table 3.2 expected depletion ratios of Fe, Na and S in the β Pic disk are calculated for Eqs. 3.23, 3.27 & 3.30, assuming an ionisation structure produced by the model of Paper VII. Depletion is defined as the ratio between the abundance of an element and the abundance of the element when originally released. Table 3.2 shows that the d(S)/d(Fe) ratio is strongly dependent on the braking scenario. A preliminary result is therefore that magnetic braking probably is not important in the β Pic disk, since the *observed* d(S)/d(Fe) ratio is $\sim$0.4 (assuming original solar abundance composition, and that 80 % of the S is ionised). However, more detailed analysis is needed for firmer conclusions.

Chapter 4

Future work

Here I detail my expectations on the future progress of the field, and a few projects I intend to participate in.

4.1 High-resolution imaging of young stars

This is the first time in history we have a chance to routinely follow young stars orbit each other, yielding dynamical mass estimates and calibrating star formation theory. By its very nature, following orbital evolution takes time. Currently, the early phases of stellar evolution are ill-constrained, due to the lack of data. In the coming years, we will start to see results from long-term monitoring programmes that will revolutionise our understanding of the important, early phases.

The modern adaptive optics systems at $8-10$ m class telescopes are sensitive enough to detect young brown dwarfs in close orbits (a few AU) around nearby stars. Even young planetary-mass objects may be found – constraining planet formation theories and addressing the "brown dwarf desert" issue.

Interferometry at infrared wavelengths will allow even higher resolutions to be probed. In a "nulling" mode, high-contrast observations of the nearest stellar environments can be searched for older yet massive planets.

4.2 The evolution of circumstellar gas disks

Due to their infrared emission, the lifetimes of dust disks have been observationally estimated (Habing et al. 1999; Haisch et al. 2001, Sect. 1.2). The lifetimes of circumstellar *gas disks* are less well understood, however. The reason is the difficulty in observing the gas of later stages. As long as the disk is accreting onto the star, its signature is clearly visible. Not all disks are active, however, and it is

expected that active disks at some point become passive. This does not necessarily mean that the gas disks disappear; they just become less visible.

By using the method we successfully applied on the β Pic gas disk to other passive (i.e. non-accreting) disks, we will be able to study how the gas in disks evolves in comparison to the dust. The advantage of this method, using a long-slit high-resolution spectrograph, is the great sensitivity; at β Pic we estimate our sensitivity to Na I to be better than 5×10^{-7} cm^{-3}, an amazingly small density.

4.3 The β Pictoris disk

The disk of β Pic still has many mysteries to unravel. The gas disk shows structure yet unexplained. We still do not know with confidence where the gas – or the dust – comes from, nor do we have any reliable estimates of the gas and dust disk masses. Our strategy to address these questions will be to model our current data better, in the hope to gain some new insights. More specifically, we will compare disk models of the ionisation structure with the observations, and obtain abundances of the more complicated elements as well (for the moment we have only studied abundance of the simple case of Na I). Abundance ratios and detailed ionisation structure models will allow us to discriminate between the radiation pressure scenarios of Sect. 3.5, inferring important properties of the disk.

In December this year (2003), we have scheduled observations to study the gas disk morphology. The disadvantage of using high-resolution spectrographs is that the field of view gets limited to a narrow slit. In the coming observations, we have therefore obtained ultra-narrow interference filters (of FWHM~5 Å) to *image* the disk in gas emission, using a coronograph in addition to the filters. Ideally we will get something like Fig. 4.1, but with much more structure.

The new sub-mm telescope APEX in the southern hemisphere will help revealing the true natures of the dust "blobs" seen by JCMT and SEST. Other scheduled observations this winter (2003–4) are ultra-deep V-band images of the outer disk of β Pic, using the FORS instrument at the VLT. If the blobs are real, we estimate that we should be able to see them in scattered light, at low surface intensity, but at much higher resolution than currently obtainable in the sub-mm (Paper V).

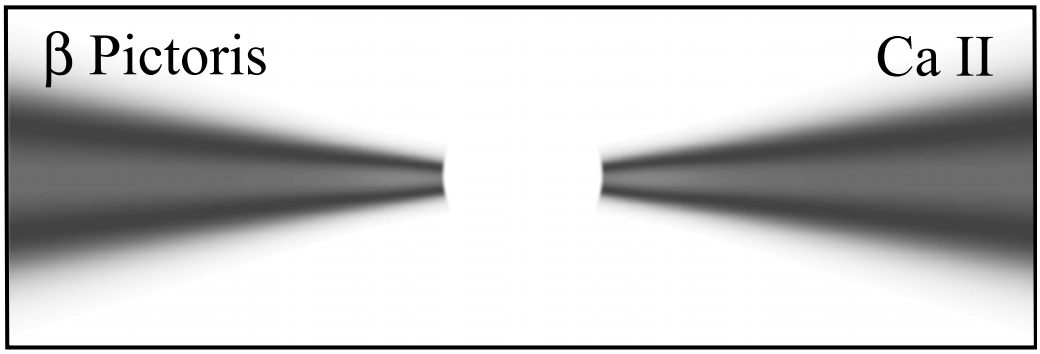

Figure 4.1: A simulated image of the Ca II H or K emission from the β Pic disk. The frame is $600\,\mathrm{AU} \times 300\,\mathrm{AU}$ in size. The flux has been normalised along the height. This is what we hope to observe in December this year (2003), but with more structure (and noise, artefacts...). Compare also to Fig. 3.1.

Appendix A

Radiation pressure theory

In this appendix I derive a few relations that relate how particles are influenced under radiation pressure.

A.1 Radiation pressure basics

The radiation pressure from the star, like gravity, is a central force $\propto r^{-2}$, where r is the distance to the star. One may therefore introduce a convenient distance independent parameter

$$\beta \equiv \frac{F_{\rm rad}}{|F_{\rm grav}|} \tag{A.1}$$

to quantify the relative strength of the force exerted by the radiation pressure, $F_{\rm rad}$, to the force of gravity, $F_{\rm grav}$. The force of gravity from a star of mass $M_\star$ on an ion of mass m is

$$F_{\rm grav} = -\frac{GM_\star m}{r^2}, \tag{A.2}$$

where G is the gravitation constant. The energy $\mathrm{d}E_i$ exciting an ion in a given transition i per time interval $\mathrm{d}t$ is

$$\frac{\mathrm{d}E_i}{\mathrm{d}t} = F_\lambda(r)\sigma_0, \tag{A.3}$$

where $F_\lambda(r)$ is the energy flux density from the star at the wavelength λ of the transition, and σ_0 is the integrated line cross section,

$$\sigma_0 = \frac{A_{jk}\lambda^4}{8\pi c}\frac{g_j}{g_k}, \tag{A.4}$$

where A_{jk} is the spontaneous emission probability (Einstein A coefficient) for the transition from level j to k, c is the velocity of light, and g_j, g_k are the statistical

weights of the levels. For the expression of σ_0, detailed balance has been assumed, i.e. that photoabsorption probability statistically equals the sum of spontaneous and stimulated emission. $F_\lambda(r)$ can be expressed as

$$F_\lambda(r) = F_\lambda(d)\left(\frac{d}{r}\right)^2, \tag{A.5}$$

where d is the distance to the Earth, and $F_\lambda(d)$ the observed energy flux density at the Earth, or

$$F_\lambda(r) = F_\lambda(R_\star)\left(\frac{R_\star}{r}\right)^2, \tag{A.6}$$

where $R_\star$ is the radius of the star and $F_\lambda(R_\star)$ the flux density at its surface. Eq. A.5 is useful when using observed fluxes to compute the radiation field, while Eq. A.6 is more useful for model atmosphere emission. Since

$$F_{\mathrm{rad},i} = \frac{1}{c}\frac{\mathrm{d}E_i}{\mathrm{d}t}, \tag{A.7}$$

we can use Eq. A.1 – A.7 to derive the expression

$$\beta_i = \frac{A_{jk}\lambda^4 R_\star^2 F_\lambda(R_\star)}{8\pi c^2 G M_\star m}\frac{g_j}{g_k}. \tag{A.8}$$

As an illustrative example, let us estimate β of the Na I, dominated by the D_2 and D_1 transitions. For Na I (D_2) we have $A_{jk} = 6.22 \times 10^7\,\mathrm{s}^{-1}$, $\lambda_{vac} = 5891.5\,\text{Å}$, $g_j = 4$, $g_i = 2$, and $m = 3.82 \times 10^{-26}\,\mathrm{kg}$. For β Pic we have $R_\star = 1.73\,R_\odot$, $M_\star = 1.75\,M_\odot$ (Kervella et al. 2003), and $F_\lambda(R_\star) = 3.27 \times 10^7\,\mathrm{erg\,s^{-1}\,cm^{-2}\,Å^{-1}}$ for $T_{\mathrm{eff}} = 8200\,\mathrm{K}$, $\log g = 4.20$ and $Z/Z_\odot = 0.0$ in the model atmosphere of Hauschildt et al. (1999). This gives $\beta_2 = 354$. For the D_1 transition, we have $\beta_1 = 176$, summing up to $\beta_{\mathrm{Na\,I}} \approx \beta_2 + \beta_1 = 530$.

Table 3.1 in Sect. 3.5 shows the radiation pressure for a number of elements.

A.2 The free-ascend solution

If left alone, a particle with high β would rapidly accelerate radially away from the star. How rapidly? Assuming the particle is released at rest with respect to the star, we have the radial equation of motion

$$\ddot{r} \equiv \frac{\mathrm{d}^2 r}{\mathrm{d}t^2} = (\beta - 1)\frac{GM}{r^2}, \tag{A.9}$$

a differential equation very similar to the equation of free fall, Eq. 1.2, except that the sign of the right-hand side differs for $\beta > 1$. This makes all the difference to

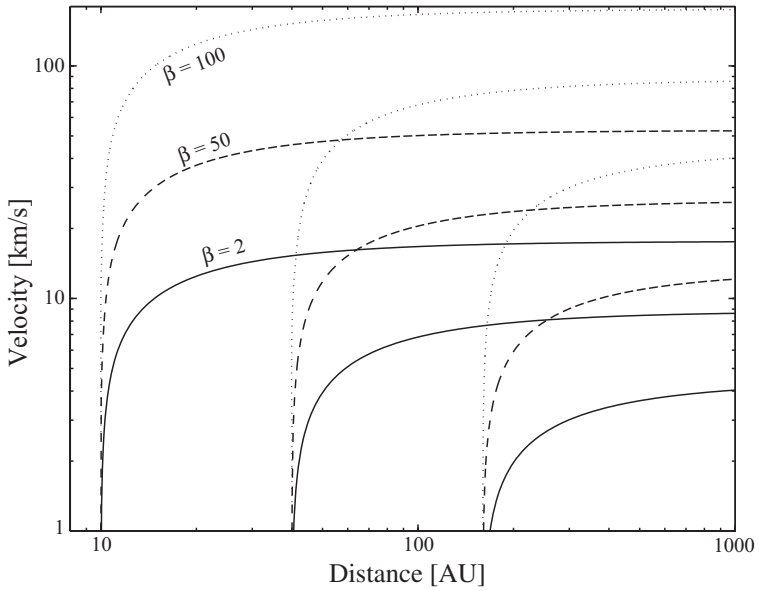

Figure A.1: Free-ascend velocity distribution for particles released at different points and with different β, in the disk of β Pic. The solid, dashed, and dotted lines correspond to $\beta = 2$, $\beta = 10$ and $\beta = 100$, respectively. The release points in the figure are at 10 AU, 40 AU, and 160 AU. See also Fig. A.3.

the solution, as it implies the reverse of free fall, "free ascend". As in the case of Eq. 1.2, the solution to this differential equation can only be obtained in implicit form.

To solve Eq. A.9, we start by multiplying the equation with $\dot{r} \equiv \mathrm{d}r/\mathrm{d}t$ and integrate it to obtain

$$\frac{1}{2}\dot{r}^2 = (1-\beta)\frac{GM}{r} + C, \tag{A.10}$$

where C is the integration constant. With the boundary conditions that $r(t=0) = r_0$ and $v(t=0) \equiv \dot{r}(t=0) = 0$, and solving for $\dot{r}/r_0$, we get

$$\frac{\dot{r}}{r_0} = \pm\sqrt{2(\beta-1)\frac{GM}{r_0^3}\left(1-\frac{r_0}{r}\right)}. \tag{A.11}$$

In order to obtain real values in Eq. A.11 for $\beta < 1$, we must have $r \leq r_0$, yielding the free-fall solution. Conversely, $\beta > 1 \Rightarrow r \geq r_0$, giving the free-ascend solution. Radial velocities for particles of different β and initial release points are shown in Fig. A.1. The particle evidently accelerates very rapidly to high velocities. From Eq. A.11 we see that the asymptotic velocity, v_∞, as $r \to \infty$, is

$$v_\infty \equiv \lim_{t\to\infty} v(t) = \sqrt{2(\beta-1)\frac{GM}{r_0}}, \tag{A.12}$$

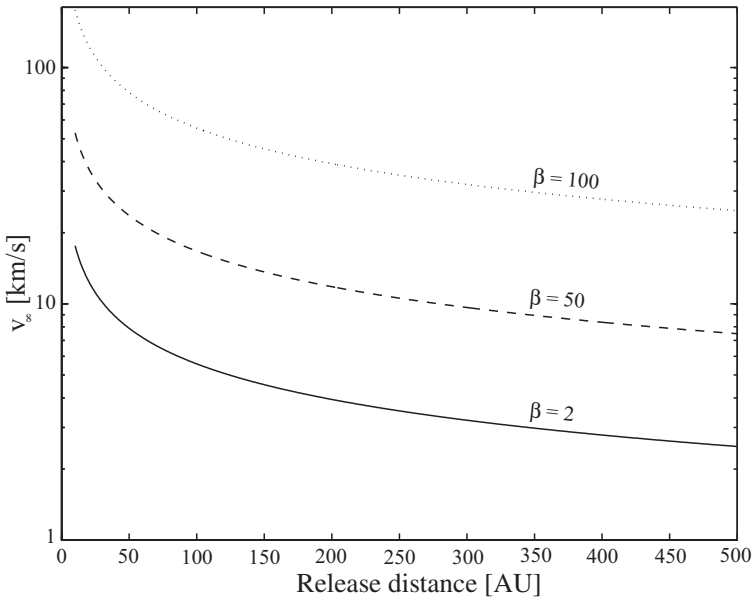

Figure A.2: Free-ascend asymptotic velocity as a funtion of release radius for particles with different β, in the disk of β Pic. The solid, dashed, and dotted lines correspond to $\beta = 2$, $\beta = 10$ and $\beta = 100$, respectively.

Fig. A.2 shows the asymptotic v_∞ as a function of release point radius for different β, in the β Pic environment.

It is also interesting to derive what kind of radial density distribution one would get from a continuous replenishing source. In steady state, the number of particles entering a particular shell around the star should equal the number of particles leaving the shell, i.e. they should fulfil the continuity equation:

$$n(r)\dot{r}(r)r^2 = \dot{\mathcal{N}}, \tag{A.13}$$

where $n(r)$ denotes the number density and $\dot{\mathcal{N}}$ is the production rate of particles per solid angle (released at r_0). Solving Eq. A.13 for $n(r)$, and using $\dot{r}$ from Eq. A.11, we have

$$n(r) = \dot{\mathcal{N}}\left[2(\beta-1)GM\left(\frac{r}{r_0}-1\right)r^3\right]^{-1/2}, \text{ with } r \geq r_0. \tag{A.14}$$

For $r \gg r_0$, $n(r) \propto r^{-2}$.

Let us derive the total column density $N_{\rm tot}$ towards the star,

$$N_{\rm tot} = \int_{r=r_0}^{\infty} n(r)\,\mathrm{d}r = \int_{r=r_0}^{\infty} \frac{\mathcal{K}\,\mathrm{d}r}{r\sqrt{(r^2 - r_0 r)}}, \text{ where } \mathcal{K} = \dot{\mathcal{N}}\sqrt{\frac{r_0}{2(\beta-1)GM}}. \tag{A.15}$$

The integral of Eq. A.15 has the solution

$$N_{\rm tot} = 2\mathcal{K} \lim_{r_1 \to \infty} \left[\frac{\sqrt{r^2 - r_0 r}}{r_0 r} \right]_{r_0}^{r_1} = \frac{2\mathcal{K}}{r_0} = \frac{2\dot{\mathcal{N}}}{\sqrt{2(\beta-1)GMr_0}}, \tag{A.16}$$

which can be checked by taking the derivative of the primitive function.

Assuming that particles are released at a constant rate, what would an observed absorption profile towards the star look like? This is equivalent to ask how many particles there are along the line of sight as a function of radial velocity. Since the velocity is increasing monotonously in time, the density of particles at a particular velocity is inversely proportional to the acceleration. Including geometrical dilution, we have that the column density as a function of radial velocity is

$$N(v) \propto \frac{1}{\ddot{r}(v) r(v)^2} \propto \{\text{Eq. A.9}\} \propto \frac{1}{\beta - 1}, \text{ for } v \in [0, v_\infty]. \tag{A.17}$$

The absorption profile would thus be rectangular of width v_∞. Using the expression for $N_{\rm tot}$ of Eq. A.16 and v_∞ of Eq. A.12,

$$N(v) = \frac{N_{\rm tot}}{v_\infty} = \frac{\dot{\mathcal{N}}}{(\beta-1)GM}, \text{ for } v \in [0, v_\infty]. \tag{A.18}$$

Let us now turn to the time evolution of the solution to Eq. A.11. For $\beta = 0$ we have the familiar homologous solution for a free fall collapse (Sect. 1.2.2) given in, e.g., Kippenhahn & Weigert (1994). To solve for $\beta > 1$, we introduce a new variable ξ, defined by

$$\cosh^2(\xi) = \frac{r}{r_0}, \tag{A.19}$$

where $\cosh(\xi)$ is the hyperbolic cosine function of ξ. Taking the time derivative of Eq. A.19 gives the relation

$$\frac{\dot{r}}{r_0} = 2\dot{\xi} \cosh(\xi) \sinh(\xi). \tag{A.20}$$

Using $\cosh^2(\xi) - \sinh^2(\xi) = 1$ and Eq. A.19 gives

$$1 - \frac{r_0}{r} = \frac{\sinh^2(\xi)}{\cosh^2(\xi)}, \tag{A.21}$$

which inserted to Eq. A.11 with Eq. A.20 implies

$$2\dot{\xi} \cosh^2(\xi) = \sqrt{2(\beta-1)\frac{GM}{r_0^3}}, \tag{A.22}$$

where we have picked the positive right-hand side of Eq. A.11, since $r \geq r_0, \forall t$. Using the identity

$$2\dot{\xi}\cosh^2(\xi) = \frac{\mathrm{d}}{\mathrm{d}t}\left(\xi + \frac{1}{2}\sinh(2\xi)\right), \tag{A.23}$$

we get the implicit solution

$$\xi + \frac{1}{2}\sinh(2\xi) = t\sqrt{2(\beta-1)\frac{GM}{r_0^3}}. \tag{A.24}$$

The timescale for a particle to leave the system can now be evaluated. Assuming, for example, that a $\beta = 10$ particle is released at $r_0 = 10$ AU and leaves the system at $r = 1000$ AU, $\xi = 3.0$ and $t = 92$ years. Released at $r_0 = 1$ AU it would leave the system in only $t = 28$ years.

A.3 Particles released from orbit

Eq. A.9 assumes that the particles start out at relative rest to the star. This is a good assumption as long as $\beta \gg 1$, and other forces are irrelevant. If we instead assume that the particles are released from a body orbiting the star at Keplerian speed, then we need to add an inertial term to the radial differential equation (see, e.g., Binney & Tremaine 1987):

$$\ddot{r} \equiv \frac{\mathrm{d}^2 r}{\mathrm{d}t^2} = (\beta-1)\frac{GM}{r^2} + \frac{L^2}{r^3}, \tag{A.25}$$

where L is the angular momentum, which is a conserved quantity in central force fields. Assuming the mother body orbits the star in a circular orbit of radius r_0, the angular momentum may be written

$$L = \sqrt{GMr_0}, \tag{A.26}$$

Eq. A.25 can be integrated the same way as Eq. A.9, resulting in

$$\frac{1}{2}\dot{r}^2 = (1-\beta)\frac{GM}{r} + \frac{GMr_0}{2r^2} + C, \tag{A.27}$$

where C again is an integration constant. Assuming that the particle is released with no initial radial velocity at r_0, we solve for $v \equiv \dot{r}$:

$$v = \pm\sqrt{2(\beta-1)GM\left(\frac{1}{r_0} - \frac{1}{r}\right) + GMr_0\left(\frac{1}{r_0^2} - \frac{1}{r^2}\right)}. \tag{A.28}$$

The asymptotic velocity at infinity is

$$v_\infty \equiv \lim_{t\to\infty} v(t) = \sqrt{(2\beta-1)\frac{GM}{r_0}}, \tag{A.29}$$

which is very similar to Eq. A.12. The only difference is that the initial Keplerian speed $\sqrt{GM/r_0}$ has been added to Eq. A.12.

Assuming that the particles are continuously replenished, we derive the expected density distribution from Eq. A.28 and the continuity equation A.13:

$$n(r) = \dot{\mathcal{N}}\left[2(\beta-1)GM\left(\frac{r}{r_0}-1\right)r^3 + GM\left(\frac{r^2}{r_0^2}-1\right)r_0 r^2\right]^{-1/2}, \text{ with } r \geq r_0. \tag{A.30}$$

For $r \gg r_0$,

$$n(r) = \dot{\mathcal{N}}\sqrt{\frac{r_0}{(2\beta-1)GMr^4}}, \tag{A.31}$$

i.e. $n(r) \propto r^{-2}$.

The absorption profile can be determined as in Eq. A.17, by evaluating the column density as a function of velocity:

$$N(v) \propto \frac{1}{\ddot{r}(v)r(v)^2} \propto \{\text{Eq. A.9}\} \propto \frac{1}{\beta - 1 + r_0/r}, \text{ for } v \in [0, v_\infty]. \tag{A.32}$$

In contrast to Eq. A.17, the column density is not constant in v. However, since $r > r_0$, the term r_0/r is always smaller than 1, and Eq. A.32 should be well approximated by Eq. A.18 for $\beta >> 1$. To evaluate Eq. A.32 exactly, one needs to express the radius r as a function of velocity v, by solving Eq. A.28 for r, which gives the slightly involved expression

$$r(v) = \frac{(\beta-1)GMr_0}{(2\beta-1)GM - v^2 r_0}\left(\sqrt{1 + \frac{(2\beta-1)GM - v^2 r_0}{GM(\beta-1)^2}} + 1\right). \tag{A.33}$$

One may verify that $r(v = 0) = 0$, and that $\lim_{v\to v_\infty} r(v) = \infty$. In Fig. A.4, normalised profiles (in both width and strength) for a number of different β are plotted. It is possible to integrate the radial density distribution A.30 analytically to get the total number density, but the resulting expression is too involved to write up. Unfortunately, it seems very difficult to solve Eq. A.28 for the radial time dependence the way we did implicitly in Eq. A.24 for Eq. A.11.

A.4 Magnetic braking

Let us investigate in some more detail what will happen to an ion of mass m, charge q and radiation pressure β released at radius r_0 in a disk with a toroidal

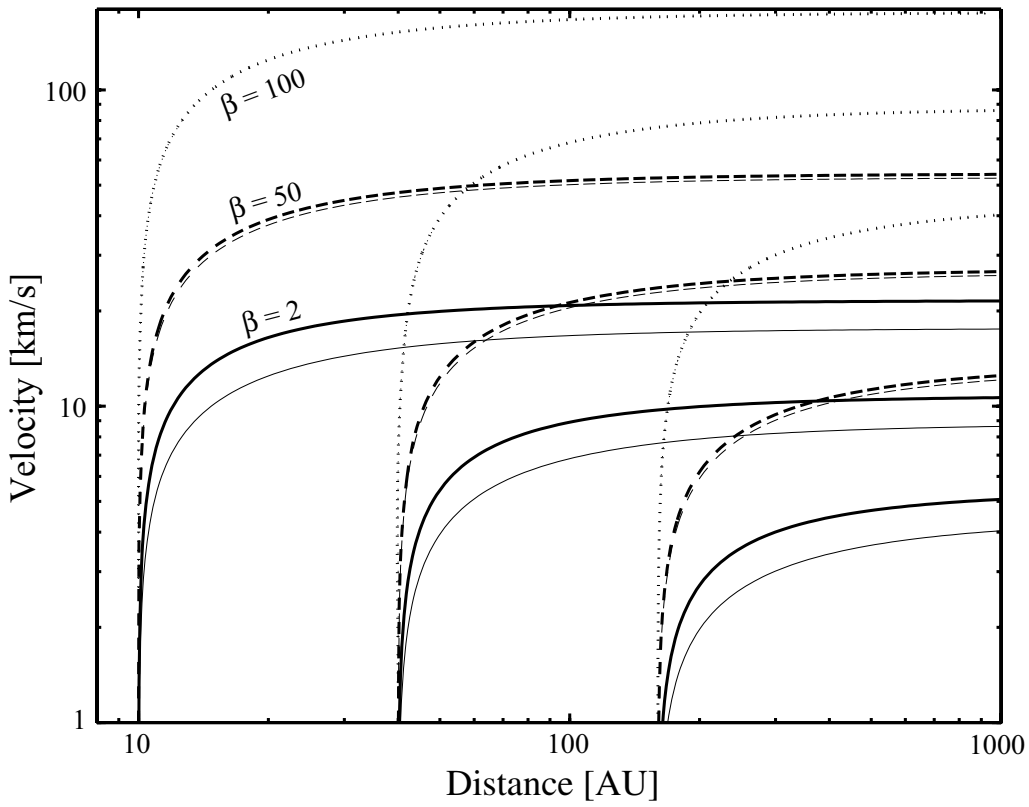

Figure A.3: Velocity distribution for particles released from mother bodies in Keplerian orbits at different radii in the disk of β Pic. The solid, dashed, and dotted lines correspond to $\beta = 2$, $\beta = 10$ and $\beta = 100$, respectively. The release points in the figure are at 10 AU, 40 AU, and 160 AU. The thin lines are the free-ascend solutions from Fig. A.1. We see that the initial Keplerian speed becomes negligible for higher β.

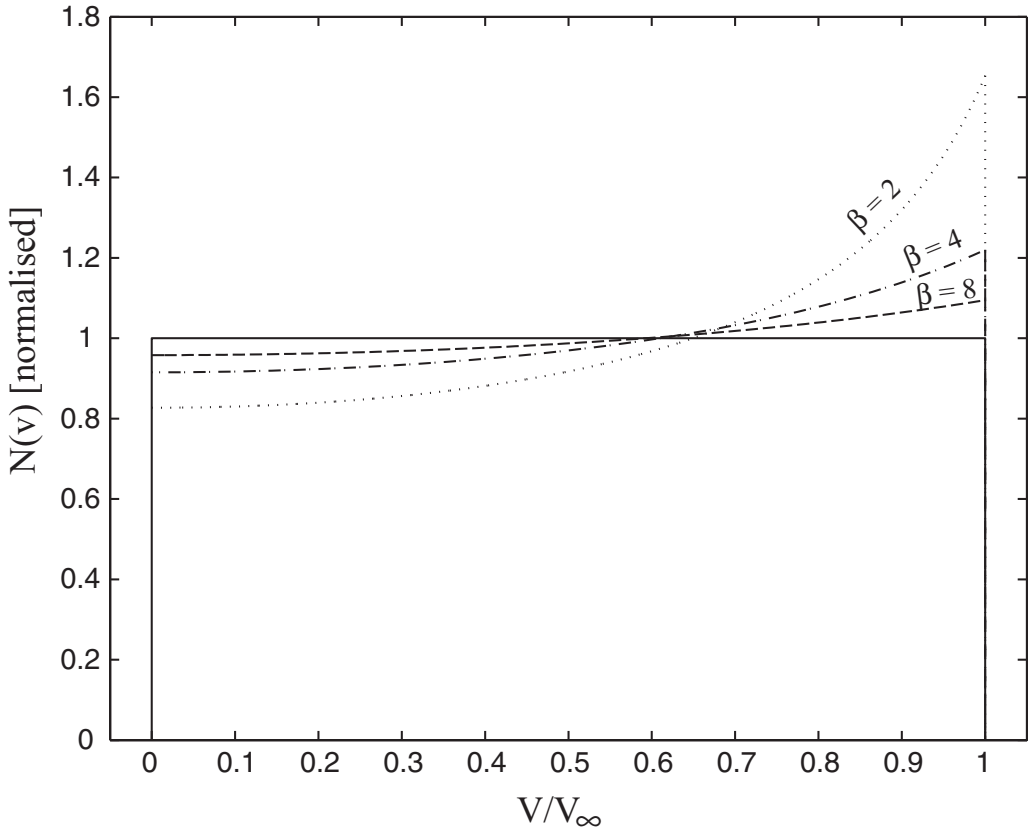

Figure A.4: Column density profile as a function of velocity, for particles of different β. This corresponds to the expected absorption profile, for particles released from mother bodies in Keplerian orbit and subject only to the radiation pressure and gravity. The solid, dashed, and dotted lines correspond to $\beta = 2$, $\beta = 4$ and $\beta = 8$, respectively. The profile quickly converges to the rectangular profile derived for the free-ascend mode (Eq. A.18 of Sect. A.2).

magnetic field of strength B. The equations of motion for a particle without azimuthal motion are

$$\ddot{\mathbf{r}} = (\beta - 1)\frac{GM}{r^2}\frac{\mathbf{r}}{r} + \frac{q}{m}\dot{\mathbf{r}} \times \mathbf{B}, \tag{A.34}$$

where $\mathbf{r} = \rho\mathbf{e}_\rho + z\mathbf{e}_z + \phi\mathbf{e}_\phi$ is the position vector, $\mathbf{B} = B\mathbf{e}_\phi$, and $\mathbf{e}_\rho$, $\mathbf{e}_\phi$, and $\mathbf{e}_z$ are unit vectors of a cylindrical coordinate system. Since we restrict ourselves to motion in a fixed plane perpendicular to the magnetic field, we have

$$\ddot{\rho} = -\frac{\dot{z}qB}{m} + (\beta - 1)\frac{GM}{r^2}\frac{\rho}{r} \tag{A.35}$$

$$\ddot{z} = \frac{\dot{\rho}qB}{m} + (\beta - 1)\frac{GM}{r^2}\frac{z}{r}. \tag{A.36}$$

If we assume that neither r nor B change much, let $z \ll r$ and therefore $\rho \approx r$, we can write the approximate equations

$$\ddot{r} = -\frac{\dot{z}qB_0}{m} + (\beta - 1)\frac{GM}{r_0^2} \tag{A.37}$$

$$\ddot{z} = \frac{\dot{r}qB_0}{m}, \tag{A.38}$$

where $B_0 = B(r = r_0, z = 0)$, and r now denotes ρ. This is a system of inhomogeneously coupled ordinary differential equations that can be solved using standard methods (e.g., Boyce & DiPrima 1986). With the initial conditions that the particle is at rest at the position $r = r_0$ and $z = 0$, we have the solution

$$r(t) = r_0 + \Delta[1 - \cos(\omega t)] \tag{A.39}$$

$$z(t) = \Delta \sin(\omega t) - \Delta\omega t, \tag{A.40}$$

where $\Delta = (\beta - 1)GM[m/(r_0 B_0 q)]^2$, and $\omega = B_0 q/m$. The velocities are

$$\dot{r}(t) = \Delta\omega \sin(\omega t) \tag{A.41}$$

$$\dot{z}(t) = \Delta\omega \cos(\omega t) - \Delta\omega, \tag{A.42}$$

meaning that the velocity amplitude observed in the radial direction is

$$v_{\max} = \Delta\omega = \frac{(\beta - 1)GMm}{r_0^2 B_0 q}. \tag{A.43}$$

It is interesting to note that while the mean radial velocity of Eq. A.41 is zero, and the particle therefore is effectively trapped in the radial direction, there is infact a net velocity in the z-direction (Fig. A.5). The result is that the ion moves out of the disk plane at the mean velocity $v_{\max}$. Moving charges in this way may significantly

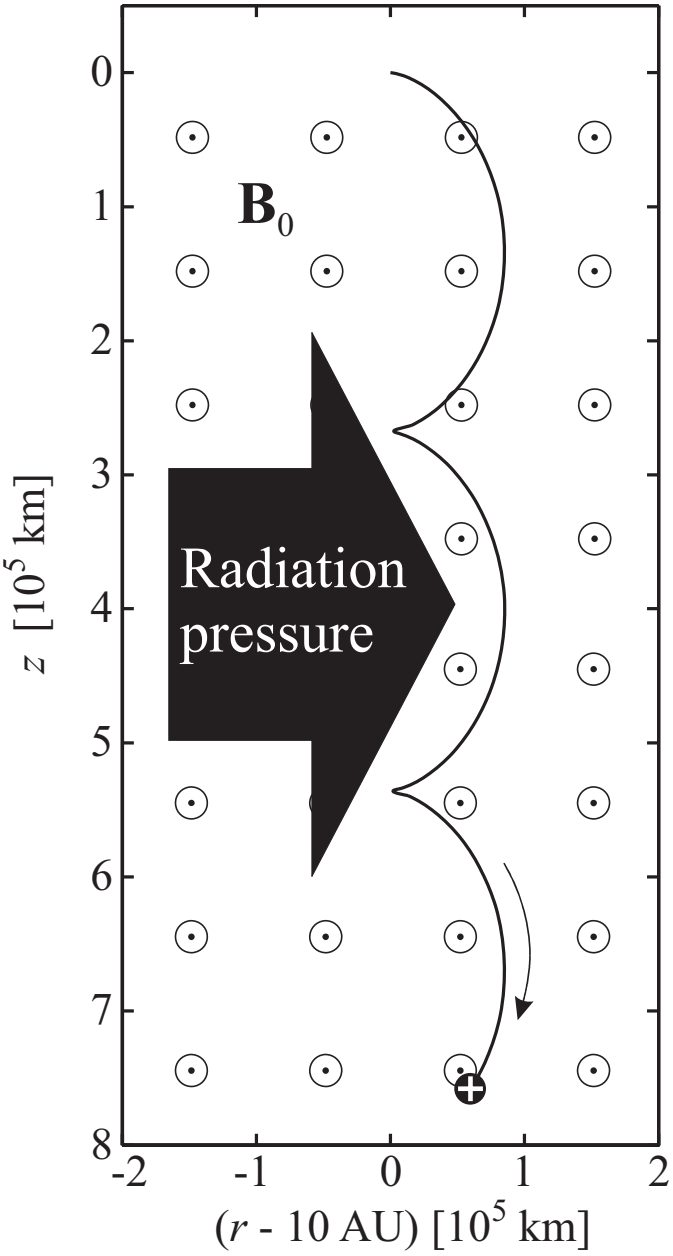

Figure A.5: The path of an Ca II ion released in the β Pic disk, pushed by the radiation pressure but withheld by a magnetic field of strength $\mathbf{B}_0 = 1\,\mu$G, resulting in a maximum radial velocity of 1 km s^{-1}. The averaged radial velocity is zero, while there is a net velocity in the height direction, resulting in a current disturbing the original field $\mathbf{B}_0$. The axes show the displacement of the ion relative to its original position, in the disk plane at radius 10 AU.

disturb the original (very weak) toroidal magnetic field, possibly completely cancelling it. Let us estimate by how much. If the number density of ions is $n\zeta$, with n the number density of particles and ζ the ionisation fraction, then the total current from the disk can be estimated as

$$I = Aqn\zeta v_{\max} \tag{A.44}$$

where $A \sim L^2$ is the area of the disk and L is the disk scale. Using Ampère's law (Eq. 3.9), we estimate that the disturbance of the magnetic field will be on the order of

$$\delta B \sim \mu_0 \frac{I}{L} = \mu_0 qn\zeta L v_{\max}. \tag{A.45}$$

With $v_{\max}$ as in Eq. A.43, the criterion $B_0 \gg \delta B$ becomes

$$B_0 \gg \sqrt{\frac{(\beta - 1)GMm\mu_0 n\zeta}{L}}. \tag{A.46}$$

Inserting typical values for β Pic ($n\zeta \sim 10\,\mathrm{cm}^{-3}$, $m \sim 30\,m_{\mathrm{H}}$, $L \sim 100\,\mathrm{AU}$, $\beta \sim 10$), we find that the disk magnetic field should be $B_0 \gg 3 \times 10^{-8}\,\mathrm{T} = 0.3\,\mathrm{mG}$ to be stable against the ions accelerated by the radiation pressure.

Let me emphasize that this imposed magnetic field is purely hypothetical, and no physical mechanism has been suggested to support it. But *if* there is such a toroidal magnetic field, *then* it will effectively brake ions. In Sect. 3.5.4, I discuss possible observable effects of a disk magnetic fields under radiation pressure on the abundances of elements.

Appendix B

Short summary of papers

Here I provide a short summary of each of the papers I include in this thesis, along with some personal notes, and detail my own contributions to them. Even though not explicitly written, it is to be understood that all co-authors (to a variable extent) contributed to the papers through mutual discussions etc. In the last section I list publications *not* included in the thesis.

B.1 Paper I: *T Tauri Multiple Systems*

Author: Alexis Brandeker

This is the written contribution from an invited short review at the IAU symposium *Star Formation at High Angular Resolutions*. I summarise the importance of studying T Tauri multiple systems, mainly focusing on the possibility to calibrate early stellar evolution theory. I review recent interesting and relevant results.

B.2 Paper II: *Discovery of a new companion and evidence of a circumprimary disk: adaptive optics imaging of the young multiple system VW Chamaeleontis*

Authors: Alexis Brandeker, René Liseau, Pawel Artymowicz, and Ray Jayawardhana

We report our finding of a $0\farcs1$ companion in the VW Cha system, and K-excess of the primary, indicating a circumprimary disk. VW Cha was part of a large target list to search for circumbinary disks with adaptive optics, but the task proved too difficult in the $\sim 1''$ seeing. Instead, we concentrated our efforts on finding tight companions (suitable for future dynamical mass estimates) and came up with the triple star VW Cha. Meeus et al. (2003) recently observed silicate features in an N-band spectrum of the star, indicating highly processed dust.

My contributions were that I was the observer, together with René Liseau, and that I reduced the data. I wrote the abstract and Sect. 1 together with Ray Jayawardhana, Sects. 2, 3, 4.1, and 4.2 myself, 4.3 with René Liseau and Sect. 5 with all co-authors. Sect. 4.4 was entirely written by Pawel Artymowicz. All sections were edited by all co-authors.

B.3 Paper III: *Discovery of close companions to the nearby young stars HD 199143 and HD 358623*

Authors: Alexis Brandeker and Ray Jayawardhana

The second time we tried to observe circumbinary disks with adaptive optics we were again unlucky with the weather. As a back-up programme we searched nearby young stars for companions, and found these two. We reduced the data and wrote the paper quickly, which apparently was very timely since there were at least three other groups that had observed these stars and found out about their binarity approximately simultaneously. Due to the unfavourable seeing conditions during our observations, we underestimated the photometry of the secondary to HD 199143 with 0.5 mag in J, as found out by subsequent reports (Chauvin et al. 2002; Neuhäuser et al. 2002; Kaisler et al. 2003).

I observed and reduced the data, wrote Sects. 2 & 3, calculated the stellar parameters of Sect. 4 and partly wrote Sects. 4 & 5. Ray Jayawardhana wrote the abstract, Sect. 1 and part of Sects. 4 & 5. Both co-authors edited the paper.

B.4 Paper IV: *Keck adaptive optics imaging of nearby young stars: detection of close multiple systems*

Authors: Alexis Brandeker, Ray Jayawardhana and Joan Najita

Ray Jayawardhana and Joan Najita were among the first to observe with the Keck adaptive optics system, and the data reported in this paper comes from their early observations. We report the finding of a *very* tight young binary, TWA 5 A, with a projected separation of 3 AU (54 mas at 55 pc). A third brown dwarf companion 2″ away, TWA 5 B, was shown to be bound to TWA 5 A with 9σ confidence. We discovered a new triple star, S 18, similar to T Tau and VW Cha in appearance and found that the once (in 1945) optical companion to UY Aur, that later turned into an IR companion (1990), again had become an optical companion, probably due to variable extinction.

I reduced the data and wrote most of the paper, except for the abstract, which was written by Ray Jayawardhana.

B.5 Paper V: *The 1.2 mm image of the β Pictoris disk*

Authors: René Liseau, Alexis Brandeker, Malcolm Fridlund, Göran Olofsson, Taku Takeuchi, and Pawel Artymowicz

We were among the first users of the SIMBA bolometric array at the Swedish-ESO Sub-millimeter Telescope (SEST), La Silla, which we used to take a deep image (21 h integration) of the β Pic dust disk at the wavelength 1.2 mm. We found that the dust disk is elongated, and a 3σ "blob" at some distance from the star, not co-incident with a previously detected "blob" by JCMT/SCUBA.

My contributions were that I reduced the data from SIMBA (using a package called MOPSI), which was quite tricky. I also produced Figs. 1 & 2, and performed calculations to show that the SCUBA "blob" is consistent with our data, and estimated the surface flux density expected in scattered light from our "blob".

B.6 Paper VI: *Widespread atomic gas emission reveals the rotation of the β Pictoris disk*

Authors: Göran Olofsson, René Liseau and Alexis Brandeker

Using an idea of Göran Olofsson, we detected gas emission from the disk of β Pictoris for the first time. We found the gas to be located in the extended disk contrary to previous expectations, and could also study the kinematics of the disk in some detail. This work is considered a break-through in the field. We were proud to submit an early version of this paper to the journal *Nature*, but were not treated well by the referees and the editor, so we re-wrote the paper for the *Astrophysical Journal Letters* instead.

I observed and reduced the data. The paper was first written by René Liseau and then completely re-written by Göran Olofsson. I wrote Sect. 2, and produced the Figs. 1 & 5 and the model of Sect. 3.1.

B.7 Paper VII: *The spatial structure of the β Pictoris gas disk*

Authors: Alexis Brandeker, René Liseau, Göran Olofsson, and Malcolm Fridlund

Using the echelle spectrograph UVES at the VLT, we greatly improved upon our previous observations of the β Pictoris gas disk. With larger spectral coverage, better spectral and spatial resolution as well as sensitivity, we found a rich source of data that will keep us busy for some time to come. In this paper we concentrate on some remarkable properties of the spatial structure of the β Pic disk. We expect

to write follow-up papers on the ionisation structure, using detailed modeling, and on the disk dynamics, taking a closer look at the gas production and evolution by numerical models.

I prepared these service observations with René Liseau, spent almost a year reducing the data (not full time, but the sheer load of data, 50 GB and 600 spectra, complicated the process), and wrote most of the article, except Sects. 5.2 & 5.3 which were mostly due to René Liseau, and Table 3, which was due to Malcolm Fridlund.

B.8 Publications not included in this thesis

- Brandeker, A., Liseau, R., Olofsson, G., Fridlund, M., 2002, "*The gas disk of β Pictoris*", in proceedings from Debris disks and the formation of planets, Eds. L. Caroff & D. Backman

- Liseau, R., Larsson, B., Brandeker, A., et al., 2003, "*First detection of NH_3 ($1_0 \rightarrow 0_0$) from a low mass cloud core. On the low ammonia abundance of the ρ Oph A core*", Astronomy & Astrophysics, 402, L73

- Haisch, K. E., Jayawardhana, R., Brandeker, A., Mardones, D., 2003, "*Close Companions to Nearby Young Stars from Adaptive Optics Imaging on VLT and Keck*", in the proceedings from Science with Adaptive Optics, Eds. W. Brandner & M. Kasper (Springer-Verlag 2004).

Appendix C

Lexicon

C.1 Constants and units

These constants are from Allen's Astrophysical Quantities (Cox 2000).

Speed of light	$c = 2.997\,924\,58 \times 10^{8}\ \mathrm{m\,s^{-1}}$
Gravitational constant	$G = 6.672\,59 \times 10^{-11}\ \mathrm{m^{3}\,kg^{-1}s^{-2}}$
Planck constant	$h = 6.626\,075\,5 \times 10^{-34}\ \mathrm{J\,s}$
Elementary charge	$q_{\mathrm{e}} = 4.803\,206\,8 \times 10^{-19}\ \mathrm{C}$
Mass of hydrogen atom	$m_{\mathrm{H}} = 1.673\,534\,4 \times 10^{-27}\ \mathrm{kg}$
Magnetic permeability	$\mu_0 = 4\pi \times 10^{-7}\ \mathrm{V\,s\,A^{-1}\,m^{-1}}$
Electric permittivity	$\varepsilon_0 = 8.854\,187\,8 \times 10^{-12}\ \mathrm{A\,s\,V^{-1}\,m^{-1}}$
Gauss unit	$\mathrm{G} = 10^{-4}\ \mathrm{T}$
erg unit	$\mathrm{erg} = 10^{-7}\ \mathrm{J}$
Astronomical Unit	$\mathrm{AU} = 1.495\,978\,706\,6 \times 10^{11}\ \mathrm{m}$
Parsec	$\mathrm{pc} = 3.085\,677\,6 \times 10^{16}\ \mathrm{m}$
Solar radius	$R_{\odot} = 6.9551 \times 10^{8}\ \mathrm{m}$
Solar mass	$M_{\odot} = 1.9891 \times 10^{30}\ \mathrm{kg}$
Earth mass	$M_{\oplus} = 5.974\,2 \times 10^{24}\ \mathrm{kg}$
Arcsecond	$1'' = 1'/\,60$
Arcminute	$1' = 1^{\circ}/\,60$
Degree	$1^{\circ} = (180\,/\,\pi)\ \mathrm{rad}$

C.2 Vocabulary

abundance The relative quantity of elements.

adaptive optics Optics designed to counteract the blurring of the atmosphere, by rapidly modifying the light path in a telescope.

angular momentum Defined as $\mathbf{L} = \mathbf{r} \times m\dot{\mathbf{r}}$, where $\mathbf{r}$ is the position vector, $\dot{\mathbf{r}}$ its time derivative, and m is the mass of the particle. Depends on the chosen coordinate system. In a central force field, the angular momentum $\mathbf{L}$ is conserved. In this thesis, the angular momentum has been defined slightly differently, by dropping the mass, as in $\mathbf{L} = \mathbf{r} \times \dot{\mathbf{r}}$.

angular resolution A quantity that describes how fine angular details one can discern. Atmospheric turbulence often limits this resolution to about one arcsecond, unless adaptive optics is used.

APEX The Atacama Pathfinder EXperiment – a sub-mm telescope built at 5 000 m altitude in the Atacama desert, Chile.

asymptotic The behaviour of a function in the ∞ limit.

bi-polar *Arising from two poles*, as in a bi-polar outflow.

brown dwarf A celestial object intermediate in mass between a giant planet and a small star. Defined to be of a too low mass to have sustained fusion of hydrogen, but massive enough to burn deuterium. Also called “failed star”.

chromosphere The outer atmosphere of a star, above the photosphere, but below the corona.

circumstellar *Around a star*.

column density An area density determined by integrating the density along the line of sight. Commonly used in astronomy, since it is the projected emission along the line of sight that is observed.

coronography An observational method where a bright source is obscured by a mask, to enhance the contrast of the observations. Sometimes called coronagraphy.

depletion If an element has a lower relative abundance than expected, then it is often called “depleted”.

dipolar A field generated by two poles, with a field strength decreasing as $\propto r^{-3}$.

disk A flattened structure, in shape similar to a disc. For circumstellar disks, the American spelling of “disc” with a “k” is the convention in the astronomical community.

dust Particles consisting of conglomerated atoms. The details of dust formation theory are not well understood. In debris disks, dust is thought to be replenished by collisions between larger bodies, planetesimals. The planetesimals, in turn, are thought to have been built up from dust in an earlier phase of planet formation.

Doppler shift The shift in wavelength due to the relative motion between a light source and an observer.

escape velocity The initial velocity required for a body to escape a gravitational source and reach infinity: $v_{\rm esc} = \sqrt{2GM/R}$, where G is the gravitational constant, M is the mass of the source, and R is the distance to the source.

ESO The European Southern Observatory – created in 1962 to "*establish and operate an astronomical observatory in the southern hemisphere, equipped with powerful instruments, with the aim of furthering and organising collaboration in astronomy*". The organisation currently consists of the European countries Belgium, Denmark, France, Germany, Italy, the Netherlands, Portugal, Sweden, Switzerland and the United Kingdom.

excitation temperature The temperature that would populate the levels according to observations, if in local thermal equilibrium (LTE). The observed gas need not actually to be in LTE for the excitation temperature to be defined.

extra-solar *Outside of the solar system.*

extra-terrestrial *Outside of the Earth.*

FEB Falling Evaporating Bodies – a theory put forward by Ferlet et al. (1987) and Beust et al. (1989) to explain transient absorption features in the spectrum of β Pic, appearing as (mostly) redshifted lines at high velocities (a few to $100\,\mathrm{km\,s^{-1}}$) that vary on a timescale of hours to days.

FORS The FOcal Reducer/low resolution Spectrograph – a combined imaging and spectrograph instrument at the VLT.

fractal A self-similar structure that need not be smooth.

FWHM Full width, half mean. Used as a measure of the width of peaks, typically spectral lines and seeing. Defined as the full width of the peak at half of its height.

galaxy A collection of up to 10^{12} stars, gravitationally bound to each other. The universe between the galaxies is very empty of ordinary matter, with the galaxies occupying roughly $10^{-6} = 0.0001\,\%$ of the volume.

GHRS Goddard High Resolution Spectrograph – a high resolution UV spectrograph flown on the HST but replaced by STIS in February 1997.

gyration When a free ion is moving in a magnetic field, the magnetic force, being perpendicular to both the direction of velocity and the magnetic field line, causes the electron to move in a circle, a motion called *gyration* (literally meaning *to move around*, or *a ring*).

homogeneous *Of the same kind, not varying.*

homologous *Of the same proportion.*

HST The Hubble Space Telescope – a 2.5 m telescope launched into orbit around the Earth in 1990.

infrared Electromagnetic waves of wavelengths longer than the wavelengths of visible light, but shorter than the microwaves: $\lambda \sim 800\,\mathrm{nm} - 400\,\mu\mathrm{m}$. Commonly abbreviated IR. Sometimes divided into the near-infrared (NIR, 800 nm – 5 μm), mid-infrared (MIR, 5 μm – 30 μm), and far-infrared (FIR, 30 μm – 400 μm), with the limits being only loosely defined.

interstellar *In between the stars.*

IRAS The InfraRed Astronomical Satellite – a satellite surveying the whole IR sky in 1983, at the wavelengths 12, 25, 60 and 100 μm.

ISO The Infrared Space Observatory – an infrared satellite telescope operational between 1995 and 1998, at the wavelengths 2.5 – 240 μm.

JCMT The James Clerk Maxwell Telescope – a sub-mm telescope located at Mauna Kea, Hawaii, sensitive to wavelengths between 0.3 mm and 2 mm.

Keplerian Whenever an orbital system fulfils the third law of Kepler, $p^2 = a^3/M$, where p is the orbital period in units of years, a is the orbital semi-major axis in units of AU, and M is the combined gravitational mass in units of solar masses.

log *g* The base 10 logarithm of the gravitational acceleration at the surface, in units of cm s^{-2}. Parameter often used in stellar atmosphere models.

LTE Local Thermal Equilibrium – the assumption that local conditions, like the excitation, ionisation, and the emission, are well described by a single temperature.

luminosity The total energy output of the full electromagnetic spectrum per time for a source.

magnitude A quantity describing the intensity of light, defined as $m_A - m_B = -2.5 \log_{10}(f_A/f_B)$, where m_A and m_B are the magnitudes of two sources, and f_A and f_B are the physical intensities for the same sources, in a specific wavelength interval. The zero point for the magnitude scale is defined by observations of photometric standard stars.

metallic gas Gas consisting of metals - metals, in this context, meaning non-volatiles (i.e. not H, He, C, N, or O).

metallicity The fraction of elements other than H or He.

multiple system A stellar system consisting of several stars gravitationally bound to each other.

photo-ionisation The ionisation of an element by the removal of at least one electron from a photon absorption.

photosphere The surface where the stellar atmosphere becomes optically thick, i.e. the surface where most of the observed light originates from.

planetesimals Objects smaller than planets, but larger than dust, orbiting a star.

poloidal The component of a field perpendicular to the equatorial plane.

protostellar phase An early phase in a star's life when the original free-fall has been stopped by the thermal pressure, but fusion processes have not yet started. See Sect. 1.2. Some authors define the protostellar phase to coincide with the free-fall phase.

proper motion The apparent angular motion of a star in the sky.

radial velocity The velocity between an observer and a source in the radial direction from the observer.

radiation pressure The pressure (force/area) exterted by radiation, i.e. by photons.

SCUBA The Submillimetre Common-User Bolometer Array – a sub-mm camera located at the JCMT.

seeing The blurring of light by the atmosphere, often referred to by giving the angular FWHM of a point source (like a star). The blurring of the atmosphere at optical wavelengths is typically around 1″.

SEST The Swedish-ESO Submillimetre Telescope – a sub-mm telescope located at La Silla, Chile, and operated by ESO. Sensitive to wavelengths between 0.8 mm and 4 mm.

significance The signal to noise, S/N, where the noise is assumed to be Gaussian, and N is the standard deviation σ of the noise. Often referred to in factors of σ, e.g. "5σ-significance".

SIMBA The Sest IMaging Bolometer Array – a sub-mm camera located at the SEST.

SIRTF The Space Infrared Telescope Facility – an infrared satellite telescope launched in 2003, sensitive to wavelengths between 3 μm and 180 μm.

solar abundance The abundance by which elements are found in the solar atmosphere.

spectral resolution The ability to resolve details in a spectrum. Often measured as the quantity $R = \Delta v/c$, where Δv is the smallest radial velocity shift observable (due to the Doppler shift), and c is the speed of light.

spectrum The intensity of light from a source, as a function of wavelength.

spectroscopic binary A star that is observed to be binary in the combined spectrum from the two stellar components.

STIS The Space Telescope Imaging Spectrograph – a high resolution specrograph operating at UV to IR wavelengths (but used mainly for UV), flown at the HST.

toroidal The component of a field in the azimuthal direction.

ultraviolet Electromagnetic waves of wavelengths shorter than the wavelengths of visible light, but longer than the X-rays: $\lambda \sim 4\,\mathrm{nm}$ – 400 nm. Commonly abbreviated as UV.

UVES The UV-Visual Echelle Spectrograph – a high resolution spectrograph at the VLT.

***V*-band** Light in the wavelength range 4600 Å– 6400 Å.

VLT The Very Large Telescope – four 8.2 m telescopes located at Paranal, Chile, and operated by ESO.

young stars What stars are defined as young depends on the context. In this thesis, stars younger than 10^8 years are considered young (our Sun is about 5×10^9 years old).

Bibliography

Artymowicz, P. 1997, Annual Review of Earth and Planetary Sciences, 25, 175

Artymowicz, P., Burrows, C., & Paresce, F. 1989, ApJ, 337, 494

Augereau, J. C., Lagrange, A. M., Mouillet, D., & Ménard, F. 1999, A&A, 350, L51

Augereau, J. C., Nelson, R. P., Lagrange, A. M., Papaloizou, J. C. B., & Mouillet, D. 2001, A&A, 370, 447

Aumann, H. H. 1985, PASP, 97, 885

Aumann, H. H., Beichman, C. A., Gillett, F. C., et al. 1984, ApJ, 278, L23

Bazell, D., & Desert, F. X. 1988, ApJ, 333, 353

Beichman, C. A., Myers, P. C., Emerson, J. P., Harris, S., Mathieu, R., Benson, P. J., & Jennings, R. E. 1986, ApJ, 307, 337

Beust, H., Lagrange-Henri, A. M., Vidal-Madjar, A., & Ferlet, R. 1989, A&A, 223, 304

Beust, H., Vidal-Madjar, A., Ferlet, R., & Lagrange-Henri, A. M. 1990, A&A, 236, 202

Binney, J., & Tremaine, S. 1987, Galactic dynamics (Princeton, NJ, Princeton University Press, 1987, 747 p.)

Bouret, J.-C., Deleuil, M., Lanz, T., Roberge, A., Lecavelier des Etangs, A., & Vidal-Madjar, A. 2002, A&A, 390, 1049

Boyce, W. E., & DiPrima, R. C. 1986, Elementary differential equations and boundary value problems (John Wiley & Sons, Inc., 1986)

Brandeker, A. 1998, Master's thesis, Royal Institute of Technology, Sweden

Brandeker, A. 2003, in IAU Symposium 221, Star Formation at High Angular Resolutions, Eds. M.G. Burton, R. Jayawardhana, & T.L. Bourke, in press

Brandeker, A., Jayawardhana, R., & Najita, J. 2003a, AJ, 126, 2009

Brandeker, A., Liseau, R., Artymowicz, P., & Jayawardhana, R. 2001, ApJ, 561, L199

Brandeker, A., Liseau, R., Olofsson, G., & Fridlund, M. 2003b, A&A, in press

Cambrésy, L. 1999, in ASP Conf. Ser. 177: Astrophysics with Infrared Surveys: A Prelude to SIRTF, Ed. M.D. Bicay, R.M. Cutri, and B.F. Madore, 256

Chauvin, G., Fusco, T., Lagrange, A.-M., et al. 2002, A&A, 394, 219

Clampin, M., Krist, J. E., Ardila, D. R., et al. 2003, AJ, 126, 385

Cox, A. N. 2000, Allen's astrophysical quantities (Allen's astrophysical quantities, 4th ed. Publisher: New York: AIP Press; Springer, 2000. Edited by Arthur N. Cox. ISBN: 0387987460)

Crawford, I. A., Spyromilio, J., Barlow, M. J., Diego, F., & Lagrange, A. M. 1994, MNRAS, 266, L65

Crifo, F., Vidal-Madjar, A., Lallement, R., Ferlet, R., & Gerbaldi, M. 1997, A&A, 320, L29

Duchêne, G. 1999, A&A, 341, 547

Elmegreen, B. G., & Falgarone, E. 1996, ApJ, 471, 816

Ferlet, R., Vidal-Madjar, A., & Hobbs, L. M. 1987, A&A, 185, 267

Freudling, W., Lagrange, A.-M., Vidal-Madjar, A., Ferlet, R., & Forveille, T. 1995, A&A, 301, 231

Habing, H. J., Dominik, C., Jourdain de Muizon, M., et al. 1999, Nature, 401, 456

—. 2001, A&A, 365, 545

Haisch, K. E., Lada, E. A., & Lada, C. J. 2001, ApJ, 553, L153

Hartmann, L. 1998, Accretion processes in star formation (Accretion processes in star formation / Lee Hartmann. Cambridge, UK ; New York : Cambridge University Press, 1998. (Cambridge astrophysics series ; 32) ISBN 0521435072.)

Hauschildt, P. H., Allard, F., & Baron, E. 1999, ApJ, 512, 377

Heap, S. R., Lindler, D. J., Lanz, T. M., Cornett, R. H., Hubeny, I., Maran, S. P., & Woodgate, B. 2000, ApJ, 539, 435

Heitsch, F., Mac Low, M., & Klessen, R. S. 2001, ApJ, 547, 280

Hobbs, L. M., Vidal-Madjar, A., Ferlet, R., Albert, C. E., & Gry, C. 1985, ApJ, 293, L29

Hoffleit, D., & Warren, W. H. 1995, VizieR Online Data Catalog, 5050

Holland, W. S., Greaves, J. S., Zuckerman, B., et al. 1998, Nature, 392, 788

Jayawardhana, R., & Brandeker, A. 2001, ApJ, 561, L111

Jayawardhana, R., Fisher, S., Hartmann, L., Telesco, C., Pina, R., & Fazio, G. 1998, ApJ, 503, L79

Jeans, J. H. 1902, Phil. Trans. R. Soc. Lond. A, 199, 1

Jolly, A., McPhate, J. B., Lecavelier, A., Lagrange, A. M., Lemaire, J. L., Feldman, P. D., Vidal Madjar, A., Ferlet, R., Malmasson, D., & Rostas, F. 1998, A&A, 329, 1028

Joy, A. H. 1945, ApJ, 102, 168

Kaisler, D., Zuckerman, B., Song, I., Macintosh, B. A., Weinberger, A. J., Becklin, E. E., Konopacky, Q. M., & Patience, J. 2003, A&A, in press

Kalas, P., & Jewitt, D. 1995a, Ap&SS, 223, 167

—. 1995b, AJ, 110, 794
Kamp, I., & Bertoldi, F. 2000, A&A, 353, 276
Kervella, P., Thevenin, F., Morel, P., et al. 2003, in IAU Symposium 219, Stars as Suns, Eds. A. Benz & A. Dupree, in press
Kippenhahn, R., & Weigert, A. 1994, Stellar Structure and Evolution (Stellar Structure and Evolution, XVI, 468 pp. 192 figs.. Springer-Verlag Berlin Heidelberg New York. Also Astronomy and Astrophysics Library)
Koerner, D. W., Ressler, M. E., Werner, M. W., & Backman, D. E. 1998, ApJ, 503, L83
Kwok, S. 1975, ApJ, 198, 583
Lagrange, A.-M., Beust, H., Mouillet, D., et al. 1998, A&A, 330, 1091
Lagrange-Henri, A. M., Gosset, E., Beust, H., Ferlet, R., & Vidal-Madjar, A. 1992, A&A, 264, 637
Lecavelier des Etangs, A., Vidal-Madjar, A., Roberge, A., et al. 2001, Nature, 412, 706
Li, A., & Greenberg, J. M. 1998, A&A, 331, 291
Liseau, R. 2003, in ESA Special Publication SP-539, in press
Liseau, R., & Artymowicz, P. 1998, A&A, 334, 935
Liseau, R., Brandeker, A., Fridlund, M., Olofsson, G., Takeuchi, T., & Artymowicz, P. 2003a, A&A, 402, 183
Liseau, R., Larsson, B., Brandeker, A., et al. 2003b, A&A, 402, L73
Lissauer, J. J. 1993, ARA&A, 31, 129
—. 2001, Nature, 409, 23
Mandelbrot, B. B. 1982, The Fractal Geometry of Nature (The Fractal Geometry of Nature, San Francisco: Freeman, 1982)
Meeus, G., Sterzik, M., Bouwman, J., & Natta, A. 2003, A&A, 409, L25
Mouillet, D., Larwood, J. D., Papaloizou, J. C. B., & Lagrange, A. M. 1997, MNRAS, 292, 896
Neugebauer, G., Habing, H. J., van Duinen, R., et al. 1984, ApJ, 278, L1
Neuhäuser, R., Guenther, E., Mugrauer, M., Ott, T., & Eckart, A. 2002, A&A, 395, 877
Olofsson, G., Liseau, R., & Brandeker, A. 2001, ApJ, 563, L77
Palla, F., & Stahler, S. W. 1999, ApJ, 525, 772
—. 2001, ApJ, 553, 299
Pantin, E., Lagage, P. O., & Artymowicz, P. 1997, A&A, 327, 1123
Pollack, J. B., Hubickyj, O., Bodenheimer, P., Lissauer, J. J., Podolak, M., & Greenzweig, Y. 1996, Icarus, 124, 62
Roberge, A., Feldman, P. D., Lagrange, A. M., Vidal-Madjar, A., Ferlet, R., Jolly, A., Lemaire, J. L., & Rostas, F. 2000, ApJ, 538, 904

Robertson, H. P. 1937, MNRAS, 97, 423
Schneider, G., Smith, B. A., Becklin, E. E., et al. 1999, ApJ, 513, L127
Shu, F. H., Adams, F. C., & Lizano, S. 1987, ARA&A, 25, 23
Slettebak, A. 1975, ApJ, 197, 137
Smith, B. A., Fountain, J. W., & Terrile, R. J. 1992, A&A, 261, 499
Smith, B. A., & Terrile, R. J. 1984, Science, 226, 1421
Spangler, C., Sargent, A. I., Silverstone, M. D., Becklin, E. E., & Zuckerman, B. 2001, ApJ, 555, 932
Steffen, A. T., Mathieu, R. D., Lattanzi, M. G., et al. 2001, AJ, 122, 997
Stutzki, J., Bensch, F., Heithausen, A., Ossenkopf, V., & Zielinsky, M. 1998, A&A, 336, 697
Takeuchi, T., & Artymowicz, P. 2001, ApJ, 557, 990
Thébault, P., Augereau, J. C., & Beust, H. 2003, A&A, 408, 775
Thi, W. F., Blake, G. A., van Dishoeck, E. F., et al. 2001, Nature, 409, 60
Torres, G., Guenther, E. W., Marschall, L. A., Neuhäuser, R., Latham, D. W., & Stefanik, R. P. 2003, AJ, 125, 825
Vidal-Madjar, A., Lagrange-Henri, A.-M., Feldman, P. D., et al. 1994, A&A, 290, 245
Wahhaj, Z., Koerner, D. W., Ressler, M. E., Werner, M. W., Backman, D. E., & Sargent, A. I. 2003, ApJ, 584, L27
Weinberger, A. J., Becklin, E. E., Schneider, G., Smith, B. A., Lowrance, P. J., Silverstone, M. D., Zuckerman, B., & Terrile, R. J. 1999, ApJ, 525, L53
Wilner, D. J., Holman, M. J., Kuchner, M. J., & Ho, P. T. P. 2002, ApJ, 569, L115
Zuckerman, B., Song, I., Bessell, M. S., & Webb, R. A. 2001, ApJ, 562, L87

Acknowledgments

Given that this is the most popular chapter in the average thesis, I have made it more extended than usual. To simplify the task of the reader to find himself/herself, I have divided the acknowledged into several groups.

Collegues

Stockholm Observatory

First, and foremost, I wish to express my sincere gratitude to my supervisor **René Liseau**. His dedication to our projects and my development as a student has been outstanding. No question I ever posed was too insignificant to deserve a lengthy discussion. I thank **Göran Olofsson** for his kind guidance, acting as a second supervisor and a great sounding board. It was Göran who introduced me to the observatory, when he invited me to work for the IR-group during the summer of 1994. I thank **Monica Huldtgren** for her infective high spirits. I acknowledge the many interesting discussions I have had with **Pawel Artymowicz**, often giving me a second point of view. Not to mention his airbourne activities. I thank **Gösta Gahm** for his useful T Tauri insights. **Sylvain Bontemps** taught me lots of data reduction basics in general, and ISOCAM reductions in particular. I thank **Alexander Men'shchikov** and **Andrei Beloborodov** for encouraging my work on fractals. The care of **Nicole van der Bliek** is greatly appreciated.

I wish to express my admiration of my two bosses **Hans Olofsson** and **Claes-Ingvar Björnsson**, for sacrificing years of research to the benefit of the department. I thank **Claes Fransson** for all his critical questions during seminars. **Peter Lundqvist** is acknowledged as a great teacher and a funny guy. I thank **Aage Sandqvist** and **Jan Högbom** for giving such a positive impression of astronomers at Stockholm Observatory, during my first astronomy course in 1994. I apologise to **Cecilia Kozma** for locking her computer up for half a day. I thank **Erik Gullbring** for providing valuable advice regarding postdoctoral studies abroad. **Garrelt Mellema** is thanked for showing Andreas and me the pubs of great beers in Leiden. I thank **Roland Svensson** for having been a great teacher. **Kay Just-**

tanont Liseau and **Taku Takeuchi** are thanked for giving the department an Asian flavour, especially for the 'lice cookies' of the latter. I acknowledge the kind help I have had from **Jan Schober**, in particular in finding odd journals.

I thank the solar guys **Göran Scharmer**, **Dan Kiselman**, **Mats Löfdahl**, **Pete Dettori** and **Bertil Dorch** for shining at the department and presenting exciting results. **Seppo Mattila** is thanked for keeping the Friday-beer tradition alive (although I almost never can attend myself). I thank **Anita Sundman** and **Margareta Malmort** for giving the observatory an artistic touch. **Göran Östlin** and **Stefan Larsson** are thanked for their cosmic visions, and **PO Lindblad** for his dedication to Stockholm Observatory.

I thank the heroines of the department, **Anne-Marie Tannenberg**, **Lena Olofsson**, **Agneta Malmort**, **Ulla Engberg** and **Sandra Åberg**, for all help they have given me. **H-G Florén** is acknowledged for his sympathy during times of PC troubles, and for his enthusiastic F & S commitment. I thank **Matt Delaney** for reforming the computer environment at the observatory, and **Sergio Gelato** for keeping it nice, and valuable help on several occasions. **Uno Wänn** is thanked for his great many stories, and having a spare adjustable spanner when needed.

(Former) fellow Ph.D. students

I am grateful to **Amanda Kaas**, who was the first person I met at the observatory and whom I worked with the first summers. She taught me a lot about IR astronomy. I thank **Luc Rouppe van der Voort** for sharing his enthusiasm for aurorae, meteors, and skating. I also thank him for bringing me two weeks to the Swedish Vacuum Solar Telescope at La Palma, and for his friendship. **Felix Ryde** is thanked for sharing his deep knowledge about scholarship applications. I thank **David Delgado**, **Luis Borgonovo** and **Miguel de Val Borro** for providing Spanish/Argentinean inspiration. **Magnus Gålfalk** is thanked for sharing his enthusiasm for great astronomical imaging, and **Per Gröningsson** for moments of sympathy in times of UVES-trouble. I thank **Jens Andersson** for being flexible in the teaching schedule. **Fredrik Schöier Larsen** is acknowledged for his hospitality in Leiden. I thank **Bengt Larsson** for always being able to help out in moments of distress. I acknowledge the interesting discussions I have had with **Anna Grigorieva**, **Adam Peplinski** and **Sven Olofsson**, mostly regarding disks, planets, and dust. **Tanja Nymark** and **Margrethe Wold** are thanked for, together with Amanda Kaas, giving the department a sense of Norwegian wonder. I sincerely thank **Andreas Lundgren Andersson** for his support and good humour. **Anestis Tziamtzis** and **Matthew Hayes** are acknowledged for exercising my Greek and English, respectively. I thank **Boris Gudiksen** for sharing his Danish lager. He has, however, not yet convinced me of its superiority to Belgian beer. I thank **Jesper Sollerman** for some ESO advice, and **Magnus Näslund** for

his quick-wittedness. **Tomas Dahlén** is thanked for being such a pleasant person, and the air captains **Roland Karlsson** and **Torsten Elfhag** for giving perspectives on graduate school.

Other collegues

I thank **Ray Jayawardhana** for his enthusiastic collaboration on numerous projects, and his great support. I am grateful to the sisters **Gunilla** (∇) and **Gwendolyn Meeus** for providing some Belgian pleasures. **Malcolm Fridlund** is thanked for his collaboration and hospitality on numerous occasions. I acknowledge the insights to the British educational system given by **Glenn White**. I thank **Gibor Basri** for his kind support in finding a postdoctoral position. The enthusiastic collaborations of **Philippe Thébault** and **Inga Kamp** are gratefully acknowledged. I am indebted to **Chas Beichman** for taking some of his valuable time to review this thesis, whatever the outcome of his review.

I sincerely thank **Laurent Cambrésy**, **Karl Haisch**, **Sally Heap**, and **Francesco Palla**, for giving me permission to reprint their figures (Figs. 1.1 & 1.2, 2.1 3.1, and 1.8, respectively).

It is my pleasure to acknowledge the great inspiration I have had from my childhood hero, **Carl Sagan**. His visions and respect for the scientific method have strongly influenced my way of thinking.

Friends

I thank **Pasta-Calle Granath** for sharing the deep appreciation for one of the great gifts of life, pasta with delicious tomato sauce. **Markus Jönsson** is thanked for countless hours of *StarStrider* programming, with beer tastings in between, and **Lovisa Bylund** for taking care of him. I also thank **Per Johansson** and **Michael Ljunggren** for their enthusiastic participation in these beer tastings. My former cohabiter **Mattias Widmark** with **Mia Berg** are acknowledged for their great friendship, and **Moa** for being such a nice girl. I thank **Magnus Aspenberg** for excursions into the lands of fantasy, mathematics, and music. **Petter Ögren** and **Karin Sigurd**, masters of robotic motion, are thanked for their generous friendship. I acknowledge the friendship with **Cecilia Albertsson**. **Marcus Lagergren** is acknowledged for developing my *C-robots* programming skills, and **Marcus Hirt** as a great keyboard-pal from the pre-internet days. I thank my best childhood friend, **Janne Kettnaker**, and his family, for great many character-shaping experiences. I am pleased to have brought together two of my best friends **Jonas Kämpe** and **Chara Tourlida**, and thank them for still remembering me (despite my strongly anti-social behaviour during these last years of thesis-production). I

also thank Chara's family and all other friends I have in Greece, too numerous to mention on a few pages.

Special thanks are sent to my original λ(ship-state) friends **Malin Siddiqi** and **Daniel Sindahl**, with whom I have spent some of my best times. I also thank them for bringing **Faik Siddiqi**, **Roland Nilsson**, **Jenny Unger** and **Pascal Cabanne** into my sphere of friends.

I thank **Lola Czerny** for encouraging my interest in astronomy early on, during the plenty of occasions when she looked after me, when I was very young. The Norwegian Greeks **Sotiris Botouroglou**, **Dimitra Biklis** and **Orestis Botouroglou** are acknowledged for the many merry Christmases, and their genuine interest in my occupation.

I thank all my fellow amateur astronomers in the Stockholm amateur astronomy club **STAR** for sharing my love for astronomy, in particular **Katarina Riesel**, for her friendship.

I am deeply grateful to **Anna Sundin** for embellishing my afternoons once a week for several years, by her musicality, positive attitude, and sheer enthusiasm.

Family

I thank my parents **Bengt Brandeker** and **Aliki Brandeker**, and my sister, **Myrto Brandeker**, for their never-failing, solid support. I thank the rest of my Stockholm family, including **Birgitta Amato**, **Gino Amato**, **Feffe Ödmann**, **Pär-Owe Brandeker**, **Marjaana Helenius**, **Peter Helenius**, **Mia Helenius**, and **Eila Brandeker Hausmann**, for their indulgence with my unearthly activities.

I thank the Greek branch of my family for taking care of me during the long, warm summers in Greece, in particular the families of my aunts **Maria Kofou** and **Frosso Athanasopoulou**. The Trollhättan relatives **Gittan**, **Bertil**, **Lasse**, and **Janne Gustafsson** are also acknowledged.

I wish to thank my family-in-law **Sture**, **Gudrun**, and **Katarina Käll**, for their great hospitality and providing a sanctuary in a remote part of Småland.

The final words of this section are directed to my wife ♡ **Erika Brandeker**: *Älskade Erika, tack för att du finns och delar min verklighet.*

Paper I

Star Formation at High Angular Resolution
ASP Conference Series, Vol. S-221, 2003
M.G. Burton, R. Jayawardhana, & T.L. Bourke

T Tauri Multiple Systems

Alexis Brandeker
Stockholm Observatory, AlbaNova University Centre,
SE-106 91 Stockholm, Sweden

Abstract. New high-resolution adaptive optics systems provide an unprecedentedly detailed view of nearby star forming regions. In particular, young nearby T Tauri stars can be probed at much smaller physical scales (a few AU) than possible just a decade ago (several tens of AU). Of major importance is closing the sensitivity gap between imaging and spectral surveys for stellar companions. This allows for 1) calibration of pre-main-sequence evolutionary tracks by obtaining accurate dynamical masses, 2) resolving confusion problems arising by placing unresolved systems in colour-magnitude diagrams, and 3) well defined and determined multiplicity fractions of young stellar systems, important for discriminating star formation scenarios. This article briefly reviews the current status of high resolution imaging of T Tauri multiple systems, and what we can expect to learn from them in the near future.

1. Introduction

Most stars, especially pre-main-sequence (PMS) stars, are part of multiple systems (Duchêne 1999; reviews by Tom Greene and Ralf Launhardt, this volume). Since single stars are only in minority, we need to understand how multiple systems are formed in order to understand star formation in general. Because it is currently not possible to deduce a star formation theory from first principles without introducing unrealistic assumptions, observations of young systems are essential for differentiating between possible hypothetical scenarios.

Over the last years, some hundred nearby T Tauri stars have been imaged with adaptive optics, and before that some hundred were studied by speckle interferometry and lunar occultations. The three examples in Fig. 1 show adaptive optics (AO) imaging of three different multiple T Tauri stars put to the same spatial scale. They may look surprisingly similar, but are actually typical in two ways: a large fraction of the systems we image are not only binary, but often triple or quadruple, and multiple stars are mostly hierarchically arranged.

Two major questions that can be addressed by high angular resolution observations of multiple stars are:

- How does the early stellar evolution depend on mass (and metallicity)?
- Does the multiplicity frequency for stellar systems evolve in time?

In the following sections I will briefly describe methods of finding answers to these questions, with some emphasis on the contributions from modern AO

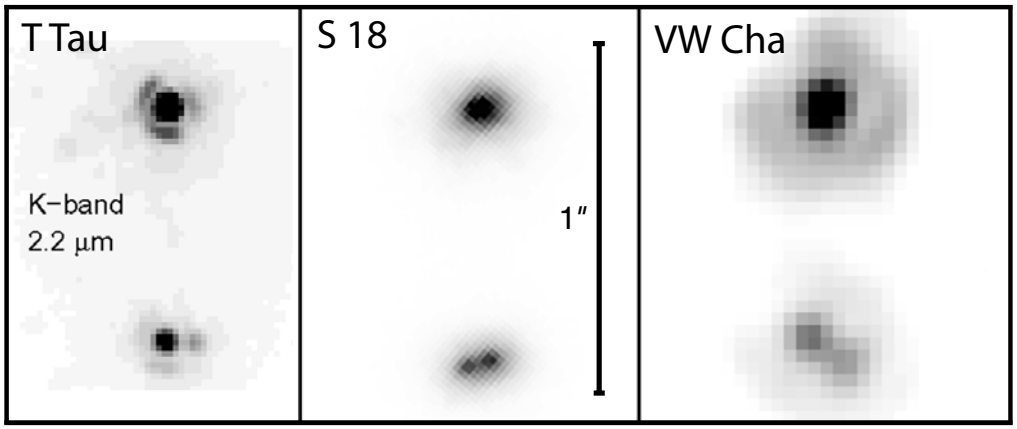

Figure 1. Three different triple T Tauri systems with a similar appearance: T Tauri, S 18 (in the MBM 12 young star association) and VW Chamaeleontis. The observations, here put to the same angular scale, are from Duchêne, Ghez, & McCabe (2002), Brandeker, Jayawardhana, & Najita (2003), and Brandeker et al. (2001) respectively. T Tau was observed in K with Keck AO, S 18 also with Keck AO but in H, and VW Cha in K with ADONIS at the 3.6 m telescope at ESO, La Silla.

systems. I will also review a few representative recent results in the area, and discuss what we may expect in the near future.

2. Calibrating PMS evolutionary tracks

Historically, binaries have played a major role in the successful theory of main sequence (MS) stellar structure. The importance of binaries in this context lies in the possibility of direct determination of stellar dynamical masses by following the orbital motion. For PMS stars, a problem has been that the nearest star forming regions are on the order of 100–150 pc distant. With observations limited by a typical seeing disc of 1″, this implies a projected physical resolution of 100–150 AU. Even for massive systems, the orbital period at the resolution separation is expected to be on the order of hundreds to thousands of years, making dynamical mass estimates impractical. Tight short-period binaries may still be found spectroscopically, since spectroscopic searches are limited by flux and not spatial scale. Without spatial information, however, only the relative masses of the stars in a binary can be deduced, unless the inclination of the orbit is known by other means.

2.1. Dynamical mass determinations

Clearly observations at higher angular resolutions are essential for dynamical mass determinations. AO systems on modern 8–10 m facilities regularly achieve diffraction limited imaging in the near infrared (NIR), corresponding to angular resolutions of 30–50 mas. At the distance of recently discovered nearby young

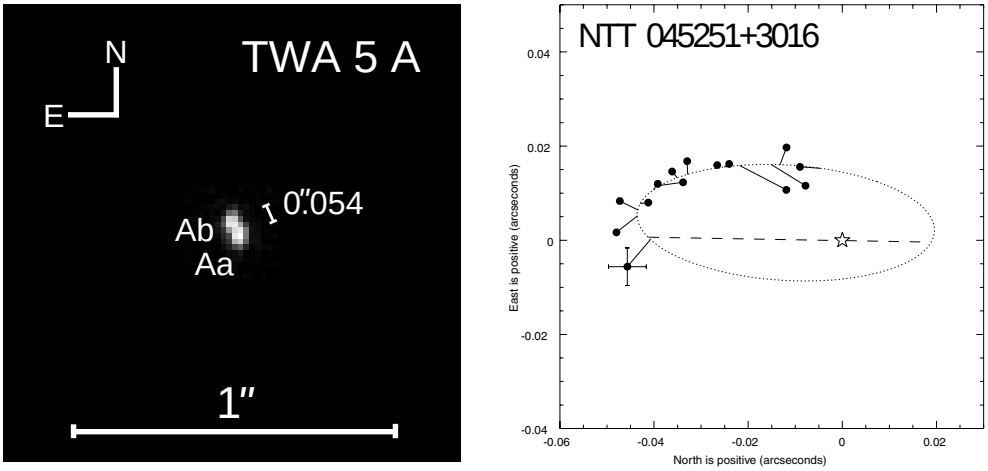

Figure 2. (*a, left panel*) The tight inner 3 AU binary TWA 5A of the TW Hydrae association. Expected period of binary is 5–10 yr. From Brandeker, Jayawardhana & Najita (2003). (*b, right panel*) Orbital solution to PMS binary NTT 045251+3016, making use of both spatially resolved observations and spectroscopic radial velocity measurements. From Steffen et al. (2001).

clusters, like the TW Hydrae association (TWA) at a distance of ∼55 pc, this translates to a projected physical scale of merely ∼2 AU. An example of a tight binary close to the resolution limit of the Keck telescope AO is shown in Fig. 2a, displaying TWA 5A with an estimated projected separation of 3 AU. By tracking the orbital motion of such tight binaries, it is possible to estimate a dynamical mass within just a few years. NTT 045251+3016 is a recent example of a binary dynamical mass estimate by Steffen et al. 2001, with their orbital solution shown in Fig. 2b. Using the Fine Guidance Sensor of the Hubble Space Telescope, they were able to reach a relative positional accuracy of 4 mas. Following the orbit during 3 years, a little less than half of the estimated orbital period, and using additional spectroscopically measured radial velocity differences between the two components, individual masses for the stars could be established as $1.45\pm0.19\,M_\odot$ and $0.81\pm0.09\,M_\odot$. Possibly surprising, a dynamical *distance* $d = 144.8\pm8.3$ pc was also derived by combining astrometric and spectroscopic data, independent of any paralactic distance. Schaefer et al. (2003) report three more systems with the system mass dynamically estimated, and show that meaningful dynamical mass estimates can be obtained even though the orbital elements remain very uncertain, as first noted by Eggen (1967).

Other methods that have been employed to determine stellar dynamical masses involve eclipsing binaries (e.g. Covino et al. 2000) and orbital motion of disk gas (Simon, Dutrey, & Guilloteau 2000). Both have their benefits and caveats: Although eclipsing binaries provide very accurate masses, they require special geometry (very small orbital inclination to the line of sight), and are consequently comparatively rare. By studying disk gas motion also the mass

of single stars can be dynamically estimated. Gas motion is, however, more sensitive to non-gravitational effects, such as the radiation pressure (see e.g. Olofsson, Liseau, & Brandeker 2001).

Accurate dynamical mass estimates of young low-mass stars ($< 1\,M_{\odot}$) remain very rare, but given the recent advances in high angular resolution instrumentation, and a few years of orbital motion, the near future will no doubt see the number of dynamically estimated masses multiply.

2.2. Resolving confusion

Another problem with seeing limited observations is that of confusion. Tight multiple systems, like those in Fig. 1, are entirely contained in a seeing disc, meaning that photometry will be measured on the system as a whole. Placing the measurements in a Hertzsprung-Russell diagram, the whole system will show an offset from the evolutionary tracks compared to the individual stars. Faint infrared companions close to the primary may show up as an IR-excess in the measured spectral energy distribution, difficult to distinguish from e.g. a warm circumstellar disk. Spectroscopic searches for faint companions are most sensitive to shorter periods, and are inefficient in finding binaries with periods of a couple of years or more. This means physical separations of a few AU or less, translating to some 40 mas or less at the typical distances of 100–150 pc. This is on the same order as the angular resolution of modern AO systems, meaning that there no longer is a sensitivity gap where stellar companions can hide.

3. Multiplicity frequency evolution

Most MS stellar systems in the solar neighbourhood are multiple (Duquennoy & Mayor 1991), and for PMS systems the multiplicity fraction in general seems to be even higher (e.g. Reipurth & Zinnecker 1993; Duchêne 1999; Barsony, Koresko, & Matthews 2003). How can this be, if we believe MS field stars to be evolved T Tauri stars? I know of three proposed explanations:

3.1. Selection effects

Maybe the multiple fraction excess among PMS stars is due to more sensitive searches (Ghez 1996). For instance, young low-mass companions are brighter and more easily seen than their older counterparts, especially in the NIR where most searches are conducted. However, a more detailed study by White & Ghez (2001) argues this to not be the case: we do see more companions among young stars, even when looking at the same mass intervals. This point illuminates the importance of finding and correcting observational biases. By closing the sensitivity gap between spectral and spatial searches for companions, corrections for unseen components can be put on a firmer ground.

3.2. Regional differences

Maybe different regions produce different multiplicity fractions, and the star forming regions we observe just by chance happen to have higher multiplicity fractions than the average. Indeed, different regions apparently do show different multiplicity fractions (Duchêne 1999). Possible parameters responsible for this

"environmental effect" are metallicity, volume stellar densities and internal velocity dispersion (see also Woitas, Leinert, & Köhler 2001; Zinnecker 2003). The statistics are still quite poor, however, so the significance of variations among different regions remains low.

3.3. Dynamical evolution

Perhaps multiple systems evolve dynamically, and in the process lose companions, either by stellar mergers or ejections (e.g. Reipurth 2000). One may also speculate that orbital evolution make companions harder to detect. One way is by shrinking a wide, easily resolved, binary to a tight, not so easily resolved binary, another is to widen a moderately wide binary to a very wide (and loose) binary, which will consequently make the companions hard to identify as such (and also make the system more sensitive to disruption due to stellar encounters). By increasing the angular resolution to the point where any stellar companion tighter than the resolution limit would be picked up spectroscopically, the hypothesis of unseen tight binaries can be ruled out. Very wide and loose binaries may be more difficult to find, but can be addressed by multiple epoch wide field studies of proper motions in combination with radial velocity observations, to assess relative space motions.

Detailed numerical studies of the early orbital evolution have produced some quantitative predictions of the low-mass stellar population in young clusters (Bates, Bonnell, & Bromm 2002, 2003) that can be checked in the near future. Companion ejection requires three-body interaction, and would thus mainly affect the companion fraction defined as $cf = (2b+3t+4q+...)/(s+b+t+q+...)$, where s, b, t, q, etc. are the number of single stars, binaries, triples, quadruples etc. The companion fraction is the average number of companions to any primary. The multiplicity fraction $mf = (b+t+q+...)/(s+b+t+q+...)$, on the other hand, should not be as strongly affected since mostly triples or higher order systems eject companions, always leaving a lower order multiple. To disrupt a binary, a stellar encounter is generally needed to provide the third body.

An interesting case where we may be observing a current ejection is the prototype system of all T Tauri stars, T Tauri. Loinard, Rodríguez, & Rodríguez (2003) used archival Very Large Array (VLA) data to follow the orbital evolution of a centimeter radio emission feature coincident with one of the southern components in the triple system, T Tau Sb. They derive an orbit of Sb around the unseen (in their data) component Sa, that from 1983 to 1997 was well described by an ellipse, but since then has departed significantly from the initial orbit (Fig. 3a). Furlan et al. (2003) dispute the identification of the radio source with the T Tau Sb companion, using recent AO NIR imaging. By following the evolution of the NIR component since 1997 (when it was first noted in speckle data by Koresko 2000), Furlan et al. (2003) derive a significantly different orbit from that of the radio emission (Fig. 3b). They argue that the centimeter emission probably comes from the ejection of a *fourth* component in the T Tau system, still unseen in the AO NIR data. Statistically, to observe an ejection in action is very unlikely, so we are extremely fortunate if this is indeed an ejection. Future AO observations in the coming decade will clarify this.

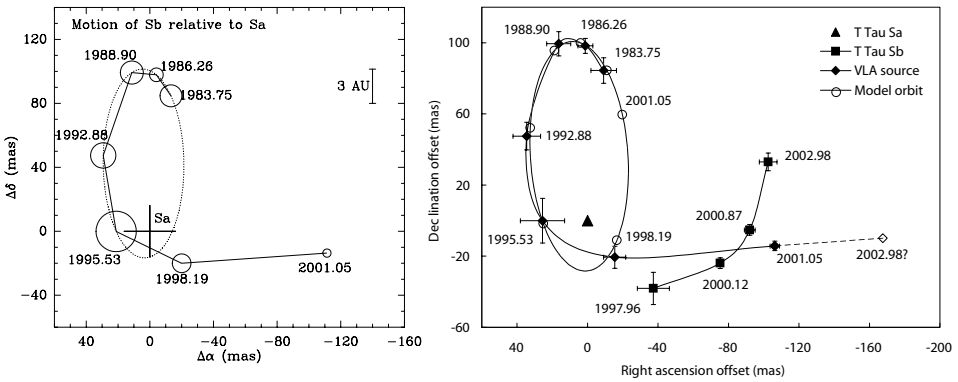

Figure 3. Orbital evolution of the T Tau S system. The left panel shows the centimeter emission feature relative to T Tau Sa, as found by VLA (from Loinard, Rodríguez, & Rodríguez 2003). After 1997, there is an apparent change of orbital path, interpreted as a possible ejection of T Tau Sb. The right panel is from Furlan et al. (2003) and adds recent AO observations that show this centimeter feature not to be associated with T Tau Sb, but possibly emanating from a fourth component being ejected.

4. Summary and outlook

Adaptive optics systems of today provide, for the first time, high enough angular resolution to determine dynamical masses of the nearest T Tauri multiple systems. A few preliminary estimates of masses have already been reported in the literature.

The coming years will see an increase both in the number of systems with dynamical mass determinations, and in the accuracy of the estimates. Looking beyond the nearest systems, optical interferometry, with notably VLTI and the Keck interferometer, will resolve binaries ten times more distant than AO alone.

By resolving multiple systems, stars can be accurately put on colour-magnitude diagrams and compared to theoretical early evolutionary tracks. In combination with accurate dynamical mass estimates, models will be much better constrained and calibrated for use in, e.g., estimating the initial mass function for different star forming regions.

High angular resolution observations in combination with spectroscopic searches have the potential to carry out a complete census of companions in nearby young clusters. Fig. 4 shows an example of the sensitivity to companions for a state-of-the-art AO system. Note that AO systems now are sensitive enough to probe the "brown dwarf desert" around young stars, as young brown dwarfs are much more luminous than older ones (Baraffe et al. 2003). By increasing the statistics and improving the observational bias corrections, the multiplicity and companion fraction as a function of separation and age may be firmly established, giving important clues to the formation of multiples and stars in general.

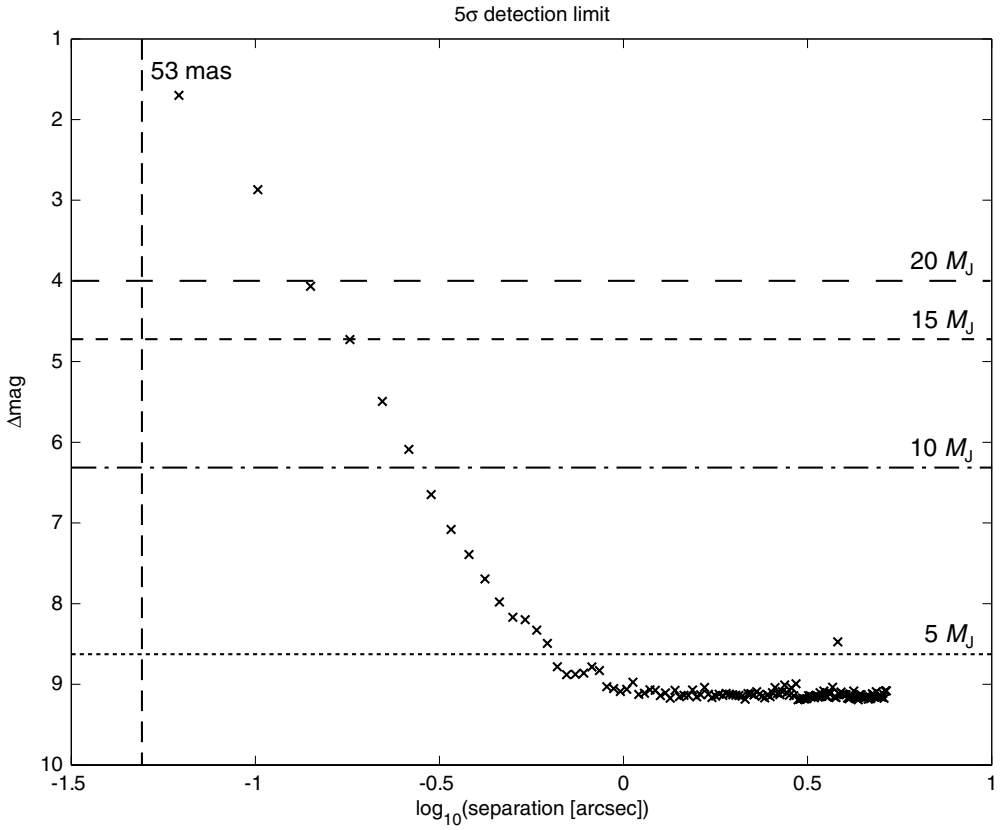

Figure 4. VLT/NACO 5σ contrast sensitivity limit in H-band as a function of separation for the binary η Cha 9 of the η Chamaeleontis association (Mamajek, Lawson, & Feigelson 1999). The vertical dashed line shows the diffraction limit, and the horizontal lines show expected flux ratios of sub-stellar companions at the distance ($\sim$100 pc) and magnitude ($H = 10$) of η Cha 9. Luminosities of the sub-stellar companions are derived from Chabrier et al. (2000) and Baraffe et al. (2003), assuming an age of 10 Myr. The exposure time was 2190×0.34 s. At small separations the noise is dominated by speckle noise from the point spread function, while the sky-noise and read-out noise dominate at larger separations. From Jayawardhana et al. (2003).

Acknowledgments. I would like to thank the organisers for inviting me to give this short review, C.F. Liljevalch j:or for a travel grant to get to Sydney, my supervisor René Liseau for supporting my participation despite being close to the deadline of my Ph.D. defence, and Ray Jayawardhana and Gösta Gahm for valuable comments and suggestions.

References

Barsony, M., Koresko, C., & Matthews, K. 2003, ApJ, 591, 1064

Bate, M. R., Bonnell, I. A., & Bromm, V. 2002, MNRAS, 336, 705

Bate, M. R., Bonnell, I. A., & Bromm, V. 2003, MNRAS, 339, 577

Baraffe, I., Chabrier, G., Barman, T. S., Allard, F., & Hauschildt, P. H. 2003, A&A, 402, 701

Brandeker, A., Jayawardhana, R., & Najita, J. 2003, AJ, 126 (in press)

Brandeker, A., Liseau, R., Artymowicz, P., & Jayawardhana, R. 2001, ApJ, 561, L199

Chabrier, G., Baraffe, I., Allard, F., & Hauschildt, P. 2000, ApJ, 542, 464

Covino, E., Catalano, S., Frasca, A., et al. 2000, in IAU Symp. 200, Birth and Evolution of Binary Stars, ed. B. Reipurth & H. Zinnecker, 9

Duchêne, G. 1999, ApJ, 341, 547

Duchêne, G., Ghez, A. M., & McCabe, C. 2002, ApJ, 568, 771

Duquennoy, A. & Mayor, M. 1991, A&A, 248, 485

Eggen, O. J. 1967, ARA&A, 5, 105

Furlan, E., Forrest, W. J., Watson, D. M., et al. 2003, submitted to ApJL

Ghez, A. M. 1996, in NATO Advanced Science Institutes Series C Vol. 477, Evolutionary Processes in Binary Stars, ed. R. Wijers & M. Davies, 1

Jayawardhana, R., Haisch, K., Brandeker, A., & Mardones, D. 2003, in prep.

Koresko, C. D. 2000, ApJ, 531, L147

Loinard, L., Rodríguez, L. F., & Rodríguez, M. I. 2003, ApJ, 587, L47

Mamajek, E. E., Lawson, W. A., & Feigelson, E. D. 1999, ApJ, 516, L77

Olofsson, G., Liseau, R., & Brandeker, A. 2001, ApJ, 563, L77

Reipurth, B. 2000, ApJ, 120, 3177

Reipurth, B. & Zinnecker, H. 1993, A&A, 278, 81

Schaefer, G. H., Simon, M., Nelan, E., & Holfeltz, S. T. 2003, AJ, in press

Simon, M., Dutrey, A., & Gulloteu, S. 2000, ApJ, 545, 1034

Steffen, A. T., Mathieu, R. D., Lattanzi, M. G. et al. 2001, ApJ, 122, 997

White, R. J. & Ghez, A. M. 2001, ApJ, 556, 265

Woitas, J., Leinert, Ch., & Köhler, R. 2001, A&A, 276, 982

Zinnecker, H. 2003, in IAU Symp. 212, A Massive Star Odyssey, from Main Sequence to Supernova, ed. K. A. van der Hucht, A. Herrero, & C. Esteban, in press

Paper II

The Astrophysical Journal, 561:L199–L202, 2001 November 10
© 2001. The American Astronomical Society. All rights reserved. Printed in U.S.A.

DISCOVERY OF A NEW COMPANION AND EVIDENCE OF A CIRCUMPRIMARY DISK: ADAPTIVE OPTICS IMAGING OF THE YOUNG MULTIPLE SYSTEM VW CHAMAELEON[1]

Alexis Brandeker,[2] René Liseau,[2] and Pawel Artymowicz
Stockholm Observatory, SCFAB, SE-10691 Stockholm, Sweden; alexis@astro.su.se, rene@astro.su.se, pawel@astro.su.se
and
Ray Jayawardhana
Department of Astronomy, University of California at Berkeley, 601 Campbell Hall, Berkeley, CA 94720; rayjay@astron.berkeley.edu
Received 2001 February 20; accepted 2001 October 1; published 2001 October 18

ABSTRACT

Since a majority of young low-mass stars are members of multiple systems, the study of their stellar and disk configurations is crucial to our understanding of both star and planet formation processes. Here we present near-infrared adaptive optics observations of the young multiple star system VW Chamaeleon. The previously known 0.″7 binary is clearly resolved already in our raw *J*- and *K*-band images. We report the discovery of a new faint companion to the secondary, at an apparent separation of only 0.″1, or 16 AU. Our high-resolution photometric observations also make it possible to measure the $J-K$ colors of each of the three components individually. We detect an infrared excess in the primary, consistent with theoretical models of a circumprimary disk. Analytical and numerical calculations of orbital stability show that VW Cha may be a stable triple system. Using models for the age and total mass of the secondary pair, we estimate the orbital period to be 74 yr. Thus, follow-up astrometric observations might yield direct dynamical masses within a few years and constrain evolutionary models of low-mass stars. Our results demonstrate that adaptive optics imaging in conjunction with deconvolution techniques is a powerful tool for probing close multiple systems.

Subject headings: binaries: close — circumstellar matter — infrared: stars — stars: formation — stars: low-mass, brown dwarfs — stars: pre–main-sequence

1. INTRODUCTION

Most stars are members of binary or multiple systems (Batten 1973; Halbwachs 1983). Yet the formation of multiple stellar systems is still poorly understood. Currently, the most promising mechanism appears to be fragmentation during the collapse of dense molecular cloud cores (Bodenheimer et al. 2000). Recent surveys of pre–main-sequence (PMS) stars in certain star-forming regions have measured a binary frequency about twice that measured in the solar neighborhood (see Mathieu et al. 2000 for a review and caveats). Whether this is an evolutionary or environmental effect is open to debate. In any case, higher order multiple systems appear to be relatively rare in both young and old stellar populations (see, e.g., Ghez et al. 1997 and references therein).

High-resolution observations of PMS multiple systems help determine the stellar and disk configurations of young objects, leading to better constraints on models of multiple star formation and early evolution. We have undertaken an adaptive optics (AO) imaging program of known PMS close binary systems to search for additional companions and to detect circumstellar or circumbinary disks. In this Letter we present our observations of one such system, VW Cha in the Cha I star-forming cloud, at a distance of ~160 pc (Whittet et al. 1997). The VW Cha system has previously been reported to consist of several components; Schwartz (1991) listed Sz 23 located 16″ away as a possible wide companion; Brandner et al. (1996) discovered a closer companion at 0.″7 separation; Ghez et al. (1997) observed these components and reported an additional companion at 2.″7 separation from the primary. Brandner & Zinnecker (1997, hereafter BZ97) obtained spatially resolved spectra of the close binary.

Here we present the discovery of a new close companion to the secondary of VW Cha and an infrared excess from the primary in the system, probably due to a dusty disk.

2. OBSERVATIONS

We observed the VW Cha system on 2000 March 11–13 with the European Southern Observatory 3.6 m telescope at La Silla, Chile, using the Adaptive Optics Near-Infrared System (ADONIS) and the SHARP II+ camera. The SHARP II+ camera is based on a 256 × 256 NICMOS3 array. We used a plate scale of 0.″035 pixel^{-1} and Nyquist-sampled the diffraction-limited point-spread function (PSF), giving an effective field of view of 8.″5 × 8.″5. The *J*-band (1.25 μm) observations of VW Cha were conducted during the first night, and *K*-band observations (2.18 μm) during the second. At *J* we obtained 60 frames, each with an integration time of 10 s, chopping the source out of the field of view for a 10 s on-sky integration between each frame. The science target itself was used as the wave front sensor of the AO system. The seeing during the VW Cha observations the first night, as reported by the La Silla seeing monitor, fluctuated in the *V* band (0.55 μm) between 0.″8 and 1.″4. The *K*-band observations of the second night were obtained in a similar manner with 10 frames of 30 s integration time each, with the difference that the sky frames were obtained after the series of on-source frames and not in between. The seeing in *V* this time was stable at about 1.″0. During both nights most frames showed a diffraction-limited core while the Strehl ratios fluctuated between 0.1 and 0.3.

After each series of observations of VW Cha, an identical series of observations with the same AO correction parameters were obtained of a PSF calibrator star for postprocessing purposes. We used the F5 V star SAO 256804 with a *V* magnitude of 8.50.

[1] Based on observations collected at the European Southern Observatory, Chile.
[2] Visiting Astronomer, European Southern Observatory, Chile.

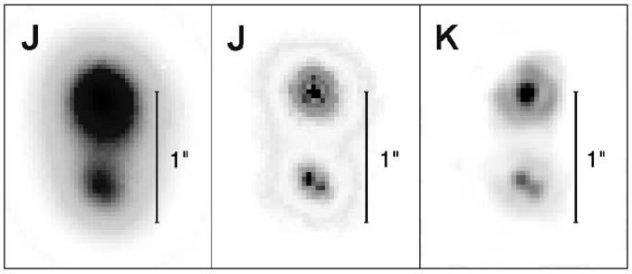

FIG. 1.—Unprocessed frame in *J* (*left panel*), and deconvolved images in *J* (*middle panel*) and *K* (*right panel*) of the VW Cha system. The secondary itself is split into a 0.″10 binary in the deconvolved images. The vertical bar in each image corresponds to 1″. North is up; east is to the left.

3. REDUCTIONS AND ANALYSIS

The basic data reductions were done in a standard way by subtracting sky frames from source frames and then dividing by a flat field obtained on-sky during dusk. The resulting frames were then not stacked together but instead were processed with the myopic deconvolution algorithm IDAC.[3]

From the PSF calibrator star observations, we obtained an initial guess of the PSF during the science data acquisition. Since the PSF calibrator star data were not obtained simultaneously with the science data, the initial guess PSF is then modified by IDAC iteratively to better match the different frames of science data. A series of PSF estimates corresponding to the science object series is thus produced along with the deconvolved image. The deconvolution procedure using IDAC took about 2 weeks of processing time on an UltraSparc workstation. We refer to Christou et al. (1999) for details on IDAC.

We performed astrometry of the VW Cha system using the deconvolved images in both *J* and *K*. The error in separation was estimated by checking the consistency of measured separations of other multiple star systems observed several times during the two nights. The error in position angle was then estimated from the error in separation by assuming positional errors to be isotropic.

For flux calibration, we used observations of 10 other SAO stars distributed over the sky and obtained during the two nights in both *J* and *K*. Their known *B* and *V* magnitudes and spectral classes were used to derive their *J* and *K* magnitudes using standard colors (Bessell & Brett 1988) and an estimate of the color excess due to extinction, using Table 1 of Mathis (1990) and assuming an optical extinction ratio $R_V = 3.1$. We then fitted a relation to the observed count rates and derived magnitudes, estimating the absolute photometric errors from the statistical error of the fit. By checking the consistency of the measured flux of stars observed several times during the two nights, we derived the relative photometric errors.

[3] Information about IDAC and the package itself may be found on the Web pages of ESO at http://www.eso.org.

4. RESULTS AND DISCUSSION

4.1. *Multiplicity of VW Cha*

In our observations, we are able to detect binaries at separations between 0.″08 and 4″, where the lower limit corresponds to the diffraction limit of the 3.6 m telescope in *J* and the upper limit is due to the 8.″5 × 8.″5 field of view. The inner 0.″7 binary is already resolved in the raw data in both *J* and *K*. After deconvolution, the secondary is split up into a tight 0.″10 binary in itself (see Fig. 1). Our results are summarized in Table 1.

The reported 2.″7 companion was not seen in any of our images. Based on the background noise levels, our 5 σ detection limits are $J = 20$ and $K = 17$, well below $K \approx 9.4 \pm 0.6$ derived from Table 2 in Ghez et al. (1997). The cause for a drop in brightness by a factor of 10^3 is hard to imagine, and we suggest that either the star has drifted out of our field of view or the detection was spurious.

4.2. *Implausibility of Chance Alignment*

Comparing our observations with measurements from 1992 (Brandner et al. 1996), we find no significant change (less than 0.″05) of the relative positions between the A and B + C components. Since VW Cha has a proper motion of about 0.″22 yr^{-1} (Frink et al. 1998), the system as a whole has moved at least 2″ over the past 10 yr. Thus, the proper motions of the components are highly correlated, corresponding to a relative velocity of less than 5 km s^{-1} at the distance of VW Cha. We therefore conclude that the VW Cha system is not a chance alignment but rather to a physical triple star.

4.3. *Stellar Parameters*

4.3.1. *Corrections for Extinction*

From observations in the visual (BZ97) and infrared (see Table 1), it follows that the primary increasingly dominates the emission at increasingly longer wavelengths. Interpolating between the flux ratios in different wave bands, we apportion the observed total *I* magnitude of 10.60 (Gauvin & Strom 1992) as 11.03 to A and 11.73 to B + C. The resulting observed colors, $(I-J)_A = 1.82$ and $(I-J)_{B+C} = 1.79$, can then be compared to the intrinsic colors of K5/K7 and K7 stars (BZ97) for a log *g*

TABLE 1

INFRARED PHOTOMETRY AND ASTROMETRY OF THE VW CHA SYSTEM[a]

Stellar Component	*J* (1.25 μm)[b] (mag)	*K* (2.18 μm)[c] (mag)	*J*−*K* (mag)	Separation[d] (arcsec)	Position Angle[d] (deg)	M_{bol} (mag)	*L* ($L_\odot$)	*M* ($M_\odot$)	Age (Myr)
A	9.21	7.03	2.18 ± 0.16	...	...	3.56	2.93	1.00	0.4
B	10.55	8.92	1.63 ± 0.16	0.661 ± 0.006	176.6 ± 0.5	4.97	0.79	0.40	0.4
C	10.87	9.32	1.55 ± 0.16	0.100 ± 0.006	233.3 ± 3.3	5.29	0.59	0.35	0.4
B + C	9.94	8.35	1.59 ± 0.20	0.683 ± 0.008[e]	179.4 ± 0.7[e]	4.37	1.38	0.75	...
A + B + C	8.76	6.75	2.01 ± 0.24	...	...	3.14	4.30	1.75	...

[a] Taken on 2000 March 11–13.

[b] Absolute error $\sigma_J = 0.06$ mag; mean relative error $\sigma_J = 0.026$ mag.

[c] Absolute error $\sigma_K = 0.08$ mag; mean relative error $\sigma_K = 0.12$ mag.

[d] Separation and position angle for components B and B + C are relative to component A, and component C is relative to component B. Position angle is measured from north to east.

[e] For B + C the astrometry is made with respect to the photocenter. The larger error is due to the shift of the photocenter with wavelength.

of 3.5 and solar metallicity of the model atmospheres by Allard, Hauschildt, & Schweitzer (2000), i.e., $(I-J)_0 = 0.80$ and 0.92, respectively. The color excess of the relatively "blue" star B + C is probably mainly due to foreground dust extinction; hence, $A_I - A_J = 0.87$, which yields $A_V = 3.03$ mag, where we have used the extinction curve for the Cha I cloud (G. Olofsson 2001, private communication; e.g., $A_V = 2.90A_J$, $A_{I_C} = 1.83A_J$, $A_K = 0.37A_J$). The assumption that this value of A_V also applies to the primary would imply excess emission from component A, at the level of about 0.1 mag at *J* and 0.9 mag at *K*. An active circumprimary disk would be a natural source of such excess radiation.

4.3.2. *Stellar Luminosities and Masses*

For the extinction-corrected and excess emission–corrected *J* magnitude of the primary, $J_{0,\,A} = 8.16$, the absolute bolometric magnitude can be obtained from Allard et al. (2000) as $M_{\rm bol,\,A} = 3.6$. For B and C, these values are 5.0 and 5.3, respectively. Consequently, the *bolometric* luminosities are $L_A = 2.9\ L_\odot$, $L_B = 0.79\ L_\odot$, and $L_C = 0.59\ L_\odot$. The "blue" components B and C contribute to the total flux mainly at shorter wavelengths. The neglect of correcting for extinction is therefore expected to underestimate the total luminosity of the system. This is indeed the case, as the *calorimetric* luminosity of $L_{\rm cal} = 3\ L_\odot$ by Prusti, Whittet, & Wesselius (1992) constitutes merely 70% of $L_{\rm bol} = 4.3\ L_\odot$. A natural explanation of this deficit would be that only a fraction of the stellar photons are reprocessed to the infrared, while the rest escape nonisotropically owing to the presence of a circumstellar disk.

The empirically determined parameters of the individual stellar components of VW Cha are consistent with those of the theoretical evolution models (for single stars)[4] by Palla & Stahler (1999) for masses of A, B, and C of 1.0, 0.40, and 0.35 $M_\odot$, respectively, at the common age of 0.4×10^6 yr (Table 1). This assumes a systematic shift of $\Delta \log T_{\rm eff} = -0.04$, which is not unreasonable.

BZ97 found the Hα line to be in emission toward both A and B + C. If dominated by disk accretion processes, some infrared excess could be expected also from the fainter pair and should thus be corrected for. However, the Hα flux is larger from A (BZ97), and the mass accretion rate $\dot{M}$ is presumably also larger for the primary. Estimates of $\dot{M}$, which are in reasonable agreement with the *K* excess, are in the range of a few times $10^{-8}\ M_\odot\ {\rm yr}^{-1}$ (Gahm et al. 1995) to $10^{-7}\ M_\odot\ {\rm yr}^{-1}$ (Hartmann et al. 1998) but are certainly much less than the large rates (10^{-6} to $10^{-4}\ M_\odot\ {\rm yr}^{-1}$) obtained by Johns-Krull, Valenti, & Linsky (2000) in the far-UV, a spectral region that is highly susceptible to extinction corrections.

VW Cha was detected by the *Infrared Space Observatory* at 6.7 and 14.3 μm (Persi et al. 2000) but not by *IRAS* at 60 and 100 μm (Prusti et al. 1992), suggesting that only small amounts of dust exist in the system, at temperatures significantly below 50 K. For the stellar properties and mass accretion rate determined above, an outer circumprimary disk radius of less than 70 AU could then be inferred from standard theory of steady state thin-disk accretion (Frank, King, & Raine 1985), using a temperature profile of the form $T_{\rm disk}(r) \propto r^{-0.4}$. This minimum temperature would be consistent also with the scenario of a tidally truncated disk around A with a size of at most twice the BC binary separation, advocated in § 4.4 (the separation of 0.″2 corresponds to 30 AU, where $T_{\rm disk} \sim 70$ K). Furthermore, the observed excess in *J* would be consistent with the presence of hot dust and thus of only a small central hole. However, as illustrated by the interpretation of the observed weakness of the 10 μm silicate feature in VW Cha (Natta, Meyer, & Beckwith 2000), some caution seems to be called for when applying simplified disk theories developed for single stars to close multiples.

It is interesting to note that the secondary in the T Tau binary system recently has been resolved into a binary in itself (Koresko 2000). The projected relative distances for A : (B + C) and B : C are about 100 and 10 AU, respectively, making the configuration very similar to VW Cha. In addition, evidence for a circumprimary disk around T Tau with a radius of ~40 AU has been presented by Akeson, Koerner, & Jensen (1998). The major difference is the much higher luminosity of the T Tau system, of $\sim 30\ L_\odot$ (Cohen & Kuhi 1979). An apparent difference is also the extremely red appearence of T Tau S. This has previously been interpreted as the (unresolved) secondary being in a considerably earlier stage of evolution than the primary. However, later results suggest that the infrared excess may be due to foreground extinction (see discussion in Akeson et al. 1998).

4.4. *Triple Star Dynamics: Stability Estimates*

We consider the possibility that VW Cha is a physical triple, bound and stable for ~1 Myr (upper limit on age). Components B and C form a tight pair B : C at the projected separation of 16 AU, while A is found at a 7 times larger projected separation of 106 AU. We first show analytically that a nearly planar three-body system similar to VW Cha, with low eccentricities, is forever stable against the disintegration of the close binary by the third massive body.

We utilize energetic constraints on the motion of a three-body system, similar to the familiar zero-velocity curves in the restricted three-body problem, where the Jacobi integral entails the so-called Hill stability, involving no exchange of components and no "ionization." A small binary B : C will never be pulled apart by component A if (Marchal & Bozis 1982; Marchal 1988) $(-EL^2) > (IU^2)_{\rm L1}$, where *E* is the total mechanical energy of the triple system, *L* its total angular momentum, *I* the semimoment of inertia (one-half times the sum of the squares of radius vectors times masses), and *U* the total potential energy of the triple. Subscript L1 denotes the value at the collinear "Lagrange point" between the two most massive bodies. Stability does not depend on either the total mass or the distance units. For example, tilting a given system with respect to the plane of the sky merely rescales the inferred periods but not the orbit shapes. If projection effects are not extreme, the orbital periods are close to those in a planar system with semimajor axes of $a_1 = 110$ AU and $a_2 = 16$ AU for the A : (B + C) and B : C pairs, i.e., on the order of 872 and 74 yr.

For the masses given in Table 1, we found that the right-hand side of the stability criterion equals $(IU^2)_{\rm L1} = 0.0152GM_{\rm tot}^2$ (where $M_{\rm tot} = 1.75\ M_\odot$ is the total mass). Our results show that if the initial orbit of the outer binary A : (B + C) is circular ($e_1 = 0$), then the B : C pair is Hill stable for a wide range of e_2-values (its initial eccentricity) of $e_2 < 0.37$ and its semimajor axis $a_2 < 26$ AU. If $e_1 = e_2 = 0$, stability can be assured for $0\ {\rm AU} < a_2 < 27$ AU. Alternatively, assuming cautiously that in the current configuration both orbits are at apocenters (maximum extension), we find that eccentricities $e_1 < 0.19$ and $e_2 < 0.20$ are required for stability. In summary, the three-body $(-EL^2)$ criterion guarantees that a nearly coplanar hierarchical system (with

[4] The validity of these models for binaries has recently been assessed by Palla & Stahler (2001).

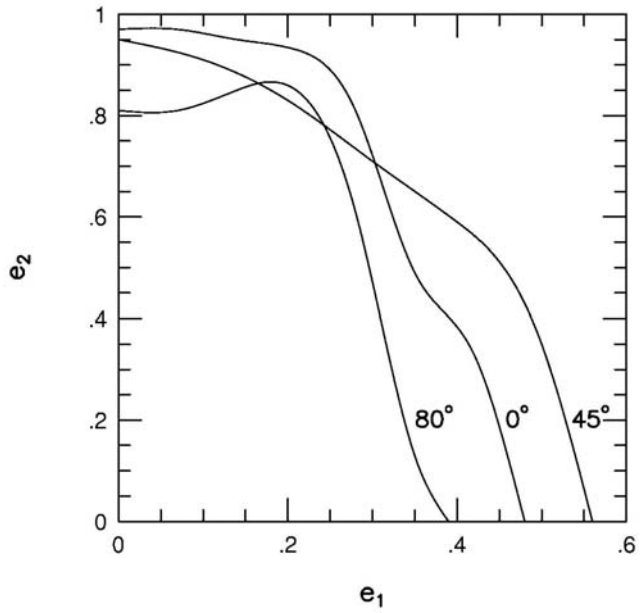

FIG. 2.—Stability diagram of a model triple system representing VW Cha. Eccentricities of a large outer and a small inner binary subsystem are denoted e_1 and e_2, and their relative inclination is marked next to the curves. The system is stable at least 1 Myr for parameter sets below the plotted curves.

geometry consistent with VW Cha), having small eccentricities, will never restructure by ejecting any star to infinity or form a close pair of either A : B or A : C.

The analytical criterion cannot guarantee that the B and C components will not physically collide. It might also indicate instability where none actually occurs on an interesting short timescale (which we fix at 1 Myr). To confirm its predictions, we therefore integrated the motion of VW Cha–like configurations with a seventh- to eighth-order Runge-Kutta method, accurate to 10 significant digits in the total energy. We assumed $a_1 = 110$ AU and $a_2 = 16$ AU. Only the ratio $a_1/a_2 \approx 7 : 1$, is decisive for stability. Mutual approaches of stars to less than 10^7 km (~10 PMS stellar radii) were treated as physical mergers following a tidal capture. We found that the analytical and numerical criteria approximately coincide. For instance, we confirmed numerically our analytical predictions discussed above.

Figure 2 presents numerical results for the planar and inclined system configurations. Curves are labeled with the starting initial inclination of the inner and outer orbits. Combinations of the eccentricities located below the plotted curves represent stable systems. All destruction modes including physical collisions of stars were observed above the curves. Strictly speaking, the lines shown in the figure result from averaging the results over such unessential initial parameters as the longitudes of pericenters, ascending nodes, and true anomalies

From Figure 2 we conclude that a wide variety of eccentricities result in stable behavior. While $e_1 < 0.45$ is generally required, larger e_2-values (up to 0.8) are consistent with stability, independent of the mutual orbital inclination (with exception of unstable, almost perpendicular orbits not presented here). We conclude that the hierarchical projected structure of VW Cha likely reflects a stable physical configuration for the estimated age of the system.

5. CONCLUSIONS

The young double star VW Cha (0.″7 separation) has been successfully observed with AO techniques in the infrared *J* and *K* bands. These AO observations led to the following main findings:

1. The secondary is a very close binary itself (0.″1 separation).
2. This physical triple system is shown to be stable over a period exceeding its estimated age of 0.4 Myr.
3. Follow-up astrometric observations may, within a few years, constrain the dynamical mass of the B : C subsystem, thus testing evolutionary models of PMS stars.
4. The primary (A) has a significant infrared excess, indicating the presence of a circumprimary disk. This disk is probably small, with a radius not exceeding ~30 AU.

Our VW Cha result shows that individual components of known binaries may be close binaries themselves, which needs to be considered while deriving ages and other parameters of such systems.

We had many helpful discussions on VW Cha with Göran Olofsson and Gösta Gahm. We are also grateful to Keith Hege for extensive support with the use of IDAC and to Wolfgang Brandner for supplying photometric data.

REFERENCES

Akeson, R. L., Koerner, D. W., & Jensen, E. L. N. 1998, ApJ, 505, 358
Allard, F., Hauschildt, P. H., & Schweitzer, A. 2000, ApJ, 539, 366
Batten, A. H. 1973, Binary and Multiple Systems of Stars (New York: Pergamon)
Bessell, M. S., & Brett, J. M. 1988, PASP, 100, 1134
Bodenheimer, P., Burkert, A., Klein, R. I., & Boss, A. P. 2000, in Protostars and Planets IV, ed. V. Mannings, A. P. Boss, & S. S. Russell (Tucson: Univ. Arizona Press), 675
Brandner, W., Alcalá, J. M., Kunkel, M., Moneti, A., & Zinnecker, H. 1996, A&A, 307, 121
Brandner, W., & Zinnecker, H. 1997, A&A, 321, 220
Christou, J., Bonaccini, D., Ageorges, N., & Marchis, F. 1999, ESO Messenger, 97, 14
Cohen, M., & Kuhi, L. V. 1979, ApJS, 41, 743
Frank, J., King, A. R., & Raine, D. J. 1985, Accretion Power in Astrophysics (Cambridge: Cambridge Univ. Press)
Frink, S., Röser, S., Alcalá, J. M., Covino, E., & Brandner, W. 1998, A&A, 338, 442
Gahm, G. F., Lodén, K., Gullbring, E., & Hartstein, D. 1995, A&A, 301, 89
Gauvin, L. S., & Strom, K. M. 1992, ApJ, 385, 217
Ghez, A. M., McCarthy, D. W., Patience, J. L., & Beck, T. L. 1997, ApJ, 481, 378
Halbwachs, J. L. 1983, A&A, 128, 399
Hartmann, L., Calvet, N., Gullbring, E., & D'Alessio, P. 1998, ApJ, 495, 385
Johns-Krull, C. M., Valenti, J. A., & Linsky, J. L. 2000, ApJ, 539, 815
Koresko, C. D. 2000, ApJ, 531, L147
Marchal, C. 1988, in The Few Body Problem, ed. M. J. Valtonen (Dordrecht: Kluwer), 5
Marchal, C., & Bozis, G. 1982, Celest. Mech., 26, 311
Mathieu, R. D., Ghez, A. M., Jensen, E. L. N., & Simon, M. 2000, in Protostars and Planets IV, ed. V. Mannings, A. P. Boss, & S. S. Russell (Tucson: Univ. Arizona Press), 703
Mathis, J. S. 1990, ARA&A, 28, 37
Natta, A., Meyer, M. R., & Beckwith, S. V. W. 2000, ApJ, 534, 838
Palla, F., & Stahler, S. W. 1999, ApJ, 525, 772
———. 2001, ApJ, 553, 299
Persi, P., et al. 2000, A&A, 357, 219
Prusti, T., Whittet, D. C. B., & Wesselius, P. R. 1992, MNRAS, 254, 361
Schwartz, R. D. 1991, ESO Sci. Rep., 11, 93
Whittet, D. C. B., Prusti, T., Franco, G. A. P., Gerakines, P. A., Kilkenny, D., Larson, K. A., & Wesselius, P. R. 1997, A&A, 327, 1194

Paper III

THE ASTROPHYSICAL JOURNAL, 561:L111–L113, 2001 November 1
© 2001. The American Astronomical Society. All rights reserved. Printed in U.S.A.

DISCOVERY OF CLOSE COMPANIONS TO THE NEARBY YOUNG STARS HD 199143 AND HD 358623[1]

RAY JAYAWARDHANA
Department of Astronomy, University of California at Berkeley, 601 Campbell Hall, Berkeley, CA 94720; rayjay@astro.berkeley.edu
AND
ALEXIS BRANDEKER
Stockholm Observatory, SCFAB, SE-106 91 Stockholm, Sweden; alexis@astro.su.se
Received 2001 September 3; accepted 2001 September 19; published 2001 October 8

ABSTRACT

Young stellar systems in the solar neighborhood provide valuable laboratories for detailed studies of star and planet formation. The bright F8 V star HD 199143 and the Li-rich late-type emission-line star HD 358623 are among the nearest young stars identified to date and may be members of a young association in Capricornus. We present high-resolution near-infrared images of these two sources, obtained using the adaptive optics system on the 3.6 m telescope at the European Southern Observatory in La Silla, Chile. Our observations reveal that both are, in fact, close binary systems. The newly discovered companion at a separation of ~1″ may account for the unusual characteristics of HD 199143—rapid rotation, emission lines, ultraviolet variability, and excess infrared emission—recently discussed by van den Ancker and coworkers. HD 199143 may be a rare example of a close binary with only a circum*secondary* disk. With the detection of a ~2″ companion, HD 358623 is now possibly one of the closest known T Tauri binaries. Both binary systems are prime targets for follow-up spectroscopic and astrometric observations.

Subject headings: binaries: close — circumstellar matter — open clusters and associations: general — stars: low-mass, brown dwarfs — stars: pre–main-sequence — techniques: high angular resolution

1. INTRODUCTION

There is growing interest in finding and characterizing young stellar systems in the solar neighborhood since their proximity offers unique advantages for improving our understanding of star and planet formation. Over the past 5 years, a number of young associations have been identified within 100 pc of the Sun, and these have become the targets of intense investigations using a variety of techniques (Jayawardhana & Greene 2001).

HD 199143 is a bright F8 V (Houk & Smith-Moore 1988) star in Capricornus with a *Hipparcos* distance of 47.7 ± 2.4 pc. It was detected as a bright extreme-ultraviolet source by the *ROSAT* and *Extreme Ultraviolet Explorer* satellites (Pounds et al. 1993; Malina et al. 1994). Recently, in a study of its optical and ultraviolet spectra, van den Ancker et al. (2000) found the emission lines of Mg II, C I, C II, C III, C IV, Si IV, He II, and N V and a high level of variability, both in the continuum and line fluxes. The authors also present evidence for very rapid (a few hundred kilometers per second) rotation of the stellar photosphere and for excess emission in the mid-infrared, detected by *IRAS* at 12 μm. Van den Ancker et al. proposed that all of these phenomena can be explained if HD 199143 has a low-mass chromospherically active companion that dominates the ultraviolet and infrared emission of the system. Episodic accretion of material from a putative T Tauri–like companion could have spun up the primary and may also account for the bursting or flaring nature of this object.

The same authors pointed out that the photometrically variable K7–M0e dwarf HD 358623 (BD −17°6128), previously studied by Mathioudakis et al. (1995), is located only 5′ from HD 199143. The optical spectrum of HD 358623 is identical to that of many classical T Tauri stars and shows strong Hα emission and Li 6708 Å absorption lines. The closeness of the two stars on the sky and the similarity of their proper motions, derived from the Tycho-2 catalog, led van den Ancker et al. (2000) to suggest that the pair belongs to a physical group that may include additional young stars. At a distance of ~48 pc, HD 358623 is estimated to be ~10^7 yr old—an age comparable to the timescales of inner disk evolution and planet formation (Jayawardhana 2001 and references therein).

Given their proximity, interesting age, and possible membership in a comoving stellar group, HD 199143 and HD 358623 are worthy of further study. Here we present the results of near-infrared adaptive optics imaging observations of both stars that reveal each to be a close binary. The newly discovered companion to HD 199143 may indeed account for the enigmatic characteristics of that system.

2. OBSERVATIONS

We observed HD 199143 and HD 358623 on 2001 May 31 to June 1 with the European Southern Observatory 3.6 m telescope at La Silla, Chile, using the adaptive optics near-infrared system and the SHARPII+ camera. The SHARPII+ camera is based on a 256 × 256 NICMOS3 array. We used a plate scale of 0.″035 pixel^{-1}, Nyquist-sampling the diffraction-limited point-spread function (PSF) in *J* and giving an effective field of view of 8.″5 × 8.″5. We observed the targets by taking a series of frames on-source and chopping out for sky frames. For HD 199143, we obtained 42 frames in *J*, each of integration time 3 s, and 42 frames in *K* of 2 s each. For HD 358623, we obtained 10 × 20 s in *J* and 22 × 10 s in *K*. The science target itself was used as the wave front sensor of the adaptive optics system. The seeing during the observations, as reported by the La Silla seeing monitor, was about 1.″3 in *V* (0.55 μm).

After each series of observations of the science targets, an identical series of observations with the same adaptive optics correction parameters were obtained of a PSF calibrator star, for postprocessing purposes. For HD 199143, we used the

[1] Based on observations collected at the European Southern Observatory, Chile.

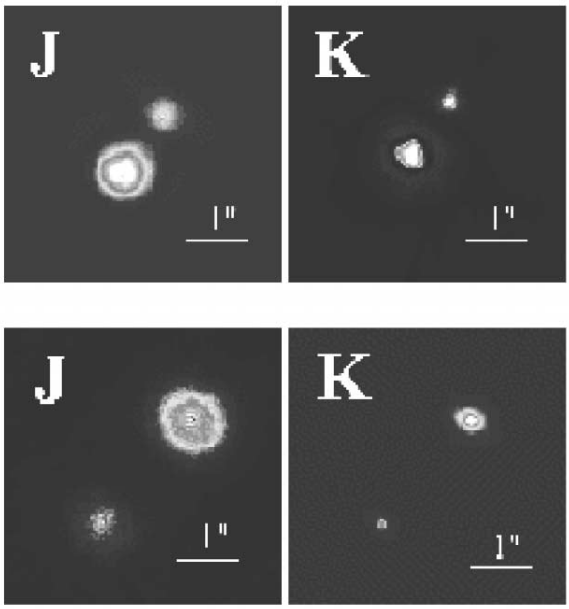

FIG. 1.—Deconvolved adaptive optics images of HD 199143 (*top*) and HD 358623 (*bottom*) in the near-infrared. The horizontal bar in each image corresponds to 1″. North is up, and east is to the left.

F3 IV star SAO 163887 with *V* magnitude of 6.8, and for HD 358623 we used the M0 star SAO 163911 with *V* magnitude of 9.8.

3. DATA REDUCTION AND ANALYSIS

The basic data reductions were done in a standard way by subtracting sky frames from source frames and then dividing by a flat field obtained on-sky during dusk. The resulting frames were then not stacked together but instead processed with the myopic deconvolution algorithm IDAC.[2]

From the PSF calibrator star observations, we obtained an initial guess of the PSF during the science data acquisition. Since the PSF calibrator star data were not obtained simultaneously with the science data, the initial guess PSF is then modified by IDAC iteratively to better match the different frames of science data. A series of PSF estimates corresponding to the science object series is thus produced along with the deconvolved image. The deconvolution procedure using IDAC took about 2 weeks of processing time on an UltraSparc workstation. We refer to Christou et al. (1999) for details on IDAC.

[2] Information about IDAC and the package itself may be found on the Web page of ESO: http://www.eso.org.

We performed astrometry of the HD 199143 and HD 358623 systems using the deconvolved images in both *J* and *K*. The error in separation was estimated by checking the consistency of measured separations in *J* and *K*. For flux calibration, we used observations of the IR standard star HD 190285 and five other SAO stars in both *J* and *K*. For the SAO stars, known *B* and *V* magnitudes and spectral classes were used to derive their *J* and *K* magnitudes using standard colors (Bessell & Brett 1988) and an estimate of the color excess due to extinction using Table 1 of Mathis (1990), where we assumed an optical extinction ratio $R_V = 3.1$. We then fitted a relation between the observed count rates and derived magnitudes.

From the fit, we estimated the absolute photometric errors, i.e., the uncertainty of the transformation from measured counts to magnitudes. By checking the consistency of the measured flux of stars observed several times during the night, we derived the relative photometric errors.

4. RESULTS AND DISCUSSION

We have resolved both HD 199143 and HD 358623 into close binaries for the first time. Figure 1 shows the deconvolved *J* and *K* images, and Table 1 presents photometric and astrometric measurements of each system. Our observations are able to detect binaries at separations between 0.″08 and 4″, where the lower limit corresponds to the diffraction limit of the 3.6 m telescope in *J* and the upper limit is due to the 8.″5 × 8.″5 field of view. A search of the Two Micron All-Sky Survey (2MASS) catalog reveals that the surface density of stars brighter than $K = 9$ within a 5° radius of our targets is ~0.004 arcmin^{-2}. Thus, it is unlikely that the companions we found are unrelated field stars.

Our $J-K$ color, as well as the $B-V$ color from the SIMBAD database, of HD 199143A is consistent that of an F8 V star with no foreground extinction. Using a distance of 48 pc and the atmosphere models of Allard, Hauschildt, & Schweitzer (2000), we find a *bolometric* luminosity of $L_{\mathrm{bol},A} = 2.45 \pm 0.12\ L_{\odot}$. Stellar evolutionary models of Palla & Stahler (1999) yield a mass of $M_A = 1.19 \pm 0.02\ M_{\odot}$ and an age of 18 ± 2 Myr for the primary. (The errors given for the stellar parameters are the formal uncertainties in statistical model fitting plus measurement errors; "true" errors—due to inherent uncertainties in the models—are likely to be larger.)

The newly discovered companion, HD 199143B, is extremely red, with $J-K = 1.368$. This near-infrared color corresponds to a model atmosphere with a temperature in the 1700–2100 K range, which (taken at face value) would imply a very young object in the brown dwarf/giant planet mass regime. However, HD 199143B most likely harbors a circumstellar disk, responsible for *K*-band excess as well as the *IRAS* 12 μm detection and ground-based mid-infrared measurements

TABLE 1

INFRARED PHOTOMETRY AND ASTROMETRY OF HD 199143 AND HD 358623

Stellar Component	J (1.25 μm)[a] (mag)	K (2.18 μm)[b] (mag)	$J-K$ (mag)	Separation (arcsec)	Position Angle[c] (deg)
HD 199143A + B	6.1816	5.7725	…	…	…
HD 199143A	6.2346	5.9054	0.329	…	…
HD 199143B	9.4869	8.1191	1.368	1.0785 ± 0.009	325.0 ± 0.7
HD 358623A + B	7.8332	7.0071	…	…	…
HD 358623A	8.0201	7.2171	…	…	…
HD 358623B	9.8359	8.8941	0.942	2.2033 ± 0.007	139.4 ± 0.5

[a] Absolute error $\sigma_J = 0.041$ mag, mean relative error $\sigma_J = 0.006$.
[b] Absolute error $\sigma_K = 0.032$ mag, mean relative error $\sigma_K = 0.023$.
[c] Position angle is measured from north to east, relative to A.

previously reported for the system (van den Ancker, Pérez, & de Winter 2001). Given the lack of optical colors and a spectral type, it is difficult to derive reliable stellar parameters for the secondary. However, assuming an age of 18 Myr and the excess to be zero at J and a free parameter at K, we find $L_{\rm bol,\,B} = 0.060 \pm 0.003\ L_\odot$, $M_B = 0.35 \pm 0.05\ M_\odot$, and a $J-K$ excess of ~0.5 mag, consistent with a T Tauri–like star.

If HD 199143B indeed harbors a dusty disk but HD 199143A does not, a scenario in agreement with our data, it would be a rare example of a close binary with only a circum*secondary* disk. In a study of 25 close, pre–main-sequence binaries, Prato (1998) found disks around both stars in 15 systems and neither star in five systems. Four others showed evidence of circum*primary* disks (also see Jayawardhana et al. 1999), while only one example of a circum*secondary* disk was identified.

Theoretical calculations suggest that circumstellar disks will be truncated by the tidal effects of a companion star in circular orbit at approximately 0.9 of the average Roche lobe radius (Artymowicz & Lubow 1994). From the *IRAS* database, van den Ancker et al. (2000) derived a flux of 0.24 ± 0.04 Jy in the 12 μm band and upper limits of 0.12, 0.12, and 0.30 Jy for the fluxes at 25, 60, and 100 μm, respectively. A tidally truncated disk around HD 199143B is consistent with the tight *IRAS* limits at 25 and 60 μm.

Our $J-K$ color and the SIMBAD $B-V$ color for HD 358623A imply very little extinction ($\leq$0.1 mag). For a K7 spectral type, assuming an age of 18 Myr to be coeval with HD 199143, we find $L_{\rm bol,\,A} = 0.21 \pm 0.04\ L_\odot$ and $M_A = 0.74 \pm 0.07\ M_\odot$ for a distance of 43 pc. Conversely, if we fix the distance at 48 pc, we get a slightly worse fit to the evolutionary models with an age of 12 ± 4 Myr, again in reasonable agreement with the age of HD 199143. Using a distance of 43 pc, stellar models yield $L_{\rm bol,\,B} = 0.034 \pm 0.002\ L_\odot$, $M_B = 0.27 \pm 0.06\ M_\odot$, and an age of 20 ± 7 Myr for the newly found secondary, HD 358623B. Van den Ancker et al. (2001) report significant mid-infrared excesses from HD 358623. Our observations do not constrain whether the dust surrounds one or both members of the binary.

5. CONCLUSIONS

Using adaptive optics techniques, we have resolved the two nearby (~48 pc) young stars HD 199143 and HD 358623 into close binaries. The newly discovered secondary may account for many of the puzzling characteristics of the HD 199143 system. If the B component harbors a dusty disk, as indicated by its near-infrared colors and consistent with previous mid-infrared detections, HD 199143 would be a rare example of a close binary with only a circum*secondary* disk. The stellar parameters we derive for each component of HD 199143 and HD 358623, while not tightly constrained, are in agreement with both systems being 15 ± 5 Myr in age at a distance of 43–48 pc. Spatially resolved spectroscopy of both binaries would allow us to determine the stellar parameters more reliably, and follow-up astrometry could yield direct dynamical masses, thus testing evolutionary models of pre–main-sequence stars. High-resolution mid-infrared imaging will be valuable for further constraining the location and nature of circumstellar dust in these two binaries. A systematic search for other young stars in the vicinity of HD 199143 and HD 358623 may reveal additional members of a comoving stellar group, enhancing our understanding of local star formation and enriching our inventory of suitable nearby targets for detailed multiwavelength studies.

We wish to thank the staff of the European Southern Observatory for their outstanding support. We are grateful to Tom Greene for a previous attempt to observe HD 199143 at the IRTF, and to the referee, Mario van den Ancker, for a prompt review. Our research made use of the ADS, SIMBAD, and 2MASS databases. R. J. holds a Miller Research Fellowship at the University of California at Berkeley. This work was supported in part by a NASA grant to R. J. administered by the AAS.

REFERENCES

Allard, F., Hauschildt, P. H., & Schweitzer, A. 2000, ApJ, 539, 366
Artymowicz, P., & Lubow, S. H. 1994, ApJ, 421, 651
Bessell, M. S., & Brett, J. M. 1988, PASP, 100, 1134
Christou, J., Bonaccini, D., Ageorges, N., & Marchis, F. 1999, Messenger, 97, 14
Houk, N., & Smith-Moore, A. 1988, Michigan Spectral Survey, Vol. 4 (Ann Arbor: Univ. Michigan Press)
Jayawardhana, R. 2001, in ASP Conf. Ser. 244, Young Stars near Earth: Progress and Prospects, ed. R. Jayawardhana & T. P. Greene (San Francisco: ASP), 185
Jayawardhana, R., & Greene, T. P., eds. 2001, ASP Conf. Ser. 244, Young Stars near Earth: Progress and Prospects (San Francisco: ASP)
Jayawardhana, R., Hartmann, L., Fazio, G., Fisher, S., Telesco, C., & Piña, R. 1999, ApJ, 520, L41
Malina, R. F., et al. 1994, AJ, 107, 751
Mathioudakis, M., et al. 1995, A&A, 302, 422
Mathis, J. S. 1990, ARA&A, 28, 37
Palla, F., & Stahler, S. W. 1999, ApJ, 525, 772
Pounds, K. A., et al. 1993, MNRAS, 260, 77
Prato, L. 1998, BAAS, 193, 89.04
van den Ancker, M. E., Pérez, M. R., & de Winter, D. 2001, in ASP Conf. Ser. 244, Young Stars near Earth: Progress and Prospects, ed. R. Jayawardhana & T. P. Greene (San Francisco: ASP), 69
van den Ancker, M. E., Pérez, M. R., de Winter, D., & McCollum, B. 2000, A&A, 363, L25

Paper IV

The Astronomical Journal, 126:2009–2014, 2003 October
© 2003. The American Astronomical Society. All rights reserved. Printed in U.S.A.

KECK ADAPTIVE OPTICS IMAGING OF NEARBY YOUNG STARS: DETECTION OF CLOSE MULTIPLE SYSTEMS

Alexis Brandeker
Stockholm Observatory, AlbaNova University Center, SE-106 91 Stockholm, Sweden; alexis@astro.su.se

Ray Jayawardhana
Department of Astronomy, University of Michigan, 830 Dennison Building, Ann Arbor, MI 48109; rayjay@umich.edu

and

Joan Najita
National Optical Astronomy Observatory, 950 North Cherry Avenue, Tucson, AZ 85719; najita@noao.edu
Received 2003 May 27; accepted 2003 June 25

ABSTRACT

Using adaptive optics on the Keck II 10 m telescope on Mauna Kea, we have surveyed 24 of the nearest young stars known in search of close companions. Our sample includes members of the MBM 12 and TW Hydrae young associations and the classical T Tauri binary UY Aurigae in the Taurus star-forming region. We present relative photometry and accurate astrometry for 10 close multiple systems. The multiplicity frequency in the TW Hydrae and MBM 12 groups are high in comparison to other young regions, although the significance of this result is low because of the small number statistics. We resolve S18 into a triple system, including a tight 63 mas (projected separation of 17 AU at a distance of 275 pc) binary, for the first time, with a hierarchical configuration reminiscent of VW Chamaeleontis and T Tauri. Another tight binary in our sample—TWA 5Aab (54 mas or 3 AU at 55 pc)—offers the prospect of dynamical mass measurement using astrometric observations within a few years and thus could be important for testing pre–main-sequence evolutionary models. Our observations confirm with 9 σ confidence that the brown dwarf TWA 5B is bound to TWA 5A. We find that the flux ratio of UY Aur has changed dramatically, by more than a magnitude in the H band, possibly as a result of variable extinction. With the smaller flux difference, the system may once again become detectable as an optical binary, as it was at the time of its discovery in 1944. Taken together, our results demonstrate that adaptive optics on large telescopes is a powerful tool for detecting tight companions and thus exploring the frequency and configurations of close multiple systems.

Key words: binaries: close — circumstellar matter — stars: pre–main-sequence — techniques: high angular resolution

1. INTRODUCTION

Nearby young stellar associations offer unique advantages for detailed studies of star and planet formation (Jayawardhana & Greene 2001). In particular, their proximity in combination with modern adaptive optics facilitates sensitive studies of individual star systems down to physical scales of ~3 AU, closing the gap between spectroscopic and visual binaries and thereby offering the prospect of a complete census of multiplicity among young pre–main-sequence (PMS) stars down to substellar masses. Completeness in sampling the binary frequency is important to avoid bias in the understanding of formation and evolution of multiple star systems. Several studies have shown multiplicity frequencies to be significantly higher among PMS stars than their main-sequence (MS) counterparts (Duchêne 1999). Suggested explanations for this discrepancy include observational sample/sensitivity bias, environmental or evolutionary effects, such as disruption of binaries by close approaches of other stars (Ghez, Neugebauer, & Matthews 1993), ejections of low-mass companions in multiple systems (e.g., Bate, Bonnell, & Bromm 2002), or even stellar mergers.

Historically, the determination of MS binary orbits, and thus their dynamical masses, have been critical for the successful theory of stellar structure developed in the early twentieth century. Unfortunately, the nearest known PMS stars, at a distance of ~150 pc, had been until recently too far away to resolve companions with reasonably short orbital periods. Resolving companions spatially is important, since spectroscopic observations by themselves only yield the relative masses of binaries. By resolving a spectroscopic binary spatially down to a physical scale of a few AU, it is not only possible to determine the dynamical masses of the components, but also to derive an independent distance to the system. Therefore, spatially resolved PMS binaries are essential tools for testing models of PMS stellar structure and evolution (Palla & Stahler 2001). An interesting recent example is the dynamical mass determination of the T Tauri binary NTT 045251+3016 by Steffen et al. (2001); using precise radial velocity and astrometric data, they show that it is now possible to derive the stellar masses without any astrophysical assumption and compare with PMS evolutionary tracks.

A third important reason to search for companions of PMS stars is to clear up the ambiguity when placing them on evolutionary luminosity-color diagrams. An unresolved PMS binary will show a luminosity (and possibly color) different from the individual components, thereby biasing any conclusions drawn from evolutionary diagrams (for an extensive review, see Mathieu 1994).

Due to their proximity, the nearby young associations MBM 12 (Luhman 2001) and TW Hydrae (Kastner et al. 1997) are prime targets for detailed studies of circumstellar

disks and close companions. Jayawardhana et al. (1999b) conducted a census of disks among TW Hydrae association (TWA) members, and Jayawardhana et al. (1999a) showed that most of the mid-infrared emitting dust in the 1.″4 binary Hen 3-600 is associated with the primary. A similar study of MBM 12 members was reported by Jayawardhana et al. (2001), who found that six of the eight stars observed harbored significant mid-infrared excess; four of these disks have now also been detected in the (sub-)millimeter (Itoh et al. 2003; Hogerheijde et al. 2003). Using adaptive optics (AO) on Gemini North, Jayawardhana et al. (2002) resolved LkHα 263 (MBM 12-3) into a 0.″415 binary and imaged a companion edge-on disk 4.″115 away. Chauvin et al. (2002) reported several additional binaries in MBM 12, and Macintosh et al. (2001) reported a 55 mas binary in TWA. In this work, we report the results of an AO survey of the inner (subarcsecond) regions of UY Aur and member stars of MBM 12 and TWA, in search of close companions. Among the 24 stars we observed, we found six close binaries and a triple not known at the time and confirmed four known binaries.

2. OBSERVATIONS

We surveyed 24 young stars on 2000 February 22–23 with the 10 m Keck II telescope on Mauna Kea, Hawaii, using AO (Wizinowich et al. 2000) and the near-infrared (NIR) camera KCam. KCam is based on a 256 × 256 pixel NICMOS3 HgCdTe array and was provided by the University of California as an early interim engineering grade camera. The pixel scale was measured on 2000 February 21 by Macintosh et al. (2001) to be 17.47 ± 0.06 mas pixel^{-1}. Since one 128 × 128 quadrant of KCam is nonfunctional, the field of view was L-shaped with 2.″24 per quadrant. We observed the targets by co-adding 1–20 exposures of integration time 0.62–60 s each and then moving the target to another quadrant of the array, so that the target was located in each of the three working quadrants at least once. The science target itself was used as a wave front sensor for the AO system, except in the case of TWA 9B, where we used TWA 9A. We observed through three different filters, J (1.26 μm), H (1.648 μm), and K' (2.127 μm), located in a cold filter wheel. The Strehl ratio during the two nights was 0.20–0.25 in H.

3. DATA REDUCTION AND ANALYSIS

The data reduction was done in a standard way by subtracting sky frames from source frames and then dividing by a flat obtained on-sky during dusk. We also corrected for the substantial number of bad pixels. Cosmic-ray hits were less of a problem because the exposures were short. For a frame with the target in a given quadrant of the array, the sky frame was obtained by averaging the frames with the target in one of the other two quadrants. For binaries with separations greater than ~2″, the secondary was only visible on one frame out of three, and only one frame was free from sources in the right quadrants to be used as a sky.

Due to the small field of view and the variability of the AO point-spread function (PSF), it is not possible to obtain accurate absolute photometry. Relative photometry and astrometry of binary systems were measured on multiple frames and then combined to get an estimate of the errors. We did aperture photometry with a diameter of 4 pixels, except for the close binaries in the TWA 5A and S18B systems where we used apertures with a diameter of only 2 pixels. The contamination from the companion into the aperture was estimated by placing an aperture also on the opposite side of the companion. To obtain accurate astrometry of these tight binaries, we used the myopic deconvolution algorithm IDAC (Christou et al. 1999). IDAC estimates the PSF simultaneously with the deconvolved image but needs a series of exposures with varying PSFs and/or accurate estimates of the PSF. For TWA 5A, we used seven frames in H, but for S18B we had only three H frames. Since S18 is a triple, however, we could make use of the primary S18A as an accurate simultaneous PSF estimate. Based on comparisons with Jayawardhana et al. (2002) and Chauvin et al. (2002), the systematic errors in our astrometry due to array orientation uncertainties are likely to be ~1°.

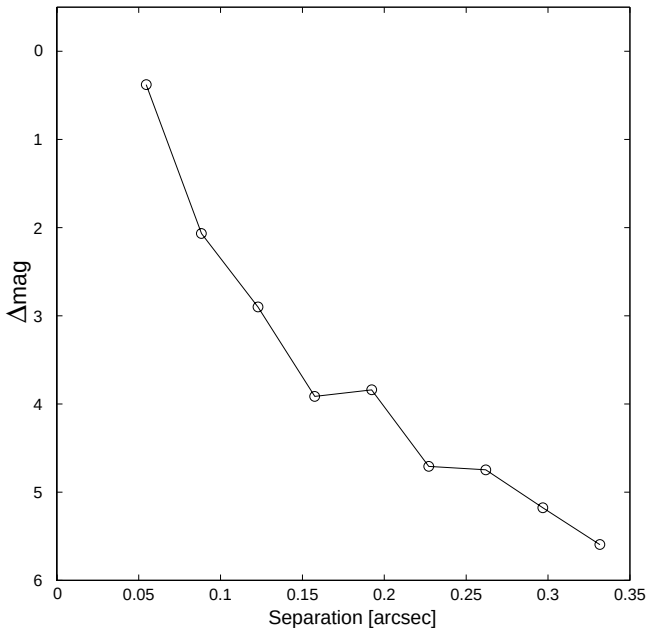

FIG. 1.—Approximate 5 σ detection contrast sensitivity as a function of separation. The inner 0.″3 are dominated by speckle noise, while sky noise causes the curve to flatten out to a flux ratio of Δmag = 6–7.

In order to estimate our sensitivity to finding close faint companions, we measured the speckle noise from observed PSFs of single stars. Our approximate 5 σ detection limit as a function of separation is shown in Figure 1.

4. RESULTS AND DISCUSSION

Among the nine proposed members in the MBM 12 association we observed, we found five to be binaries, all previously reported by Chauvin et al. (2002) and one to be a new triple (Table 1). To calculate the multiplicity frequency of the 12 proposed members of MBM 12 (Luhman 2001), we assume that LkHα 262 and LkHα 263 are part of the same quadruple system (Jayawardhana et al. 2002) and count LkHα 264 and MBM 12-10 as binaries (Chauvin et al. 2002).[1] The multiplicity frequency, defined as mf = (b +

[1] HD 17332, RX J0255.3+1915, and RX J0306.1+1921 are not counted because they are not likely to be PMS members of MBM 12 (see Jayawardhana et al. 2001 and Luhman 2001).

TABLE 1
MULTIPLE STARS OBSERVED ON 2000 FEBRUARY 22–23

OBJECT DESIGNATION	FLUX RATIOS			SEPARATION (arcsec)	POSITION ANGLE[a] (deg)
	J (1.26 μm)	H (1.65 μm)	K' (2.13 μm)		
HD 17332	...	1.58 ± 0.05	...	3.66 ± 0.02	309.39 ± 0.02
RX J0255.3+1915	31.5 ± 0.5	24.7 ± 0.1	24 ± 5[b]	1.025 ± 0.004	160.27 ± 0.03
RX J0255.4+2005	1.01 ± 0.01	1.00 ± 0.01	1.05 ± 0.05	0.533 ± 0.003	101.81 ± 0.04
LkHα 263	1.25 ± 0.03	1.10 ± 0.02	0.89 ± 0.05	0.416 ± 0.003	232.67 ± 0.05
E02553+2018	1.06 ± 0.05	1.37 ± 0.03	1.7 ± 0.2	1.144 ± 0.005	163.77 ± 0.03
S18A/(Ba+Bb)	1.25 ± 0.02	1.35 ± 0.01	1.3 ± 0.2	0.747 ± 0.005	130.34 ± 0.4
S18Ba/Bb	...	1.13 ± 0.05	...	0.063 ± 0.004	56.52 ± 1.6
UY Aur	...	1.47 ± 0.01	...	0.894 ± 0.004	228.82 ± 0.03
TWA 2	...	1.98 ± 0.07	...	0.547 ± 0.003	30.49 ± 0.04
TWA 3	...	1.8 ± 0.1	...	1.477 ± 0.006	215.78 ± 0.09
TWA 5(Aa+Ab)/B	120 ± 20	112 ± 13	98 ± 26[b]	1.954 ± 0.008	359.16 ± 0.08
TWA 5Aa/Ab	0.94 ± 0.05	1.09 ± 0.08	1.11 ± 0.07	0.054 ± 0.003	24.15 ± 2.8

[a] Position angles are measured from north to east. Quoted errors are relative; the systematic errors, due to array orientation uncertainties, are likely to be ~1°.
[b] These relatively large errors are due to unfortunate placements of the secondary on some bad pixels in the array.

$t + q)/(s + b + t + q)$, where s, b, t, and q are the number of single, double, triple, and quadruple systems, respectively, is found to be $(5 + 1 + 1)/(4 + 5 + 1 + 1) = 0.64 \pm 0.16$, where the quoted error is statistical. Similarly, the average number of companions per star system, defined as $\mathrm{csf} = (b + 2t + 3q)/(s + b + t + q)$ (Duchêne 1999), equals $(5 + 2 \times 1 + 3 \times 1)/(4 + 5 + 1 + 1) = 0.91 \pm 0.30$.

In TWA, we found no new companion candidates apart from the TWA 5A 54 mas binary, which was also found independently by Macintosh et al. (2001). The corresponding multiplicity numbers for TWA are $\mathrm{mf} = 0.58 \pm 0.12$ and $\mathrm{csf} = 0.84 \pm 0.22$, where we have counted the companions in the systems TWA 1–19, as reported by Webb et al. (1999) and Zuckerman et al. (2001). TWA 5 was assumed to be a quadruple system, including the brown dwarf TWA 5B and a spectroscopic binary in TWA 5A (see 4.2). This only affects csf, since mf is insensitive to multiple companions. Both TWA and MBM 12 have multiplicity numbers that are on the high side compared with those reported for other young associations (Duchêne 1999), although the significance of this result is low due to the small number statistics.

In Table 2, we give the coordinates and absolute NIR fluxes for the components as inferred from the Two Micron All-Sky Survey (2MASS). We plainly divided the unresolved 2MASS flux to the stars according to our measured flux ratios. Note that the epoch of the 2MASS observations differ by ~2 yr from ours, so variations in flux may introduce errors in addition to the propagated errors quoted in the table. In Table 3, we present stars that did not reveal close companions in our survey.

4.1. *S18*

S18 in MBM 12 was reported to be a 0.″753 binary by Chauvin et al. (2002). In our H-band observations, we resolve the secondary B into a tight Ba/Bb 63 mas binary in itself (Fig. 2). Note the close similarity in configuration and scale with the triple stars VW Chamaeleontis (Brandeker et al. 2001) and T Tauri (Duchêne, Ghez, & McCabe 2002). In J and K, we were unable to resolve B sufficiently to measure the flux ratio accurately. If we assume the distance to MBM 12 to be ~275 pc (Luhman 2001), then the projected distance between the stars is ~17 AU. Using Kepler's third

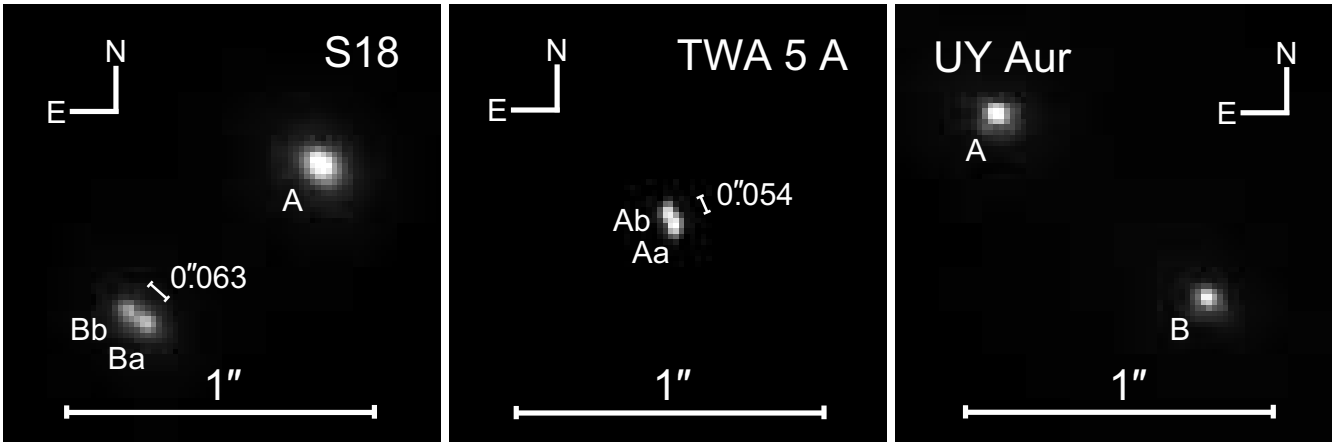

FIG. 2.—Sharpest H-band frames obtained of the young multiple star systems S18, TWA 5A, and UY Aur. The image scale is 17.5 mas pixel^{-1}. North is up, and east is to the left.

TABLE 2
INFERRED PHOTOMETRY OF MULTIPLE SYSTEM COMPONENTS

OBJECT DESIGNATION	α (J2000.0)	δ (J2000.0)	IR MAGNITUDES[a]		
			J	H	K_s
HD 17332A	02 47 27.42	19 22 18.6	...	6.10 ± 0.03	...
HD 17332B			...	6.59 ± 0.04	...
RX J0255.3+1915A	02 55 16.60	19 15 01.5	9.36 ± 0.02	9.10 ± 0.03	9.02 ± 0.03
RX J0255.3+1915B			13.10 ± 0.04	12.58 ± 0.03	12.49 ± 0.25
RX J0255.4+2005A	02 55 25.78	20 04 51.7	10.54 ± 0.03	9.93 ± 0.03	9.72 ± 0.05
RX J0255.4+2005B			10.54 ± 0.03	9.93 ± 0.03	9.77 ± 0.05
LkHα 263A	02 56 08.42	20 03 38.6	11.26 ± 0.03	10.55 ± 0.03	10.32 ± 0.05
LkHα 263B			11.50 ± 0.04	10.65 ± 0.03	10.19 ± 0.05
E02553+2018A	02 58 11.23	20 30 03.5	9.98 ± 0.05	9.09 ± 0.04	8.60 ± 0.06
E02553+2018B			10.04 ± 0.05	9.43 ± 0.04	9.18 ± 0.09
S18A	03 02 21.05	17 10 34.2	11.31 ± 0.03	10.49 ± 0.03	10.18 ± 0.09
S18B(a+b)			11.55 ± 0.03	10.82 ± 0.03	10.47 ± 0.11
S18Ba			...	11.51 ± 0.05	...
S18Bb			...	11.64 ± 0.05	...
UY Aur A	04 51 47.38	30 47 13.4	...	8.26 ± 0.07[b]	...
UY Aur B			...	8.68 ± 0.10[b]	...
TWA 2A	11 09 13.81	−30 01 39.8	...	7.37 ± 0.05	...
TWA 2B			...	8.11 ± 0.07	...
TWA 3A	11 10 28.0	−37 31 53	...	7.53 ± 0.05	...
TWA 3B			...	8.15 ± 0.07	...
TWA 5Aa	11 31 55.27	−34 36 27.4	8.46 ± 0.05	7.69 ± 0.07	7.45 ± 0.05
TWA 5Ab			8.39 ± 0.05	7.79 ± 0.08	7.56 ± 0.06

NOTES.—Units of right ascension are hours, minutes, and seconds, and units of declination are degrees, arcminutes, and arcseconds. Coordinates are from Luhman 2001, Webb et al. 1999, or the Tycho-2 Catalogue (Høg et al. 2000). The absolute photometry has been inferred from 2MASS measurements (the All-Sky Data Release) of the unresolved systems together with our obtained flux ratios.

[a] The reported uncertainties are only the propagated errors from the 2MASS photometry and our flux ratios. The epoch difference (~1998 for 2MASS and 2000 for our data) introduces an additional, but unknown, error due to the variability of the stars.

[b] For the primary UY Aur A, we adopt the H magnitude of Close et al. (1998) and then assume that the observed change of flux ratio is entirely due to the companion getting brighter. See also § 4.3.

law and assuming a circular orbit, we get the orbital period $P = 71(M_B\alpha^3)^{-1/2}$ yr, where α is the projection factor [observed (projected) separation/real separation], and M_B is the system mass of S18Ba/Bb in solar units. This corresponds to an average motion in position angle of $5.0(M_B\alpha^3)^{1/2}$ deg yr^{-1}, and should be readily detected within a year. Similarly, the relative radial velocity amplitude is $7.3(M_B\alpha)^{1/2}$ (sin i) km s^{-1}, which may also be measurable over the period of a few decades unless the inclination i, the angle between the orbital plane, and the plane of sky is very small.

TABLE 3
STARS WITHOUT DETECTED CLOSE ($\lesssim 1\farcs6$) COMPANIONS

Object Designation	α (J2000.0)	δ (J2000.0)	Observed Band
LkHα 262	02 56 07.99	20 03 24.3	H, K'
LkHα 264	02 56 37.56	20 05 37.1	H, K'
RX J0258.3+1947	02 58 16.09	19 47 19.6	J, H
RX J0306.1+1921	03 06 33.1	19 21 52	J, H, K'
TWA 6	10 18 28.8	−31 50 02	H
TWA 7	10 42 30.3	−33 40 17	H
TWA 1	11 01 51.9	−34 42 17	H
TWA 8B	11 32 41.4	−26 52 08	H
TWA 8A	11 32 41.5	−26 51 55	H
TWA 9B	11 48 23.6	−37 28 49	H
TWA 9A	11 48 24.2	−37 28 49	H
TWA 10	12 35 04.3	−41 36 39	H
TWA 11B	12 36 00.8	−39 52 15	H
TWA 11A	12 36 01.3	−39 52 09	H

NOTES.—Coordinates are from Luhman 2001, Hearty et al. 2000, Webb et al. 1999, or the Tycho-2 Catalogue (Høg et al. 2000). Our observations are sensitive to separations between $0\farcs042$ (diffraction limit at H) and $1\farcs6$ (smallest field-of-view radius, but in some directions out to $3\farcs4$). The contrast sensitivity as a function of separation is depicted in Fig. 1.

4.2. *TWA 5A and 5B*

We found TWA 5A to be a tight 54 mas binary, as also reported by Macintosh et al. (2001). At the distance of TWA (~55 pc; Perryman et al. 1997), this corresponds to a projected separation of only 3 AU. The orbital period is thus $P = 5.2(M_A\alpha^3)^{-1/2}$ yr, corresponding to an average position angle motion of $69(M_A\alpha^3)^{1/2}$ deg yr^{-1}. The radial relative velocity amplitude is $17.3(M_A\alpha)^{1/2}$ sin i km s^{-1}. Follow-up studies of this system have the potential to obtain an accurate dynamical mass estimate within a few years. One possible complication may be the presence of an additional *spectroscopic binary* in the TWA 5A system, as suggested by Webb et al. (1999) and Torres et al. (2003).

Our observations also reveal the brown dwarf companion TWA 5B discovered by Lowrance et al. (1999). With a flux ratio of ~100 (5 mag) and a separation of $1\farcs954$, the companion was not always ideally placed in our L-shaped array. In our K'-band observations, the star was close to the edge, which accounts for large estimated errors in the photometry. The astrometry, however, is excellent, and we can use

this to increase the significance of the companion hypothesis, as previously argued by Neuhäuser et al. (2000). Weintraub et al. (2000) used the *Hubble Space Telescope* to measure accurate relative astrometry on 1998 July 12. By combining their astrometry with our measurements, we conclude that the relative positions between TWA 5A and 5B has changed by $\Delta\alpha = 9.5 \pm 27$ mas and $\Delta\delta = -6 \pm 10$ mas during the 1.61 yr between the epochs. The proper motion of TWA 5A, as found in the Tycho-2 Catalogue (Høg et al. 2000), is $\mu_\alpha = -81.6 \pm 2.5$ mas yr^{-1}, $\mu_\delta = -29.4 \pm 2.4$ mas yr^{-1}. The expected position of a background object is thus excluded at 9 σ, somewhat higher than the 5 σ obtained by Neuhäuser et al. (2000) and consistent with their estimated orbital motion 13.4 ± 4.2 mas yr^{-1} of a bound system.

4.3. *UY Aurigae*

In addition to the young stars in the nearby associations MBM 12 and TWA, we also observed the classical T Tauri binary system UY Aur in the Taurus star-forming region. UY Aur is unique in that it was first discovered as an optical binary in 1944 by Joy & van Biesbroeck (1944) with a flux ratio 0.4–0.5 mag in *V*. By 1992, the companion was no longer visible in optical wavelengths and at least 5 mag fainter than the primary in *R* (0.71 μm) (Herbst, Koresko, & Leinert 1995). The system is obviously variable, with *K*-band flux ratios having varied from $\Delta K = 0.76 \pm 0.06$ mag (White & Ghez 2001) to $\Delta K = 1.38 \pm 0.08$ mag (Leinert et al. 1993). The system was also the second detected to show a circumbinary disk (Dutrey et al. 1996; Duvert et al. 1998; Close et al. 1998). Our *H*-band observation of UY Aur has a too small a field of view and is not sensitive enough to detect the circumbinary disk. We find, however, that the flux ratio in *H* is significantly smaller, 1.47 ± 0.01, than previous measurements, 4.33 ± 0.36 (Close et al. 1998). Unfortunately, we cannot assess whether it is the primary that has dimmed or the secondary that has brightened (or both). Close et al. (1998) derived an extinction of $A_V = 1.0$ mag and $A_V = 9.2$ mag for the primary and secondary, respectively, explaining the very red color of the secondary. If the observed change in flux ratio in *H* is due to a variable extinction, then the implied change in extinction is $\Delta A_H = 1.2$ mag, corresponding to $\Delta A_V = 5.8$ mag (assuming the extinction law $R_V = 5.0$ in Table 1 of Mathis 1990). A crude estimate, using the spectral classes K7 and M0 for the primary and secondary, respectively (Herbst et al. 1995), suggests that the flux ratio in *R* has evolved from $\Delta R = 6.6$ in 1996 October 24 (Close et al. 1998) to $\Delta R = 2.0$ in 2000 February 22 (this work). The system may thus once again have become detectable as an optical binary, just as it was at the time of its discovery in 1944.

5. CONCLUSIONS

We have conducted a survey of the inner regions of nearby young star systems and measured accurate astrometry of epoch 2000 February 22–23 for eight binaries and two triples, as well as flux ratios. Our main conclusions are as follows:

1. The multiplicity frequency and average companion number of the young associations MBM 12 and TWA are very high, although the significance of this result is low because of small number statistics.
2. The T Tauri star S18 is actually a triple system, with a tight binary (0$''$.063 $\sim$17 AU). Its hierarchical configuration is very similar to VW Cha and T Tau. Follow-up astrometric observations may constrain the mass within a few decades.
3. The T Tauri star TWA 5A is resolved into a very tight binary in itself (0$''$.054 $\sim$ 3 AU). Follow-up astrometric and spectroscopic observations within a few years have the potential to accurately measure the dynamical mass of individual components, as well as an independent distance, thus providing an ideal system to test evolutionary models of PMS stars.
4. The brown dwarf TWA 5B is shown to be bound to TWA 5A with 9 σ confidence.
5. The classical T Tauri binary star UY Aur has changed its flux ratio dramatically by more than a magnitude in *H*. The secondary may have once again turned into an optically detectable companion, as it was when first discovered in 1944.

We thank an anonymous referee for helpful comments. We would like to acknowledge the great cultural significance of Mauna Kea for native Hawaiians, and express our gratitude for permission to observe from its summit. We also thank the Keck Observatory staff for their outstanding assistance over the past several years. We have made use of the NASA/IPAC Infrared Science Archive, NASA's Astrophysics Data System Bibliographic Services, the SIMBAD database, and data products from the Two Micron All Sky Survey in our research. This work was supported in part by NASA Origins grant NAG 5-11905 to R. J.

REFERENCES

Bate, M. R., Bonnell, I. A., & Bromm, V. 2002, MNRAS, 336, 705
Brandeker, A., Liseau, R., Artymowicz, P., & Jayawardhana, R. 2001, ApJ, 561, L199
Chauvin, G., Meńard, F., Fusco, T., Lagrange, A.-M., Beuzit, J.-L., Mouillet, D., & Augerau, J.-C. 2002, A&A, 394, 949
Christou, J., Bonaccini, D., Ageorges, N., & Marchis, F. 1999, Messenger, 97, 14
Close, L. M., et al. 1998, ApJ, 499, 883
Duchêne, G. 1999, A&A, 341, 547
Duchêne, G., Ghez, A. M., & McCabe, C. 2002, ApJ, 568, 771
Dutrey, A., Guilloteau, S., Duvert, G., Prato, L., Simon, M., Schuster, K., & Menard, F. 1996, A&A, 309, 493
Duvert, G., Dutrey, A., Guilloteau, S., Menard, F., Schuster, K., Prato, L., & Simon, M. 1998, A&A, 332, 867
Ghez, A. M., Neugebauer, G., & Matthews, K. 1993, AJ, 106, 2005
Hearty, T., Fernández, M., Alcalá, J. M., Covino, E., & Neuhäuser, R. 2000, A&A, 357, 681
Herbst, T. M., Koresko, C. D., & Leinert, C. 1995, ApJ, 444, L93
Høg, E., Fabricius, C., Makarov, V. V., Urban, S., Corbin, T., Wycoff, G., Bastian, U., Schwekendiek, P., & Wicenec, A. 2000, A&A, 355, L27
Hogerheijde, M., Johnstone, D., Matsuyama, I., Jayawardhana, R., & Muzerolle, J. 2003, ApJ, 593, L101
Itoh, Y., et al. 2003, ApJ, 586, L141
Jayawardhana, R., & Greene, T. P., ed. 2001, ASP Conf. Ser. 244, Young Stars Near Earth: Progress and Prospects (San Fransisco: ASP)
Jayawardhana, R., Hartmann, L., Fazio, G., Fisher, R. S., Telesco, C. M., & Piña, R. K. 1999a, ApJ, 520, L41
———. 1999b, ApJ, 521, L129
Jayawardhana, R., Luhman, K. L., D'Alessio, P., & Stauffer, J. R. 2002, ApJ, 571, L51
Jayawardhana, R., Wolk, S. J., Barrado y Navascués, D., Telesco, C. M., & Hearty, T. J. 2001, ApJ, 550, L197
Joy, A. H., & van Biesbroeck, G. 1944, PASP, 56, 123
Kastner, J. H., Zuckerman, B., Weintraub, D. A., & Forveille, T. 1997, Science, 277, 67

Leinert, C., Zinnecker, H., Weitzel, N., Christou, J., Ridgway, S. T., Jameson, R., Haas, M., & Lenzen, R. 1993, A&A, 278, 129
Lowrance, P. J., et al. 1999, ApJ, 512, L69
Luhman, K. L. 2001, ApJ, 560, 287
Macintosh, B., et al. 2001, in ASP Conf. Ser. 244, Young Stars Near Earth: Progress and Prospects, ed. R. Jayawardhana & T. P. Greene (San Fransisco: ASP), 309
Mathieu, R. D. 1994, ARA&A, 32, 465
Mathis, J. S. 1990, ARA&A, 28, 37
Neuhäuser, R., Guenther, E. W., Petr, M. G., Brandner, W., Huélamo, N., & Alves, J. 2000, A&A, 360, L39
Palla, F., & Stahler, S. W. 2001, ApJ, 553, 299
Perryman, M. A. C., et al. 1997, A&A, 323, L49
Steffen, A., et al. 2001, AJ, 122, 997
Torres, G., Guenther, E. W., Marschall, L. A., Neuhäuser, R., Latham, D. W., & Stefanik, R. P. 2003, AJ, 125, 825
Webb, R. A., Zuckerman, B., Platais, I., Patience, J., White, R. J., Schwartz, M. J., & McCarthy, C. 1999, ApJ, 512, L63
Weintraub, D. A., Saumon, D., Kastner, J. H., & Forveille, T. 2000, ApJ, 530, 867
White, R. J., & Ghez, A. M. 2001, ApJ, 556, 265
Wizinowich, P., et al. 2000, PASP, 112, 315
Zuckerman, B., Webb, R. A., Schwartz, M., & Becklin, E. E. 2001, ApJ, 549, L233

Paper V

A&A 402, 183–187 (2003)
DOI: 10.1051/0004-6361:20030194
© ESO 2003

Astronomy & Astrophysics

The 1.2 mm image of the β Pictoris disk*

R. Liseau[1], A. Brandeker[1], M. Fridlund[2], G. Olofsson[1], T. Takeuchi[3], and P. Artymowicz[1]

[1] Stockholm Observatory, SCFAB, Roslagstullsbacken 21, 106 91 Stockholm, Sweden
e-mail: alexis@astro.su.se, olofsson@astro.su.se, pawel@astro.su.se
[2] ESTEC/ESA, PO Box 299, 2200AG Noordwijk, The Netherlands
e-mail: malcolm.fridlund@esa.int
[3] Lick Observatory, University of California Santa Cruz, CA 95064, USA
e-mail: taku@ucolick.org

Received 26 July 2002 / Accepted 5 February 2003

Abstract. We present millimeter imaging observations in the 1200 μm continuum of the disk around β Pic. With the 25″ beam, the β Pic disk is unresolved perpendicularly to the disk plane ($\leq$10″), but slightly resolved in the northeast-southwest direction (26″). Peak emission is observed at the stellar position. A secondary maximum is found 1000 AU along the disk plane in the southwest, which does not positionally coincide with a similar feature reported earlier at 850 μm. Arguments are presented which could be seen in support of the reality of these features. The observed submm/mm emission is consistent with thermal emission from dust grains, which are significantly larger than those generally found in the interstellar medium, including mm-size particles, and thus more reminiscent of the dust observed in protostellar disks. Modelling the observed scattered light in the visible and the emission in the submm/mm provides evidence for the particles dominating the scattering in the visible/NIR and those primarily responsible for the thermal emission at longer wavelengths belonging to different populations.

Key words. stars: individual: β Pictoris – circumstellar matter – planetary systems: formation – protoplanetary disks – ISM: dust, extinction

1. Introduction

Since its discovery by IRAS (e.g., Aumann 1984), the β Pictoris system has presented the prime example of a dusty disk around a main sequence star, partly because of its high degree of "dustiness" ($L_{\rm IR}/L_\star = 2.5 \times 10^{-3}$, e.g. Lagrange et al. 2000) and partly because of its relatively close distance to the Earth (19.3 pc, Crifo et al. 1997), which makes it possible to obtain high quality data over the entire spectral range. Recent papers reviewing the physics of the disk around β Pic include those of Artymowicz (2000), Lagrange et al. (2000) and Zuckerman (2001). Considerable uncertainty existed regarding the age of the system, but most recent estimates place the stellar age close to only ten million years (12^{+8}_{-4} Myr, Zuckerman et al. 2001). This could open up the possibility that planet formation (nearing its final phases?) might actually become observable.

Since these reviews were written, new relevant information has been added to our knowledge of the β Pic system: Olofsson et al. (2001) reported the discovery of widespread atomic gas in the disk, a result recently confirmed and extended by Brandeker et al. (2002). These observations revealed the sense of disk rotation and that the northeast (NE) part of the gaseous disk is extending to the limit of the observations by Brandeker et al., viz. to at least 17″ (330 AU) from the star. Several difficulties were encountered with these discoveries, such as the observed fact that the gas stays on (quasi-)Keplerian orbits, although radiation pressure forces in the resonance lines should accelerate the gas to high velocities and remove it on time scales comparable to the orbital period.

This needs to be addressed in the context of the origin and evolution of the gas and dust, i.e. whether one or both components are presently produced in situ in the disk or whether they (at least to some degree) constitute "left-overs" from the star formation process, being of primordial origin. Takeuchi & Artymowicz (2001) have considered the interaction of gas and dust in a circumstellar disk, the dynamical evolution of which is critically dependent on the relative abundance of these species (see also Lecavelier des Etangs et al. 1998). Possible observational consequences, even relatively far from the central star, may become assessible with modern mm/submm cameras. With the aim to compare and to extend the results obtained at 850 μm with SCUBA by Holland et al. (1998), we performed imaging observations at longer wavelengths and, in this paper, we present the image of the β Pic disk at 1200 μm (1.2 mm).

The SIMBA observations and the reduction of the data are presented in Sect. 2. Our basic result, i.e. the 1.2 mm image

Send offprint requests to: R. Liseau, e-mail: rene@astro.su.se

* Based on observations collected with the Swedish ESO Submillimeter Telescope, SEST, in La Silla, Chile.

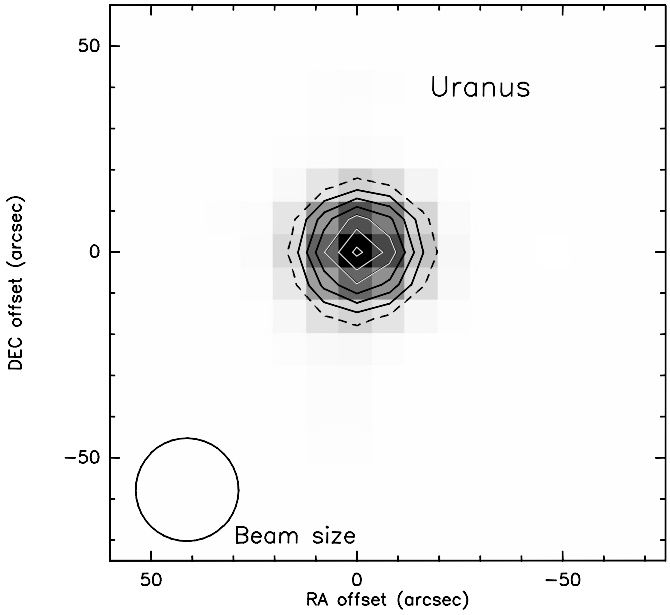

Fig. 1. The normalised SIMBA 1.2 mm image with 8″ pixels of the flux calibrator Uranus, the size of which was 3.″5 in diameter at the time of our observations and, hence, appeared point-like to SIMBA. Offsets in Right Ascension and Declination are in arcsec and the derived circular Gaussian beam of 25″ *FWHM* is shown in the lower left corner. During the scanning alt-az observations, the image rotates which would smear out any low-level features. Contour levels as in Fig. 2.

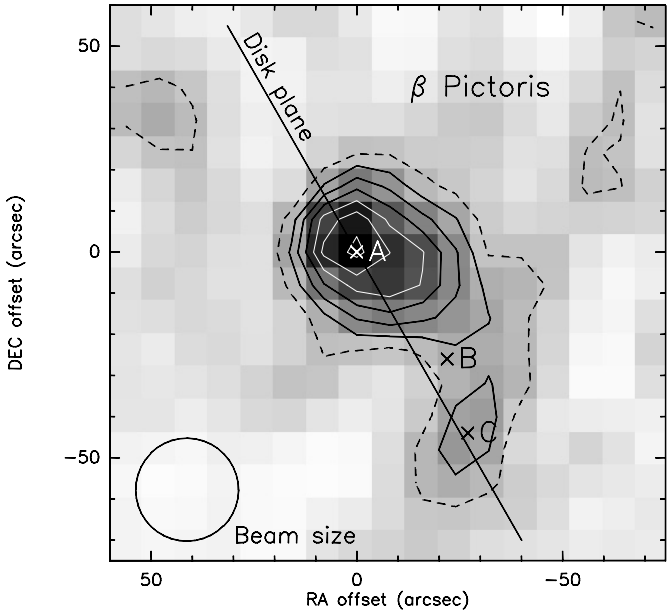

Fig. 2. The β Pic disk imaged at 1.2 mm with a pixel sampling of 8″. The lowest (dashed) contour corresponds to 2σ and increments are by 1σ = 3 mJy/beam. The center coordinates (0, 0) refer to the stellar position and offsets are in arcsec. Features discussed in the text are marked and the optical disk midplane is shown by the straight line at position angle 31.°5. The circular Gaussian beam of 25″ *FWHM* (∼500 AU) is shown to scale in the lower left corner.

of β Pic and its circumstellar disk, is found in Sect. 3, and in Sect. 4 the possible implications of these observations are discussed, where also other data are consulted. Finally, in Sect. 5, we briefly summarise our main conclusions from this work.

2. SIMBA observations and data reductions

The observations were performed with the SEST Imaging Bolometer Array (SIMBA) at the 15 m Swedish-ESO Submillimeter Telescope (SEST), La Silla, Chile, during the periods November 17–23 and 27–29, 2001. SIMBA has been developed by the Max-Planck-Institut für Radioastronomie, Bonn, in collaboration with the Astronomisches Institut der Ruhr-Universität Bochum. The 37 liquid helium cooled semiconductor elements are n-doped silicon chips, mounted on a saphire substrate. Projected on the sky, the 37 horn antennae have each an HPBW of 23″ and are spaced by 44″ in a hexagonal arrangement, covering about 4′. The spectral band pass is centered at 250 GHz (1200 μm) and has a full width at half maximum (*FWHM*) of 90 GHz.

As map centre, the equatorial coordinates of β Pic were used, viz. $05^{\rm h}47^{\rm m}17^{\rm s}.1$, $-51°03'59''$ (J 2000). Generally, the mapping was done in fast mode by scanning 600″ in azimuth and 400″ in elevation at the rate of 80″ per second and with a step size in elevation of 8″, oversampling the beam by about a factor of three. The zenith opacities were obtained by means of frequent sky dips and were on the average 0.22 at the beginning of our observing run, but improved to about 0.15 after a couple of days. The pointing of the telescope was regularly checked using the extragalactic radio source 0537−441 and/or the planet Saturn and was found to be within a third of the beamwidth.

Flux calibrations were based on observations of the planet Uranus. The brightness temperature of 94.8 K at 250 GHz implies a Uranus flux density of 38 Jy/beam, with an uncertainty of 5% (Griffin & Orton 1993). As is evident from Fig. 1, the spatial flux distribution of this point source (diameter 3.″5) is consistent with a circular Gaussian telescope beam, with the measured $FWHM(\parallel, \perp) = (24.''9 \pm 0.''3,\ 24.''6 \pm 0.''3)$. The deviation from a circularly symmetric Gaussian beam pattern occurs at the 1% level of the peak value (−20 db).

In total, we recorded 171 maps with 21 hours of integration. These data were reduced by making use of the MOPSI reduction software package[1] developed by Robert Zylka. This involved correcting for atmospheric extinction, cosmic rays and the variable sky background, as well as producing maps from the fast scanning mode. The sky noise was greatly reduced by correlating and removing the simultaneous flux level variations of the different bolometer channels.

3. Results

The 1200 μm image of the β Pic region is displayed in Fig. 2, where the displayed contours are chosen in compliance with Holland et al. (1998). The flux maximum, designated as feature *A* in the figure, is centered on the position of the star

[1] `http://www.ls.eso.org/lasilla/Telescopes/SEST/SEST.html`

β Pic (0″, 0″). At position angle 237° relative to *A*, an elongation of the emission in the NE–SW direction is discernable. For an assumed Gaussian source flux distribution, the deconvolved minor and major axes are ≤10″ and 26″, respectively, the latter corresponding to 500 AU. The disk emission extends to at least 55″ (1050 AU) in the SW direction. In addition, faint emission protrudes south toward a "blob" at (−27″, −44″). This feature *C*, at position angle 211.°5, is 52″ (1000 AU) distant from the star and is thus not (whether real or not) positionally coincident with the 850 μm-SW blob of Holland et al. 1998 at (−21″, −26″) and identified as *B* in Fig. 2, but we note the following important facts: (1) this faint emission, extending straight south, is also apparent in the 850 μm image, (2) as is evident in Fig. 2, the position angle to blob *C* coincides with that of the midplane of the β Pic disk inferred from optical data (= 31.°5 + 180°; Kalas & Jewitt 1995, Heap et al. 2000), and (3) faint dust scattered light in this direction has been observed far from the star (1450 AU, Larwood & Kalas 2001). Toward the NE, the scattering disk has been claimed to extend even further from the star, to 1835 AU.

An about 2σ feature at (+48″, +32″) and PA = 57° (1100 AU) is discernable in our image, but which would again be significantly offset from a similar blob at (+28″, +25″) in the 850 μm data. In order to assess the reality of these faint features we have divided the raw data into different portions and then applied the same reduction procedures to these subsamples. The result of this exercise indicates that the (+48″, +32″) feature is an artefact introduced by the noise, as it is not seen in all frames, whereas blob *C* is persistently present in the final sub-maps.

The flux densities of both the β Pic disk (*A*) and the SW features (*B* and *C*) are presented in Table 1. The result for the peak flux obtained by Chini et al. (1991)[2] with a single element bolometer at the SEST at 1300 μm, viz. 24.9 ± 2.6 mJy/beam, is in agreement with our array value of 24.3 ± 3.0 mJy/beam at 1200 μm (cf. Fig. 3). The ratio of the peak flux *A* to that of blob *C* is 2.5 ± 0.8.

Table 1. SIMBA 1200 μm flux densities of the β Pic disk.

Feature	Relative Offset (″)	F_ν(1200 μm) (mJy/beam)	Remarks
A	(0, 0)	24.3 ± 3.0	β Pic disk
		35.9 ± 9.7	integrated over a radius of 40″
B	(−21, −26)	...	SW blob (Holland et al. 1998): contaminated by β Pic disk
C	(−27, −44)	9.7 ± 3.0	SW blob (this paper)

4. Discussion

4.1. The β Pic disk

For widely adopted parameters, the stellar disk subtends an angle in the sky of less than 1 mas and the photosphere generates a flux density at the Earth of less than 1 mJy at 1200 μm. The stellar contribution to our SEST measurements can therefore be safely ignored. Also, any line emission in this band pass is likely to be totally negligible (Liseau & Artymowicz 1998; Liseau 1999 and references therein).

Assuming an opacity law of the form $\kappa_\nu = \kappa_0 (\nu/\nu_0)^\beta$, the flux density at long wavelenghts from an optically thin source of a certain dust population can be expressed as

$$F_\nu = \frac{2k\kappa_0\Omega}{c^2\nu_0^\beta}\,\nu^{2+\beta}\int T_{\rm dust}(z)\,{\rm d}z\ . \qquad (1)$$

[2] We assume that these data refer to β Pic and not to α Pic as written in their Table 1.

If the particles dominating the emission at 850 μm and 1200 μm, respectively, can be assumed to yield the same integral, e.g. because they share the common temperature $T_{\rm dust}$ and/or occupy similar locations in space along the line of sight *z*, the average spectral index β can be obtained from our 1200 μm and the 850 μm fluxes by Holland et al. (1998), using

$$\beta = -2 + \frac{{\rm d}\log F_\nu}{{\rm d}\log\nu} = -2 + \frac{\log(F_{850}/F_{1200})}{\log(1200/850)}\ , \qquad (2)$$

yielding $\beta = 0.5$ for a point source at the stellar location. The index becomes $\beta = 1$, if we use the fluxes for the extended source, viz. integrated over a radius of 40″ centered on the star. This includes blob *B*, contributing some 20% to the 850 μm flux. A "correction" for this would again indicate a lower β value and we conclude that the dust in the β Pic disk has a shallow opacity index, perhaps even below unity (Dent et al. 2000 suggest $\beta = 0.8$). This is illustrated in Fig. 3, which displays the long wavelength spectral energy distribution of β Pic, together with weighted Rayleigh-Jeans spectra for $\beta = 0$, 1 and 2, and could mean that the grains dominating the millimeter-wave emission are different from those scattering most efficiently in the visual and the near infrared. This value of β is significantly lower than those found in the interstellar medium (ISM), where typically $\beta \sim 2$ (Hildebrand 1983), but it is similar to that found in *protostellar* disks (e.g., Beckwith et al. 1990; Mannings & Emerson 1994; Dutrey et al. 1996), indicating significant differences between the dust particles in the ISM and those in the β Pic disk. As was also already concluded by Chini et al. (1991), the presence of relatively large grains is suggested, with maximum radii in excess of 1 mm ($\max a/\lambda \gtrsim 1$). Intriguing, however, is the existence of such large grains possibly as far away as 1000 AU from the star (see, e.g., Takeuchi & Artymowicz 2001; Lecavelier des Etangs et al. 1998).

4.2. Weak dust features in the 1.2 mm image

The asymmetric flux distribution displayed in Fig. 2 may be surprising. In agreement with our observations, Chini et al. (1991) and Dent et al. (2000) too were unable to detect any emission in the northeast part of the disk, where we place a 3σ-upper limit on the mass of 0.2 $M_\oplus$ (see below; the dust temperature at 500 AU $T_{\rm dust} = 45$ K, when $T_{\rm dust}(r) = 110\,(r/26\ {\rm AU})^{-0.3}$ K, see Liseau & Artymowicz 1998).

Given the low signal-to-noise ratio (S/N), the reality of this lopsidedness is difficult to assess, but asymmetries in the β Pic

disk have been noticed also at other wavelengths. For instance, in scattered light, the receding NE side of the disk extends much further and is much brighter than the SW disk. In contrast, the shorter, approaching SW disk seems much thicker (Kalas & Jewitt 1995; Larwood & Kalas 2001). The situation is reversed in the thermal infrared (albeit on smaller spatial scales), where the SW disk appears significantly brighter and more extended than the NE side (Lagage & Pantin 1994; Wahhaj et al. 2002; Weinberger et al. 2002). This could be due to a "Janus-effect", i.e. the NE being dominated by "bright" dust particles (high albedo, silicates), whereas in the SW, the majority of dust grains is "dark" (high absorptivity, carbonaceous?). What would accomplish such uneven distribution in the disk is not clear, but large differences in albedo, by more than one order of magnitude, are not uncommon, for instance, in solar system material. Also, in order to understand the nature of feature *C* (and *B*) velocity information would be valuable.

Blob *C* would be situated in the disk midplane and on the *second* contour in the scattered light image of Larwood & Kalas (2001) ($22 < R < 25\,\mathrm{mag/arcsec^2}$, see also Kalas & Jewitt 1995). No obvious distinct feature is seen at its position. However, to be detectable with SIMBA at the SEST, any point source at mm-wavelengths would not be point-like at visual wavelengths, and its optical surface brightness could be very low.

To gain some quantitative insight we ran numerical models, exploiting Mie-theory, for a variety of plausible dust mixtures regarding the chemical composition and grain size distributions (for details, see Pantin et al. 1997). The equilibrium temperatures were found to be in the interval 16 K to 58 K and depending on the dust albedo and scattering phase function, the predicted integrated scattered light, to be consistent with our SEST observations, spans 8 magnitudes. The two most extreme cases considered were (1) bright cold dust (albedo = 1 at visual wavelengths, $T_{\rm dust} = 16$ K) which is scattering isotropically and has albedo = 0.2 at thermal wavelengths, which results in a spatially integrated *R*-magnitude of 17.3 and (2) dark warm dust (albedo = 0.02 in the visual, $T_{\rm dust} = 58$ K) which gives rise to "comet scattering", i.e. 14% of isotropic at 90°, and has zero albedo at thermal wavelengths, resulting in an integrated *R*-magnitude of 25.6. These extreme cases are felt to be either too optimistic or too conservative and an intermediate case might be more appropriate. Our adopted model includes isotropically scattering dust at $T_{\rm dust} = 25$ K with albedo = 0.2 at visual and zero albedo at thermal wavelengths, yielding an integrated *R*-magnitude of 20. An about 10″ source ($R = 25\,\mathrm{mag/arcsec^2}$) would thus be consistent with both the optical data and our SIMBA measurement and a deep *R*-band search might become successful. Similarly, the integrated 850 μm flux density is predicted to be slightly less than 18 mJy and should become readily detectable. However, blob *C* is situated outside the figure of Holland et al. 1998.

Feature *C* is perfectly aligned with the optical disk plane, and its (hypothetical) mass can be estimated from

$$M_{\rm dust} = \frac{D^2\, F_\nu}{\kappa_\nu\, B_\nu(T_{\rm dust})}\ , \qquad (3)$$

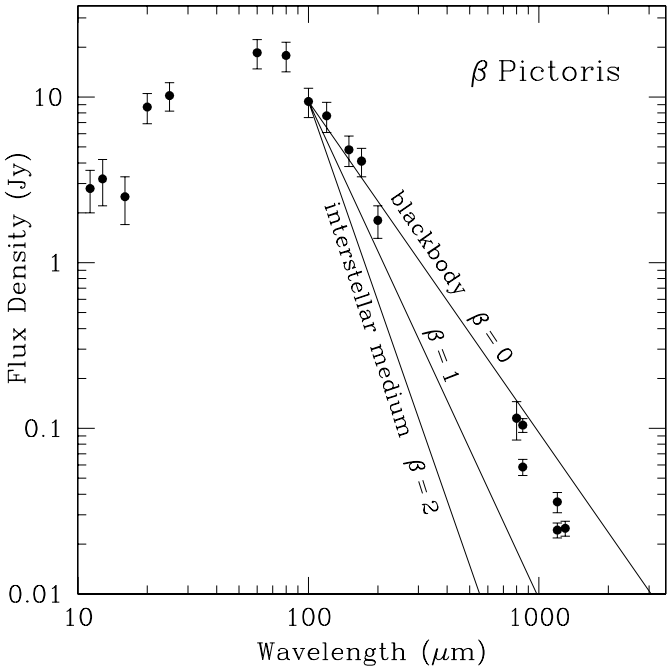

Fig. 3. The SED of the β Pic disk from 10 to 1300 μm. Data up to 200 μm are from Heinrichsen et al. (1999) (52″ to 180″). The datum at 800 μm is from Zuckerman & Becklin (1993) (integrated over a radius = 25″). The 850 μm data are from Holland et al. (1998) and refer to a 14″ beam and to the integrated flux over a radius = 40″. The latter should be comparable to our 1200 μm point for 40″; the lower is for a 25″ beam, and that at 1300 μm (24″ beam) is from Chini et al. (1991). For reference, the spectral slopes longward of 100 μm for three values of the dust emissivity index β, discussed in the text, are shown by the straight lines.

where the distance *D* is assumed to be that of β Pic and the adopted *dust* absorption coefficient $\kappa_{250\,\mathrm{GHz}} \sim 1\,\mathrm{cm^2\,g^{-1}}$. This estimate of κ_ν is probably correct within a factor of three (Beckwith et al. 2000 and references therein). For the dust temperature $T_{\rm dust} = 25$ K, the dust mass is of the order of ten lunar masses ($0.16\,M_\oplus$), which would be comparable to the dust mass of the disk proper, being overall much warmer. Another factor of about three uncertainty stems thus from the dust temperature, provided $10\,\mathrm{K} < T_{\rm dust} < 60\,\mathrm{K}$.

The famous "SW-blob" in the 850 μm image has received considerable interest by the debris disk community. According to Dent et al. (2000), this feature, labelled *B* in Fig. 2, is real. It is not readily apparent in our 1200 μm image, however, presumably due to the combination of low contrast and reduced angular resolution. To test this idea, we performed numerical experiments, i.e. convolving two point sources, at the appropriate positions of *A* and *B* and with varying flux ratios, with the SIMBA beam. Flux ratios, normalised to the peak value, which are consistent with our observations are in the range 0.25–0.45, with the most compelling being about 0.3 (comparable to that for blob *C*). In combination with feature *C*, blob *B* accounts for the southward bridge seen in Fig. 2.

For radiation mechanisms generating power law spectra and/or thermal dust emission from blob *B*, the spectral slope is given by $\alpha = \beta_A + 2 - \Delta \log R_\lambda / \Delta \log \lambda$, where β_A,

as before, refers to $A = (0'', 0'')$, i.e. the β Pic disk, and where $R_\lambda = [F_\nu(A)/F_\nu(B)]_\lambda$ and $\lambda = 850\,\mu$m or $1300\,\mu$m. Because of the relatively low S/N of the SCUBA and SIMBA data, the actual flux ratios are highly uncertain and, furthermore, calibration uncertainties and telescope beam effects could potentially introduce large errors. The combined observations of blob B suggest $\log(R_{850}/R_{1200}) \sim 0$, yielding $\beta_B \sim \beta_A$, i.e. consistent with the spectrum of A.

5. Conclusions

Based on $1200\,\mu$m imaging observations of the circumstellar dust of β Pic we conclude the following:

- At $25''$ resolution, the $1200\,\mu$m image of the β Pic disk is slightly resolved in the NE–SW direction, but remains unresolved perpendicularly (NW–SE). In addition, the emission appears asymmetric and extends further SW–S to more than 1000 AU away from the star. Maximum emission (= 24 mJy) is observed toward the position of the star.
- Combining our $1200\,\mu$m map with that by Holland et al. (1998) at $850\,\mu$m we infer that the dust size distribution in the β Pic disk is significantly different from that in the general interstellar medium and appears more reminiscent of that found in protostellar disks. We argue that the thermal emission is dominated by dark big particles and that these grains constitute a population different from that dominating the scattering in the visible/NIR part of the spectrum.
- From the examination and numerical simulations of the available data (optical and submm/mm) for the southwestern blobs/extensions seen in the SIMBA maps we conclude that their reality can at present neither be excluded nor can, on the basis of the available evidence, their existence be fully confirmed.

Acknowledgements. We are grateful to Dr. José Afonso, who made available to us the Uranus calibration data, and to the SEST staff for providing additional observations. The critical comments by the anonymous referee are highly appreciated.

References

Artymowicz, P. 2000, SSR, 92, 69
Aumann, H. H. 1984, BAAS, 16, 483
Beckwith, S. V. W., Sargent, A. I., Chini, R. S., & Güsten, R. 1990, AJ, 99, 924
Beckwith, S. V. W., Henning, T., & Nakagawa, Y. 2002, in Protostars and Planets IV, ed. V. Mannings, A. P. Boss, & S. S. Russell (University of Arizona), 533
Brandeker, A., Liseau, R., Olofsson, G., & Fridlund, M. 2002, in Debris disks and the formation of planets: a Symp. in memory of Fred Gillet, ed. L. Caroff, & D. Backman (ASP), in press
Chini, R., Krügel, E., Shustov, B., Tutukov, A., & Kreysa, E. 1991, A&A, 252, 220
Dent, W. R. F., Walker, H. J., Holland, W. S., & Greaves, J. S. 2000, MNRAS, 314, 702
Dutrey, A., Guilloteau, S., Duvert, G., et al. 1996, A&A, 309, 493
Crifo, F., Vidal-Madjar, A., Lallement, R., Ferlet, R., & Gerbaldi, M. 1997, A&A, 320, L 29
Griffin, M. J., & Orton, G. S. 1993, Icarus, 105, 537
Heinrichsen, I., Walker, H. J., Klaas, U., Sylvester, R. J., & Lemke, D. 1999, MNRAS, 304, 589
Heap, S. R., Lindler, D. J., Lanz, T. M., et al. 2000, ApJ, 539, 435
Hildebrand, R. H. 1983, QJRAS, 24, 267
Holland, W. S., Greaves, J. S., Zuckerman, B., et al. 1998, Nature, 392, 788
Kalas, P., & Jewitt, D. 1995, AJ, 110, 794
Lagage, P. O., & Pantin, E. 1994, Nature, 369, 628
Lagrange, A.-M., Backman, D. E., & Artymowicz, P. 2000, in Protostars and Planets IV, ed. V. Mannings, A. P. Boss, & S. S. Russell (University of Arizona), 639
Larwood, J. D., & Kalas, P. G. 2001, MNRAS, 323, 402
Lecavelier des Etangs, A., Vidal-Madjar, A., & Ferlet, R. 1998, A&A, 339, 477
Liseau, R. 1999, A&A, 348, 133
Liseau, R., & Artymowicz, P. 1998, A&A, 334, 935
Mannings, V., & Emerson, J. P. 1994, MNRAS, 267, 361
Olofsson, G., Liseau, R., & Brandeker, A. 2001, ApJ, 563, L 77
Pantin, E., Lagage, P. O., & Artymowicz, P. 1997, A&A, 327, 1123
Takeuchi, T., & Artymowicz, P. 2001, ApJ, 557, 990
Wahhaj, Z., Koerner, D. W., Werner, M. W., & Backman, D. E. 2002, in Debris disks and the formation of planets: a Symp. in memory of Fred Gillet, ed. L. Caroff, & D. Backman (ASP), in press
Weinberger, A., Becklin, E., & Zuckerman, B. 2002, in Debris disks and the formation of planets: a Symp. in memory of Fred Gillet, ed. L. Caroff, & D. Backman (ASP), in press
Zuckerman, B. 2001, ARA&A, 39, 549
Zuckerman, B., & Becklin, E. E. 1993, ApJ, 414, 793
Zuckerman, B., Song, I., Bessell, M. S., & Webb, R. A. 2001, ApJ, 562, L 90

Paper VI

THE ASTROPHYSICAL JOURNAL, 563:L77–L80, 2001 December 10
© 2001. The American Astronomical Society. All rights reserved. Printed in U.S.A.

WIDESPREAD ATOMIC GAS EMISSION REVEALS THE ROTATION OF THE β PICTORIS DISK[1]

GÖRAN OLOFSSON, RENÉ LISEAU, AND ALEXIS BRANDEKER
Stockholm Observatory, SCFAB, SE-106 91 Stockholm, Sweden; olofsson@astro.su.se
Received 2001 October 2; accepted 2001 October 30; published 2001 November 26

ABSTRACT

We present high-resolution Na I D spectroscopy of the β Pictoris disk, and the resonantly scattered sodium emission can be traced from less than 30 AU to at least 140 AU from the central star. This atomic gas is coexistent with the dust particles, suggestive of a common origin or source. The disk rotates toward us in the southwest and away from us in the northeast. The velocity pattern of the gas finally provides direct evidence that the faint linear feature seen in images of the star is a circumstellar disk in Keplerian rotation. From modeling the spatial distribution of the Na I line profiles, we determine the effective dynamical mass to be $1.40 \pm 0.05\ M_{\odot}$, which is smaller than the stellar mass, $1.75\ M_{\odot}$. We ascribe this difference to the gravity opposing the radiation pressure in the Na I lines. We argue that this is consistent with the fact that Na is nearly completely ionized throughout the disk (Na I/Na $< 10^{-4}$). The total column density of sodium gas is $N(\mathrm{Na}) = 10^{15}\ \mathrm{cm}^{-2}$.

Subject headings: circumstellar matter — planetary systems: protoplanetary disks — stars: individual (β Pictoris)

1. INTRODUCTION

The β Pictoris disk has been the subject of intense studies ever since it was shown to have excess emission in the thermal infrared by the *IRAS* mission (Aumann 1985). The dust particles giving rise to the infrared emission also scatter the stellar light, and coronagraphic techniques revealed an elongated structure (Smith & Terrile 1984) that recently has been extremely well characterized by means of *Hubble Space Telescope* (*HST*) observations (Heap, Lindler, & Lanz 2000). Although the general impression of these images is that of a high degree of smoothness and symmetry, Heap et al. (2000) show that the peak of the elongated scattered emission has wiggles that suggest that the inner part of the disk is tilted relative to the outer part. There is also evidence for asymmetries and structures in the radial light distribution of this inner disk. Asymmetries have also been observed in the mid-IR (Pantin, Lagage, & Artymowicz 1997).

These asymmetries and the remarkable discovery (Vidal-Madjar et al. 1994; Lagrange, Backman, & Artymowicz 2000) of comet-like bodies occasionally occulting the star and giving rise to high-velocity absorption lines reveal dynamical activity that generally is interpreted as evidence for planetary disturbances (Artymowicz 1997; Augereau et al. 2001).

When it comes to the gas component in the disk, the situation is at present confusing. Absorption spectroscopy in the optical and UV shows a stable component at the same radial velocity as the star (Vidal-Madjar et al. 1986; Lagrange et al. 1998). One would expect radial expansion of this gas, caused by the radiation pressure of the star, and as a possible explanation a ring of atomic hydrogen has been proposed (Lagrange et al. 1998). If present, such a ring must be close to the star since widespread H I is not detected at 21 cm (Freudling et al. 1995). CO has been detected by means of UV spectroscopy (Roberge, Feldman, & Lagrange 2000), but sensitive searches for CO emission in the radio region have failed to detect this molecule (Liseau & Artymowicz 1998). Molecular hydrogen is not detected in UV absorption spectra (Lecavelier des Etangs et al. 2001), but, on the other hand, *Infrared Space Observatory*/Short-Wave Spectrometer spectroscopy (Thi et al. 2001) indicates H_2 emission lines that, if real (the signal-to-noise ratio is low), require large amounts of molecular hydrogen in a spatial distribution that has a void in the line of sight toward the star.

So far, it has not been possible to directly probe the velocity pattern along the disk, lacking the detection of spatially resolved gas emission (except a possible detection of Fe II emission very close to the star; Lecavelier des Etangs, Hobbs, & Vidal-Madjar 2000). In the present Letter, we report the detection of the resonance Na I doublet lines at 5990 and 5996 Å.

2. OBSERVATIONS AND RESULTS

The star β Pic was observed in 2001 January 2–4 with the echelle spectrograph ESO Multi-Mode Instrument on the 3.5 m New Technology Telescope at ESO, La Silla, Chile. For the Na I D1/D2 observations, we used a 5′ long slit and therefore omitted the cross-disperser. Instead, we inserted an order-sorting interference filter, which was centered at 5890 Å and had a width of 60 Å. We have measured the filter profile and are in control of the leakage from the neighboring orders (less than 3% and 4%, respectively). With a wavelength resolution of 6×10^4 ($\Delta v = 5\ \mathrm{km\ s}^{-1}$), this instrumental setup can be viewed as some sort of a "spectroscopic coronagraph," in which the high dispersion is used to prevent the saturation of the detector (CCD) by the very bright stellar point source. Still, the overheads of the observing time were dominated by detector readout times since integration times of individual observations were typically only 300 s. The total integration time was chosen such that the co-added spectra should permit the detection of the faint light scattered off the disk by the dust, which was also achieved. Parallel with the disk (at position angle 30.°75; Kalas & Jewitt 1995), this time was 2.5 hr, whereas we spent a total of 36 minutes for observations with the slit oriented perpendicular to the disk. The seeing values determined from these observations are 1.″2, whereas the width of the slit was kept at 1.″0 in order to sample (on the CCD) the spectral resolution at the Nyquist frequency.

In addition to the two telluric emission lines, the parallel observations also show spatially extended Na I D emission, with both lines consistently redshifted to the heliocentric velocity of β Pic ($21\ \mathrm{km\ s}^{-1}$). These observations are displayed

[1] Based on observations collected at the European Southern Observatory, Chile.

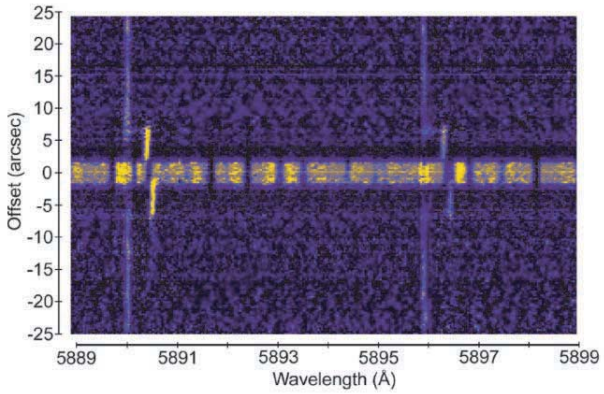

FIG. 1.—Spectral region around the Na I D lines toward β Pic. The dispersion is along the horizontal axis, with wavelengths increasing to the right, and the scale is 0.035 Å pixel^{-1} (1.8 km s^{-1} pixel^{-1}). The spatial dimension is along the vertical axis, with the 1″ wide and 300″ long slit oriented along the position angle of 30°.75. The scale is 0″.27 pixel^{-1} (5 AU pixel^{-1}), with positive values toward the southwest and the negative values toward the northeast. The (deliberately very much reduced) stellar continuum at the center of the figure is covered with telluric absorption lines, whereas the terrestrial ionospheric Na I D1/D2 emission lines extend over the entire vertical space. The Na I line emission from the β Pic disk is seen redshifted with respect to the sky lines and with the intensity ratio 1 : 2. On either side of the star, the disk lines are either blue- or redshifted with respect to the systemic rest wavelength, represented by the disk gas absorption seen against the stellar continuum.

in Figure 1. In Figure 2, the distribution of the Na I emission along the slit, on either side of the stellar spectrum, is compared with the corresponding distribution of the dust. Evidently, both gas and dust show similar light distributions, suggestive of the coexistence of these species in the β Pic disk.

3. DISCUSSION

3.1. *The Rotation of the Disk*

We first address the question of Keplerian rotation. Justified by the indications that there is no significant outward motion, we simply assume circular rotation. The distance to the star is 19.3 pc (Crifo et al. 1997). In order to interpret the velocity pattern, we must first find a radial density distribution of the Na gas component that results in the observed light distribution. For the moment, we ignore the difference between the two

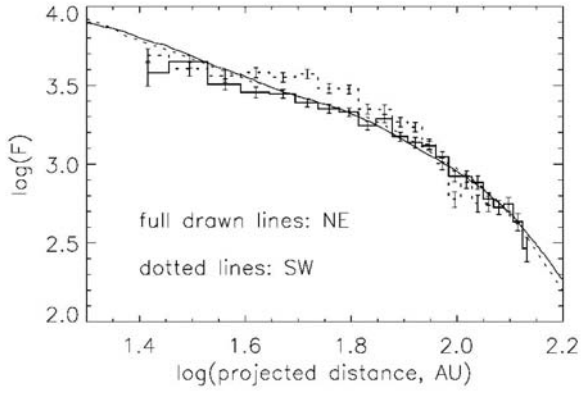

FIG. 2.—Radial distribution, for the two sides of the disk, of the Na I D2 line emission with error bars compared with that of the scattered stellar radiation caused by the dust (from Heap et al. 2000). The flux scale is arbitrary and adjusted to facilitate the comparison.

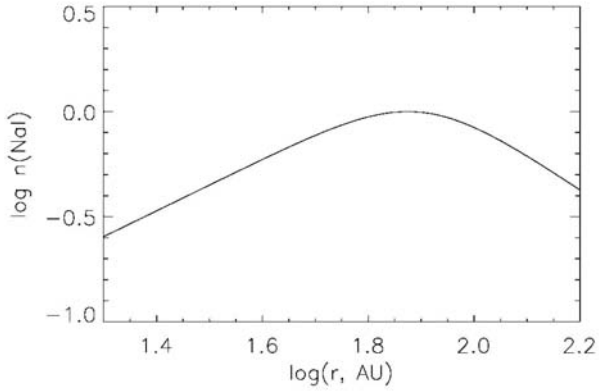

FIG. 3.—Derived radial distribution for Na I (normalized at the peak)

sides (Fig. 2) and use the average light distribution. Adopting a functional relation that is suitable for a broken power law,

$$n(\mathrm{Na\ I}) \propto [(r/a)^{2b} + (r/a)^{2c}]^{-1/2},$$

where n(Na I) is the volume density of Na I at the radial distance r (within the 1″ slit), we get a quite satisfactory fit to the observed projected light distribution with the following numerical values: $a = 89.5$ AU, $b = -1.28$, and $c = 3.44$. The distribution function is shown in Figure 3, and the fit to the observations in Figure 4.

Our observations are consistent with the circular Keplerian rotation of the gas (see Fig. 5), in which we have taken the measured seeing and spectral instrumental profile (using telluric absorption lines) into account. The best-fit mass, in a χ^2 sense, equals $1.40 \pm 0.05\ M_\odot$. This model mass is less than that deduced from the stellar position in the H-R diagram, viz., $1.75\ M_\odot$ (e.g., Crifo et al. 1997). It is possible that this difference is due to radiation pressure (see § 3.3).

3.2. *The Light Budget*

The origin of the "stable gas" absorption has been extensively discussed, and there are arguments for a location very close to the star (Lagrange et al. 1998). If, on the other hand, the sodium emission far out in the disk is caused by the resonance scattering of stellar radiation, then, at least partly, the stable gas absorption must originate throughout the disk along the line of sight. We

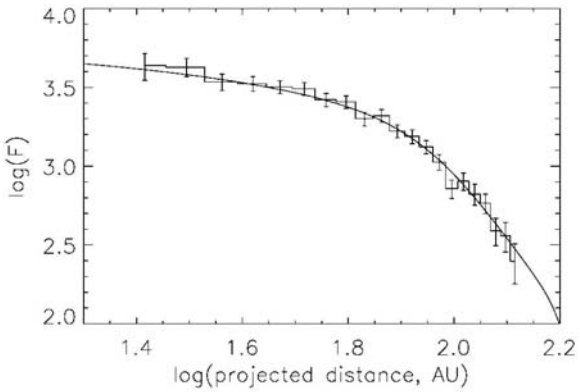

FIG. 4.—Projected radial distribution of the Na I D2 emission of the model (*solid line*) compared with that observed (the average of the southwest and northeast sides).

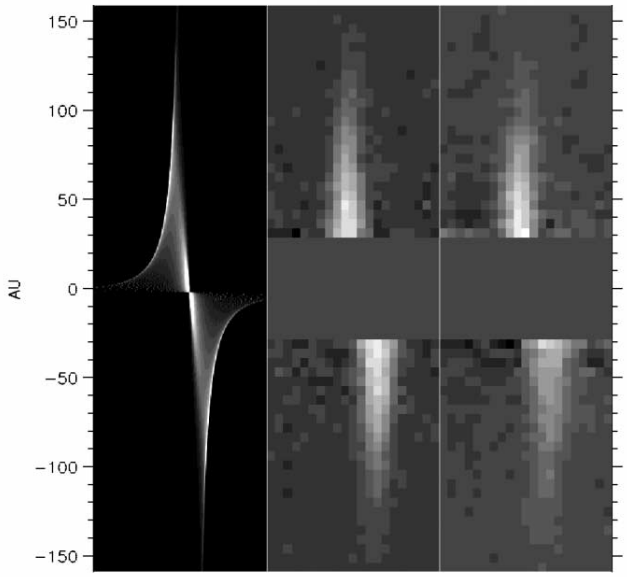

FIG. 5.—Comparison of the observed Na I D2 line with the results of theoretical model calculations. To the left, the model is displayed at spatial and spectral resolutions 10 times better than that observed. In the middle, we show the model degraded to the quality of the observations (including noise). As is seen, it compares well with the observations (to the right).

measure an Na I D2 equivalent width in absorption of 9.4 mÅ, implying a column density of $N(\mathrm{Na\ I}) = 7 \times 10^{10}$ cm^{-2}, in agreement with previous observations by Vidal-Madjar et al. (1986). In emission, a total equivalent width of 0.72 mÅ is obtained. This latter number is of course a lower limit since it does not include any line emission originating outside the 1″ wide slit of the spectrograph. It means that the disk, as seen from the star, must occupy at least a latitudinal angle of 8°.8. We start to detect the line emission at a distance of 30 AU, and at this distance the required thickness of the disk would be at least 4.6 AU. Since the slit width covers 19 AU, these estimates do not lead to any contradiction regarding the light budget under the assumption of resonance scattering. On the other hand, there is not much margin for the proposed dense H I ring (Lagrange et al. 1998) to contribute to the stable Na I absorption lines.

3.3. *The Radiation Pressure*

How, then, can we understand why the radiation pressure does not quickly accelerate the Na I outward in the same sense as it does, for instance, in comets (see Cremonese et al. 1997)? We first note that the momentum transfer caused by the resonance scattering vastly exceeds the gravity. Assuming a stellar mass of 1.75 $M_\odot$, we find that the force caused by the radiation pressure exceeds the gravitational force by a factor of 300. A possible explanation as to why we do not observe a radial velocity component is the presence of a relatively dense gas component. However, this would require very large amounts of gas far out in the disk. As an example, we consider the distance of 100 AU. Our observations exclude a radial velocity component exceeding 5 km s^{-1}, and assuming that the main gas component is atomic hydrogen, we find that the gas density must be at least 10^5 cm^{-3}. Since the thickness (or scale height) of the gas component of the disk is unknown, it is hard to judge if this minimum density is in conflict with other observations.

Even though we cannot at present rule out this explanation for the balancing of the radiation pressure, we propose an alternative. Due to the low-ionization potential of Na I (5.1 eV), one would expect the stellar UV radiation to provide a high degree of ionization. Since Na II lacks strong transitions within the range of the stellar spectrum, the radiation pressure on the ionized sodium gas does not counterweigh the gravitation. Thus, if the gas density is low, a sodium atom will quickly take up speed outward. But it will stay neutral just for a short time, and then, as singly ionized, it will have a long time to adapt to the motion of the main gas component.

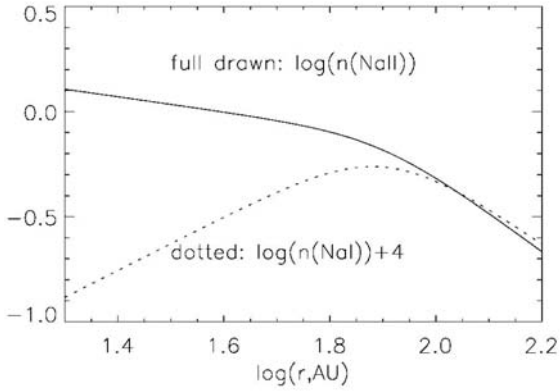

FIG. 6.—Derived number density (in units of cm^{-3}) for Na I and Na II. Only a small fraction ($<10^{-4}$) of the sodium is neutral.

To quantitatively test this idea, we estimate the degree of ionization. Since we can exclude higher ionization stages (the ionization potential is 47 eV for Na II), the equation of ionization equilibrium reads

$$\frac{n(\mathrm{Na\ II})}{n(\mathrm{Na\ I})} = \frac{\omega(r)\Gamma_0}{\alpha_{\mathrm{tot}}[T(r)]n_e(r)},$$

where ω is the dilution factor of the radiation density at the distance r from the star compared with that at the stellar surface, Γ_0 is the ionization rate at the stellar surface, α_{tot} is the total recombination coefficient, and n_e is the electron density. Using a model atmosphere from Allard, Hauschildt, & Schweitzer (2000) and cross sections from Cunto et al. (1993), we estimate that $\Gamma_0 = 205$ s^{-1}. Assuming 100 K as a typical electron temperature in the disk, we get $\alpha_{\mathrm{tot}} = 3.85 \times 10^{-12}$ cm^3 s^{-1} (Verner & Ferland 1996). The electron density remains to be estimated. The stellar far-UV continuum does not suffice to ionize H, He (if at all present), C, N, and O. Assuming solar abundances (Holweger & Rentzsch-Holm 1995) for elements with ionization potentials $\leq$8.3 eV (longward of 1500 Å), we estimate that $n_e \sim 50n(\mathrm{Na\ II})$. If we finally assume a constant thickness of the disk (the half-power width of the dust disk is in fact close to constant from 30 AU and outward; see Heap et al. 2000), we can use the radial distribution derived for Na I in combination with the column density to derive the degree of ionization as a function of the distance to the star. We find that sodium is indeed highly ionized with $n(\mathrm{Na\ I})/n(\mathrm{Na}) < 10^{-4}$ throughout the disk. In Figure 6, we show the radial distribution of n(Na I) and n(Na II). These analytical results have been confirmed by self-consistent photoionization computations, which produce the observed line fluxes. The details will be given in a forthcoming paper.

We conclude that the radiation pressure on sodium, averaged over time, would be small. However, we must also estimate the speed that a neutral atom would typically achieve before

it becomes ionized. Both the UV continuum and the sodium D lines are optically thin throughout the disk, and thus both the ionization rate and the resonance scattering rate roughly scale as the inverse square of the distance to the star. Therefore, the number of scattered photons per period of neutral state is constant, and we find that typically 1.5×10^4 scattering events will occur before an atom becomes ionized. The scattered radiation is essentially isotropic, and the transferred momentum would cause an outward velocity of merely 0.4 km s^{-1}. After that, there will be a long period of time during which the sodium ion will interact with the main gas components and conform to the general velocity pattern, whether it be basically circular Keplerian rotation or not. This also means that the radiation pressure may cause a slow, stepwise motion of each sodium atom outward, resulting in a net flow from the inner to the outer parts of the disk.

3.4. *The Amount of Atomic Gas in the Disk*

From the radial distribution of Na I, we were able to derive the radial distribution of Na II (Fig. 6). The number density is typically $n(\mathrm{Na}) = 1$ cm^{-3}, and the column density from 30 to 140 AU is $N(\mathrm{Na}) = 10^{15}$ cm^{-2}. If the Na/H ratio were solar, this would indicate a hydrogen column density of $N(\mathrm{H}) = 5 \times 10^{20}$ cm^{-2}. Further discussion of these aspects will be deferred to a forthcoming paper.

4. CONCLUSIONS

We have observed Na I D1 and D2 emission along the disk of β Pic from a projected distance of 30–140 AU. The velocity pattern mimics circular Keplerian rotation, but the deduced mass is somewhat lower than that expected for an A5 V star ($1.4\ M_\odot$ compared with $1.75\ M_\odot$). This difference is probably due to the radiation pressure that to some extent counterbalances the gravity. We find that the sodium gas is mainly ionized, with Na II/Na I around 10^4, and for this reason, the radiation pressure does not accelerate the sodium gas component to high velocities. This is simply because the number of scattering events during a neutral period of a sodium atom would only suffice to give an outward velocity of 0.4 km s^{-1}, and then, during the typically 10^4 times longer period of a singly ionized state, the radiation pressure is negligible. So there is plenty of time for the sodium gas to conform, through gas friction, to the motion of the main gas component (i.e., H, O, C, and N) that has only a weak direct interaction with the radiation field.

Finally, it is clear that the observations presented in the present Letter mark only a starting point of spectroscopic investigations since both the spectral and spatial resolutions as well as the stray-light level can be significantly improved on. In addition, other lines like the Ca II H and K doublet and a number of resonance lines in the UV, accessible from, e.g., the *HST*, will probably be detected in the disk.

REFERENCES

Allard, F., Hauschildt, P. H., & Schweitzer, A. 2000, ApJ, 539, 366
Artymowicz, P. 1997, Annu. Rev. Earth. Planet. Sci., 25, 175
Augereau, J. C., Nelson, R. P., Lagrange A. M., Papaloizou, J. C. B., & Mouillet, D. 2001, A&A, 370, 447
Aumann, H. H. 1985, PASP, 97, 885
Cremonese, G., et al. 1997, ApJ, 490, L199
Crifo, F., Vidal-Madjar, A., Lallement, R., Ferlet, R., & Gerbaldi, M. 1997, A&A, 320, L29
Cunto, W., Mendoza, C., Ochsenbein, F., & Zeippen, C. J. 1993, A&A, 275, L5
Freudling, W., Lagrange, A.-M., Vidal-Madjar, A., Ferlet, R., & Forveille, T. 1995, A&A, 301, 231
Heap, S. R., Lindler, D. J., & Lanz, T. M. 2000, ApJ, 539, 435
Holweger, H., & Rentzsch-Holm, I. 1995, A&A, 303, 819
Kalas, P., & Jewitt, D. 1995, AJ, 110, 794
Lagrange, A.-M., Backman, D. E., & Artymowicz, P. 2000, in Protostars and Planets IV, ed. V. Mannings, A. P. Boss, & S. S. Russell (Tucson: Univ. Arizona Press), 639
Lagrange, A.-M., et al. 1998, A&A, 330, 1091
Lecavelier des Etangs, A., Hobbs, L. M., & Vidal-Madjar, A. 2000, A&A, 356, 691
Lecavelier des Etangs, A., et al. 2001, Nature, 412, 706
Liseau, R., & Artymowicz, P. 1998, A&A, 334, 935
Pantin, E., Lagage, P. O., & Artymowicz, P. 1997, A&A, 327, 1123
Roberge, A., Feldman, P. D., & Lagrange, A.-M. 2000, ApJ, 538, 904
Smith, B. A., & Terrile, R. J. 1984, Science, 226, 1421
Thi, W. F., et al. 2001, Nature, 409, 60
Verner, D. A., & Ferland, G. J. 1996, ApJS, 103, 467
Vidal-Madjar, A., Hobbs, L. M., Ferlet, R., Gry, C., & Albert, C. E. 1986, A&A, 167, 325
Vidal-Madjar, A., et al. 1994, A&A, 290, 245

Paper VII

Astronomy & Astrophysics

The spatial structure of the β Pictoris gas disk⋆

A. Brandeker[1], R. Liseau[1], G. Olofsson[1], and M. Fridlund[2]

[1] Stockholm Observatory, AlbaNova University Centre, 106 91 Stockholm, Sweden
e-mail: rene@astro.su.se, olofsson@astro.su.se
[2] ESA/ESTEC, PO Box 299, 2200 AG Noordwijk, The Netherlands
e-mail: Malcolm.Fridlund@esa.int

Received 17 September 2003 / Accepted 7 October 2003

Abstract. We have used VLT/UVES to spatially resolve the gas disk of β Pictoris. 88 extended emission lines are observed, with the brightest coming from Fe I, Na I and Ca II. The extent of the gas disk is much larger than previously anticipated; we trace Na I radially from 13 AU out to 323 AU and Ca II to heights of 77 AU above the disk plane, both to the limits of our observations. The degree of flaring is significantly larger for the gas disk than the dust disk. A strong NE/SW brightness asymmetry is observed, with the SW emission being abruptly truncated at 150–200 AU. The inner gas disk is tilted about 5° with respect to the outer disk, similar to the appearance of the disk in light scattered from dust. We show that most, perhaps all, of the Na I column density seen in the "stable" component of absorption, comes from the extended disk. Finally, we discuss the effects of radiation pressure in the extended gas disk and show that the assumption of hydrogen, in whatever form, as a braking agent is inconsistent with observations.

Key words. stars: individual: β Pictoris – circumstellar matter – planetary systems: formation – protoplanetary disks

1. Introduction

The young, near-by main-sequence star β Pictoris has been the subject of intense studies ever since it was discovered to harbour circumstellar cold dust (Aumann 1985), distributed along a linear shape (Smith & Terrile 1984), interpreted as a "debris disk" (Backman & Paresce 1993). These studies have been largely motivated by the possibility of observing an analogue to the solar system in its early stages, in the hope of finding clues to the mechanisms of planet formation. Asymmetries found in the disk from light *scattered* by the dust (Kalas & Jewitt 1995; Heap et al. 2000) have indeed been suggested to be the signature of perturbing planet(s) (Moulliet et al. 1997; Augereau et al. 2001), but so far no direct detection of a planet around β Pic has been made. Asymmetries have also been detected in *thermal emission* from the dust (Liseau et al. 2003; Weinberger et al. 2003 with references therein). Recent papers reviewing the β Pic disk are those by Artymowicz (2000), Lagrange et al. (2000) and Zuckerman (2001).

Circumstellar *gas*, seen in absorption against the star, was also found early on (Hobbs et al. 1985), thanks to the favourable edge-on orientation of the disk. Finding and characterising the gas content is important for understanding its relation to the dust and the general evolution of the disk (Artymowicz 2000). Gas is also useful as a probe of physical conditions in the disk, where density, composition, temperature and bulk velocities under favourable conditions can be directly estimated.

The gas found at relative rest to β Pic, consisting of metals, raised the problem why it is not blown away from the system by the high radiation pressure. Lagrange et al. (1998) made some detailed calculations and found that the gas drag from a dense enough H I ring ($n_{\rm H\,I} \geq 10^5\,{\rm cm}^{-3}$) close to the star (~0.5 AU) could brake migrating particles sufficiently, provided they started out inside the ring. The picture was complicated by the announcement of H_2 detected in emission by the Infrared Space Observatory (Thi et al. 2001), implying large quantities (~50 $M_\oplus$) of molecular hydrogen, and the subsequent report of sensitive upper limits ($N(H_2) \lesssim 10^{18}\,{\rm cm}^{-2}$) of H_2 from FUV absorption lines using β Pic as a background source (Lecavelier des Etangs et al. 2001). In addition, Olofsson et al. (2001, hereafter Paper I) found spatially resolved widespread gas emission from Na I in the disk, stretching out to at least 140 AU.

Here we present observations improved by a factor of two in both spatial and spectral resolution, as well as a greatly increased spectral coverage, compared to Paper I. We put emphasis on the observed spatial structure of the gas disk, derive an empirical density profile of Na I atoms and use a photoionisation code to construct disk models consistent with our observations. We discuss implications of the radiation pressure under various conditions derived from these models. Results from a

Send offprint requests to: A. Brandeker,
e-mail: alexis@astro.su.se

⋆ Based on observations collected at the European Southern Observatory, Chile.

Table 1. VLT/UVES observation log.

UT Date	β Pic[a]	Grating[b]	Width[c]	Length[c]	Offset[d]	Orientation[d]	Exposures
2001-12-02 T 03:38	ON	437	0.″4	10″	–4.″4	Parallel	69 × 15 s
2001-12-02 T 03:38	ON	860	0.″3	12″	–4.″4	Parallel	47 × 25 s
2001-12-02 T 05:31	ON	390	0.″4	8″	–3.″4	Parallel	62 × 20 s
2001-12-02 T 05:31	ON	580	0.″3	12″	–3.″4	Parallel	48 × 25 s
2002-01-03 T 06:21	ON	390	0.″4	8″	–3.″4	Parallel	62 × 20 s
2002-01-03 T 06:21	ON	580	0.″3	12″	–3.″4	Parallel	48 × 25 s
2002-01-06 T 05:51	OFF	390	0.″4	8″	–3.″0	Orthogonal	3 × 1205 s
2002-01-06 T 05:51	OFF	580	0.″3	12″	–3.″0	Orthogonal	3 × 1195 s
2002-01-16 T 02:47	OFF	390	0.″4	8″	–11″	Parallel	3 × 1205 s
2002-01-16 T 02:47	OFF	580	0.″3	12″	–11″	Parallel	3 × 1195 s
2002-01-16 T 03:51	OFF	390	0.″4	8″	–6.″0	Orthogonal	3 × 1205 s
2002-01-16 T 03:51	OFF	580	0.″3	12″	–6.″0	Orthogonal	3 × 1195 s
2002-01-19 T 03:11	ON	390	0.″4	8″	3.″4	Parallel	62 × 20 s
2002-01-19 T 03:11	ON	580	0.″3	12″	3.″4	Parallel	48 × 25 s
2002-01-19 T 04:25	ON	390	0.″4	8″	3.″4	Parallel	62 × 20 s
2002-01-19 T 04:25	ON	580	0.″3	12″	3.″4	Parallel	48 × 25 s
2002-02-09 T 03:55	OFF	390	0.″4	8″	3.″0	Orthogonal	3 × 1205 s
2002-02-09 T 03:55	OFF	580	0.″3	12″	3.″0	Orthogonal	3 × 1195 s
2002-02-10 T 03:19	OFF	390	0.″4	8″	11″	Parallel	3 × 1205 s
2002-02-10 T 03:19	OFF	580	0.″3	12″	11″	Parallel	3 × 1195 s
2002-02-11 T 04:04	OFF	390	0.″4	8″	6.″0	Orthogonal	3 × 1205 s
2002-02-11 T 04:04	OFF	580	0.″3	12″	6.″0	Orthogonal	3 × 1195 s
2002-09-24 T 08:09	OFF	437	0.″4	10″	–3.″0	Orthogonal	3 × 1205 s
2002-09-24 T 08:09	OFF	860	0.″3	12″	–3.″0	Orthogonal	3 × 1195 s

[a] ON means that the star was inside the spectroscopic slit, OFF that it was outside.
[b] The gratings correspond to the following wavelength ranges: 326–445 nm for grating 390, 373–499 nm for grating 437, 476–684 nm for grating 580, and 660–1060 nm for grating 860.
[c] Width and Length refer to the dimensions of the slit.
[d] Offset is the centre of the slit relative to β Pic in the plane of the disk, where positive offsets are to the north-east. The orientation of the slit is relative to the disk plane.

detailed study of the observed chemical abundances will be discussed in a forthcoming paper.

2. Observations

The star β Pictoris was observed with the echelle spectrograph UVES on the 8.2 m Kueyen telescope at the Very Large Telescope of ESO, Paranal, Chile. The observations were made in service mode to take advantage of the excellent seeing conditions occasionally provided by the site. Service mode means that the observers prepare observation blocks that are executed by the local telescope operators provided certain conditions (like air mass and seeing) are met. A total of 12 observation blocks during 2001–2002 (see Table 1) lasting about an hour each were successfully executed. The air mass and seeing at zenith were always below 1.5 and 0.″6, respectively. The UVES spectrograph was used in standard dichroic modes, meaning that a dichroic mirror was used to split the light into two wavelength ranges, each using its own echelle grating and CCD detectors. Two types of gratings were used for each arm, together covering the wavelengths 3300 Å to 10 400 Å with a spectral resolution ranging from $R \sim 80\,000$ in the blue to $R \sim 110\,000$ in the red. The blue arm was equipped with a single CCD of type EEV 44-82 and size 4096 × 4096 pixels, while the red arm had a mosaic of two CCDs of sizes 2048 × 4096 each, of the types EEV 44-82 and MIT-LL CCID-20. The spectroscopic slits were 0.″4 and 0.″3 wide in the blue and red arm, respectively. To adequately separate the echelle orders, slits were restricted to lengths between 8″ and 12″, depending on setting (see Table 1). Slits were positioned at 4 overlapping locations along the β Pic dust disk, and at 4 locations orthogonal to the disk, reaching a distance of 17″ from the star in the disk plane, and a height of 6″ above the plane (see Fig. 1). From the data, we determined the positioning of the slits, with respect to β Pic, to be better than ∼0.″2. Calibration data (flat-fields, bias frames, Th-Ar lamp wavelength calibration spectra, flux standard stars, etc.) were provided by the UVES calibration plan.

3. Data reduction

3.1. Pipeline reduction

The data were reduced using a modified version of the UVES pipeline 1.2, that runs in the ESO MIDAS environment. The pipeline automatically generates the appropriate calibration

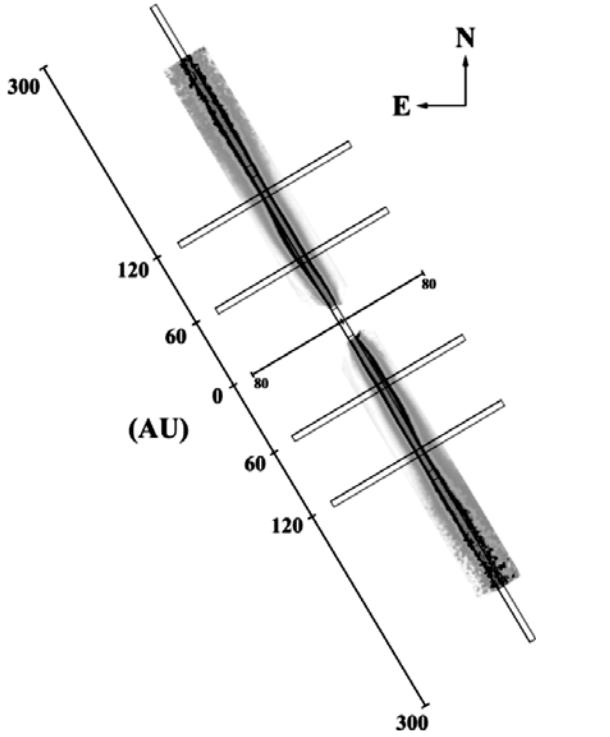

Fig. 1. Orientations and positions of the 8 different slit settings used. The background image shows observations of the dust as obtained by HST/STIS (Heap et al. 2000).

sets from the calibration data obtained as a part of the UVES calibration plan, and apply them to the science frames. The raw frames are bias subtracted, flat-fielded, background subtracted, order extracted, and wavelength calibrated. An error was corrected in the pipeline version 1.2, that associated a wavelength calibration to the wrong order when 2D extraction was selected without merging the orders.

The orders of the echelle grating are slightly inclined on the CCD with respect to pixel columns. Since the observations with the star on slit were performed under excellent seeing (the seeing measured in the spectra was $\sim$0.″7), this resulted in a very high flux gradient between the pixels on and off the star. By default, the orders are resampled linearly, but this caused the spectrum to show a periodic "spiky" pattern in the flux. We found that linear interpolation does not work properly due to the strong non-linear shape of the point spread function (PSF) at the pixel resolution. By modifying the order extracting routine to use a third order Catmull-Rom spline interpolation instead of linear, we found the spikes to be greatly reduced (though not completely eliminated).

The reduction procedure was complicated by the sheer load of data. With about 600 spectra, each 4096×4096 pixels, plus calibration frames etc., the raw data were close to 50 GB.

The end product of the pipeline reduction consisted of individual orders separated into individual files with the spatial information along the slit preserved, and a wavelength calibration guaranteed to be better than 0.5 km s^{-1}.

3.2. PSF subtraction

To trace the circumstellar gas emission as close as possible to the star, we had to subtract the scattered light from the star, in the cases where the star was in the slit. To do this, we estimated the stellar spectrum S by centering a small aperture on the star. To allow for slow gradients, we took advantage of the fact that the gas emission lines are narrow (a few pixels) and produced a median filtered version M of the stellar spectrum S, using a window of 30–60 pixels. We also obtained the median filtered spectrum m_i at each spatial position i, using the same median filter window. The stellar PSF subtracted spectrum was then estimated as $s_i = r_i - m_i S/M$, where r_i is the spectrum at position i. For the observations where the star was off the slit, we just subtracted the median filtered background scattered light (scattered both locally by the dust disk and in the atmosphere / telescope), $s_i = r_i - m_i$.

3.3. Flux calibration

To flux-calibrate the data, we made use of the master response curves provided by the UVES team. The master response curves are generated from long-time monitoring of the sensitivity trends of the instrument, and are provided for various standard settings and periods in time. The claimed absolute flux calibration is 10%, but comparing with standard flux stars observed (with an open slit) the same nights as β Pic we found the derived fluxes to deviate by as much as 40% from tabulated values for these stars. We thus used the master response curves to correct only for the over-all sensitivity dependence on wavelength, and used the standard star spectra obtained in connection with the β Pic observations to correct the absolute flux calibration. By looking at the variations of the derived absolute fluxes of disk emission lines observed several times, we estimate that the error on the absolute flux is about 5–10%. Since we use a narrow slit (0.″3–0.″4), the slit losses from a point source like β Pic are substantial and very seeing dependent. The error of the absolute flux from the star is therefore expected to be substantially higher. Our main concern, however, is the flux of the disk emission, which, due to its spatial extension, is much more stable with regard to seeing variations.

3.4. Heliocentric wavelength correction

The wavelength calibration obtained from the UVES pipeline does not correct for the velocity of the instrument relative to the centre of the Sun. To transform the observed spectrum to a heliocentric frame, we made use of the software program RV written by P. T. Wallace and C. A. Clayton[1]. The obtained accuracy in the transformation is better than 0.01 km s^{-1}, fully adequate for our purposes.

3.5. Line flux measurements

From the reduced, PSF subtracted and wavelength calibrated spectra, the disk emission lines were measured in several steps.

[1] RV is available from `http://star-www.rl.ac.uk`

First the lines were identified by correlating their measured wavelengths with the atomic line database provided by NIST[2]. This procedure was greatly simplified by the high accuracy of the wavelength calibration, better than 0.5 km s^{-1}, corresponding to 0.01 Å at 6000 Å. A median systematic velocity was then calculated for the brightest and most accurately measured emission lines, assuming all shared the same systematic radial velocity. For the brightest lines, the measured flux as a function of apertures centred on the systematic velocity was evaluated. A large aperture samples more signal, but also more noise. We were therefore interested in finding the best balance, in order to achieve the highest signal to noise (S/N). The apertures used to measure emission lines were consequently chosen as a function of line strength and background noise, with smaller apertures for fainter lines. We assumed that all lines from a particular ion share the same spatio-spectral profile, and scaled the flux measured in small apertures of fainter lines with the ratio between equally sized and maximum sized apertures placed on the sum of several bright lines. In this way we estimated the signal from a faint line without integrating up too much noise. The method is analogous to methods used in aperture photometry to measure star fluxes in, e.g., a CCD image.

For the slits placed orthogonally to the disk, we summed up all flux in the spatial direction, i.e. along the height of the disk (Table 2). The quantity thus derived has the unit of flux per arcsecond.

4. Results

We detected 88 spatially extended emission lines from the β Pic gas disk, identified as emission from Fe I, Na I, Ca II, Ni I, Ni II, Ti I, Ti II, Cr I and Cr II. Table 2 shows a selection of the brightest lines. Following the brightest emission lines ($S/N \sim 50$) from Na I and Fe I radially (Figs. 2 and 3), we observe a strong asymmetry between the north-east (NE) and the south-west (SW) parts of the disk, similar to the brightness asymmetry in the dust emission (Kalas & Jewitt 1995), but asymmetric to a much higher degree. The NE gas emission extends smoothly to the limits of our observations (17″, corresponding to 330 AU at the distance of β Pic), whereas the SW emission is abruptly truncated at 150–200 AU. In the inner regions, the SW emission dominates over the NE part, in agreement with Fig. 2 of Paper I.

Determining the centre of emission from the orthogonal profiles, it becomes apparent that the inner part of the disk is slightly tilted with respect to the outer parts, in particular on the NE side (Fig. 4). We estimate this tilt to be $5^\circ \pm 2^\circ$ (1σ), similar to the 4°–5° tilt observed by HST/STIS in the inner dust disk (Heap et al. 2000).

The scale height ($FWHM$) of the gas disk, estimated on observations deconvolved with a Gaussian of 0.″7 to simulate the seeing, is ∼20 AU at 3″ (58 AU), similar to the dust disk scale height (Heap et al. 2000). At 6″ (116 AU), however, the gas disk is significantly thicker, ∼30 AU compared to ∼15 AU for the dust (see Fig. 5).

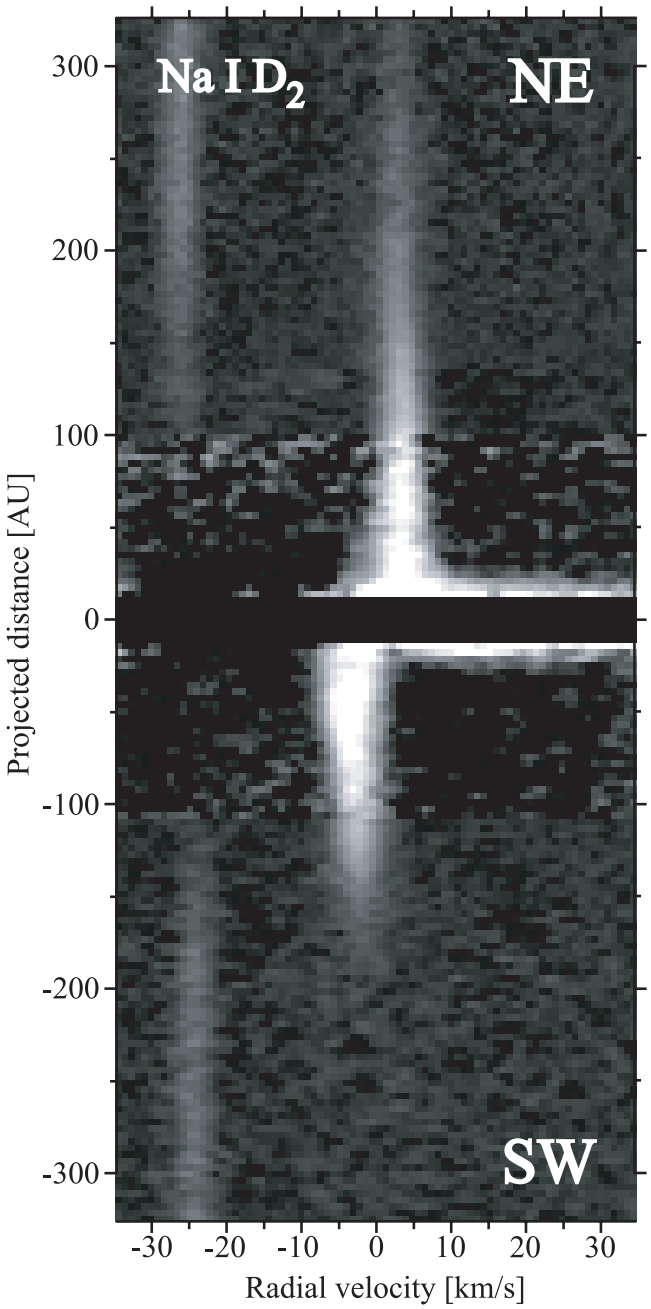

Fig. 2. Na D$_2$ ($\lambda_{\rm air}$ = 5889.951 Å) emission from the β Pic disk, as seen through four slits parallel to the disk (see Fig. 1). The vertical axis is along the spatial direction, with positive offsets north-east of the star, while the spectral dispersion is along the horizontal axis, centred on the β Pic rest frame of the Na D$_2$ line. The inner 11 AU, showing mostly residual noise from the PSF subtraction, have been masked out. The velocity shift of the NE and SW side is due to Keplerian rotation of the disk, with the SW rotating towards us (Paper I). The grey scale has been scaled non-linearly with the intensity, in order to bring out the bright disk structure close to the star as well as the faint features at greater distances. The emission in the NE can be traced out to the limits of our observations at 323 AU, while the emission in the SW ends abruptly at 150–200 AU (see also Fig. 3). Close to −25 km s^{-1}, telluric Na D$_2$ emission is seen covering the slit. The relative velocity of the sky emission to β Pic varies slightly between the mosaiced observations due to the orbital motion of the Earth between the epochs.

[2] http://physics.nist.gov

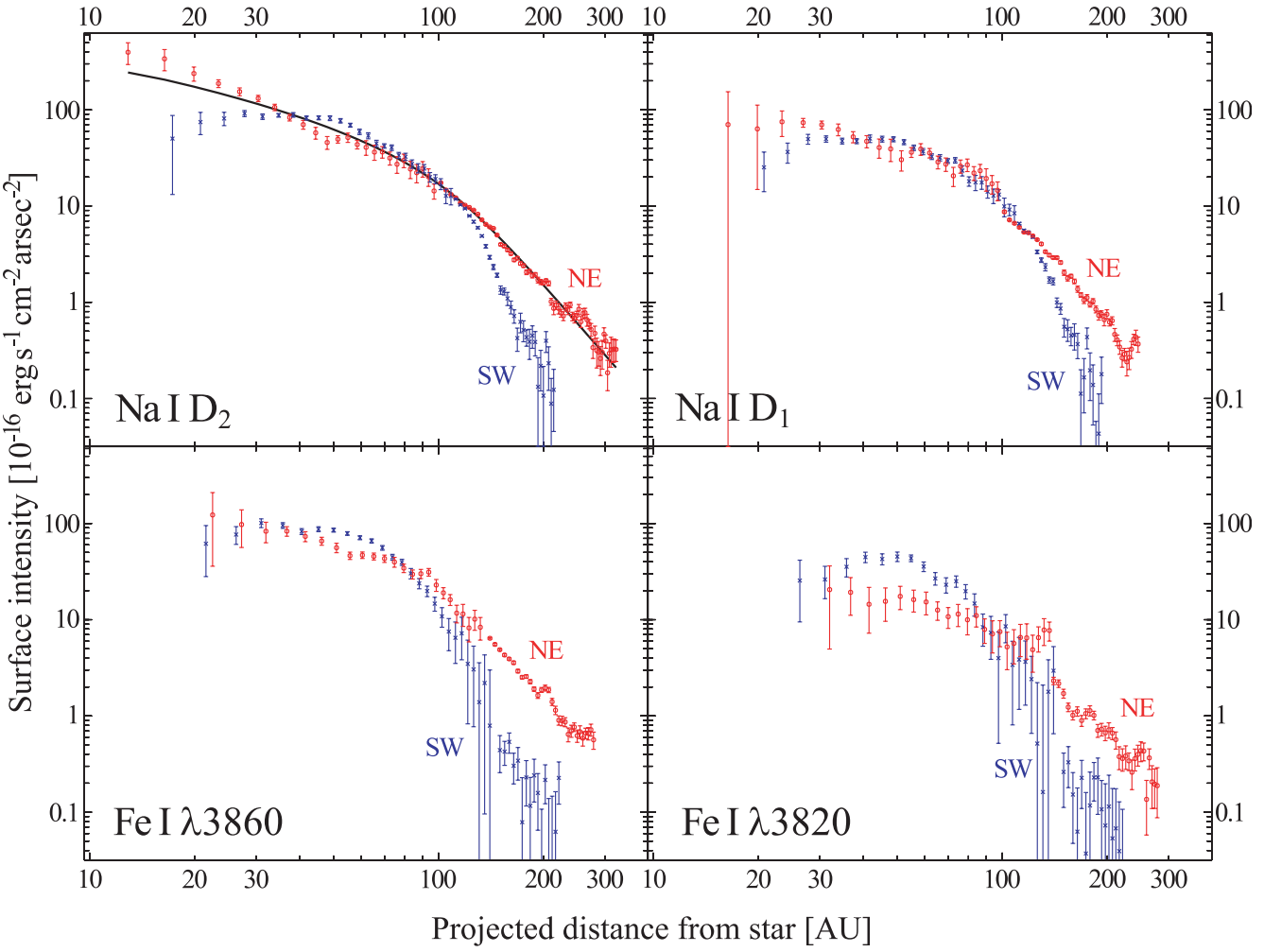

Fig. 3. Determined surface intensity as a function of radial distance in NE and SW for Na D$_{1,2}$ and Fe I λ3859.911, λ3820.425. The fit of Sect. 5.1 is shown for Na I D$_2$ as a an unbroken line. Note the sharp decrease in flux in the SW at 150 AU–200 AU.

Table 2. Selected gas emission lines, 3″ SW in disk.

Line	λ^{a}_{air}	Flux^{b}	σ^{b}_{flux}	E^{c}_{low}	E^{c}_{high}
Fe I	3820.425	61.3	2.5	0.859	4.103
Fe I	3859.911	111.3	3.4	0.000	3.211
Na I D$_2$	5889.951	79.2	4.0	0.000	2.104
Na I D$_1$	5895.924	42.4	2.5	0.000	2.102
Ca II K	3933.663	12.0	1.0	0.000	3.151
Ca II H	3968.468	16.8	1.2	0.000	3.123

[a] Wavelength of transition in air, in units of Å.
[b] Flux in units of 10^{-16} erg s^{-1} cm^{-2} arcsec^{-1}; see Sect. 3.5.
[c] Lower and upper energy levels of transition, in units of eV.

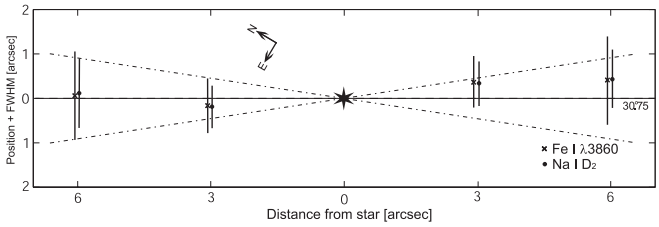

Fig. 4. Measured positions of the Na I and Fe I gas emission relative to the plane at position angle 30.°75. The bars correspond to derived scale heights, obtained by deconvolving the observed height profiles with a Gaussian of 0.″7 *FWHM* simulating the seeing. The inclined dash-dotted lines show the empirical opening angle of the gas disk, corresponding to $H/r = 0.28$ (see Sect. 5.1). The error in positioning of the slits is on the order of 0.″1.

A very complex height profile is shown by the Ca II H & K lines (Figs. 5 and 6). Especially at 6″ distance from the star, the emission from the disk midplane is much fainter than the emission away from the midplane. In particular, the detected Ca II emission, at 6″ SW of the star, keeps increasing to the limits of the spectroscopic slit 4″ above the disk midplane, meaning that there is a significant number of Ca II ions at 77 AU height above the midplane at 116 AU distance from the star. From Fig. 6 it is evident that the radial velocities of these Ca II ions are small – on the order of a few km s^{-1}. Implications of this fact are discussed in Sect. 5.2.

In order to determine the heliocentric velocity of β Pic accurately, we averaged the heliocentric gas velocities as observed on each side at the distances 3″ and 6″ from the star. In this way, we can assess the system velocity independently from the

Table 3. Radial velocities relative β Pic of ions measured in absorption.

Ion	Δv[a] km s^{-1}	$\sigma_{\Delta v}$[b] km s^{-1}
Fe I	−0.0	0.3
Na I	−1.2	0.3
Ca II[c]	−0.3	2.1
Ti II	0.2	0.8
Ni I	0.4	0.4
Ni II	2.8	3
Cr II	2.2	3

[a] The positive direction is radially away from us, towards β Pic.
[b] Errors are relative only. An additional systematic error of 0.5 km s^{-1} comes from the uncertainty in the system velocity of β Pic.
[c] The radial velocity of Ca II is measured on the infrared lines λ7291.47 and λ7323.89, and not the optically thick Ca II H & K lines.

lines observed in absorption, which are sensitive to possible radial velocities of the absorbers (caused by, e.g., radiation pressure). We determined the heliocentric radial velocity of β Pic to be 20.0 ± 0.5 km s^{-1}, with the error mainly due to the uncertainty in wavelength calibration.

In the spectrum of the star, we measured the absorption profiles corresponding to observed ground state emission lines. Most lines were found to be at, or close to, the system velocity of β Pic (Table 3).

5. Discussion

We proceed by inverting the observations of the projected disk to a radial density law for Na I, and then extend the result by calculating the ionisation structure to find an estimate on the total Na density. By making assumptions of the abundances we construct two models with distinct H densities, test how well the models compare with observations of H I and H_2, and examine how the kinematics of ions in these models are affected by radiation pressure.

5.1. Sodium gas density profile

From the spatial emission profiles we estimate the density distribution of the observed gas by making the following assumptions:

1. The disk is axisymmetric and the density of the emitting medium is well described by

$$n(r,h) = n_0 \left[\left(\frac{r}{r_0}\right)^{2a} + \left(\frac{r}{r_0}\right)^{2b} \right]^{-\frac{1}{2}} \exp\left[-\left(\frac{h}{\alpha r}\right)^2 \right], \quad (1)$$

   where r and h are the cylindrical coordinates describing the midplane distance and height over the midplane, respectively, n_0 is a normalising density, r_0 is the broken power-law break distance, a and b are power-law exponents of the inner and outer regions respectively, and α is related to the scale height H of the disk at midplane distance r as $H/r = 2\sqrt{\ln 2}\,\alpha$.
2. The inclination of the disk is close to zero, i.e. we see it edge-on.
3. The emission is optically thin and isotropic.
4. The emitting gas traces the full gas population of that ion.

The observed disk is, of course, not axisymmetric but quite asymmetric in appearance (Figs. 2, 3 and 6). The difference between the NE and SW parts of the inner disk is not that dramatic, though, less than a factor of two in the region where most gas is located (30–120 AU). Thus the assumption of axisymmetry is probably not too bad.

We chose the Na I $D_{1,2}$ lines for the inversion because (A) the S/N is high (~50), (B) the line ratio between D_2 and D_1 is close to 2, implying that the emission is optically thin, and (C) we expect nearly all Na I atoms to be in their ground state (see Sect. 5.3), meaning the resonance $D_{1,2}$ lines trace all of the Na I population. The parameters of Eq. (1) were fitted by constructing a numerical model, simulating observed spatial profiles as a function of the parameters and χ^2-minimising the difference between the model and the observations. In more detail, the model was initiated on a three dimensional grid of height × width × depth dimensions 40 AU × 800 AU × 2000 AU at 1 AU resolution. The central star was assumed to emit 4.5×10^{30} erg s^{-1} Å^{-1} at wavelengths close to the Na I D_2 line, and $A_{ji} = 6.22 \times 10^7$ s^{-1} was used as the D_2 transition Einstein coefficient for spontaneous emission, in calculating the scattering cross-section. For each cell, a specific line luminosity was calculated, summed up along the line of sight and geometrically diluted to the distance of the observer at 19.3 pc. This "ideal" image of the disk was then convolved with a Gaussian of $FWHM = 0\farcs7$, simulating the atmospheric seeing, and sampled along the various spectroscopic slit settings of Fig. 1 to fit the observations. In the fit we used the midplane radial emission distribution from 13 AU out to 323 AU of the NE, and the orthogonal profiles at 3″ and 6″ NE of the star. The derived parameters of Eq. (1) for Na I are:

$n_0 = (1.02 \pm 0.04) \times 10^{-5}$ cm^{-3}
$r_0 = 117 \pm 3$ AU
$a = 0.47 \pm 0.06$
$b = 3.16 \pm 0.04$
$H/r = 0.28 \pm 0.05$,

where the quoted errors are 1σ formal fitting errors obtained by making an additional number of fits to artificial data generated by adding random noise, at the estimated noise level, to the observed profile. We have over plotted the Na I fit into Fig. 3.

We can use Eq. (1) with the above parameters to estimate the midplane column density of Na I, to compare with column densities estimated from Na I absorption in the stellar spectrum seen through the disk. If we integrate only over the radii where we are sensitive to Na I emission, that is, from 13 AU out to 323 AU, we obtain a column density of $N(\mathrm{Na\,I}) = 3.0 \times 10^{10}$ cm^{-2}. Extrapolating Eq. (1) to all radii, that is, from zero radius out to infinity, we increase the Na I column density

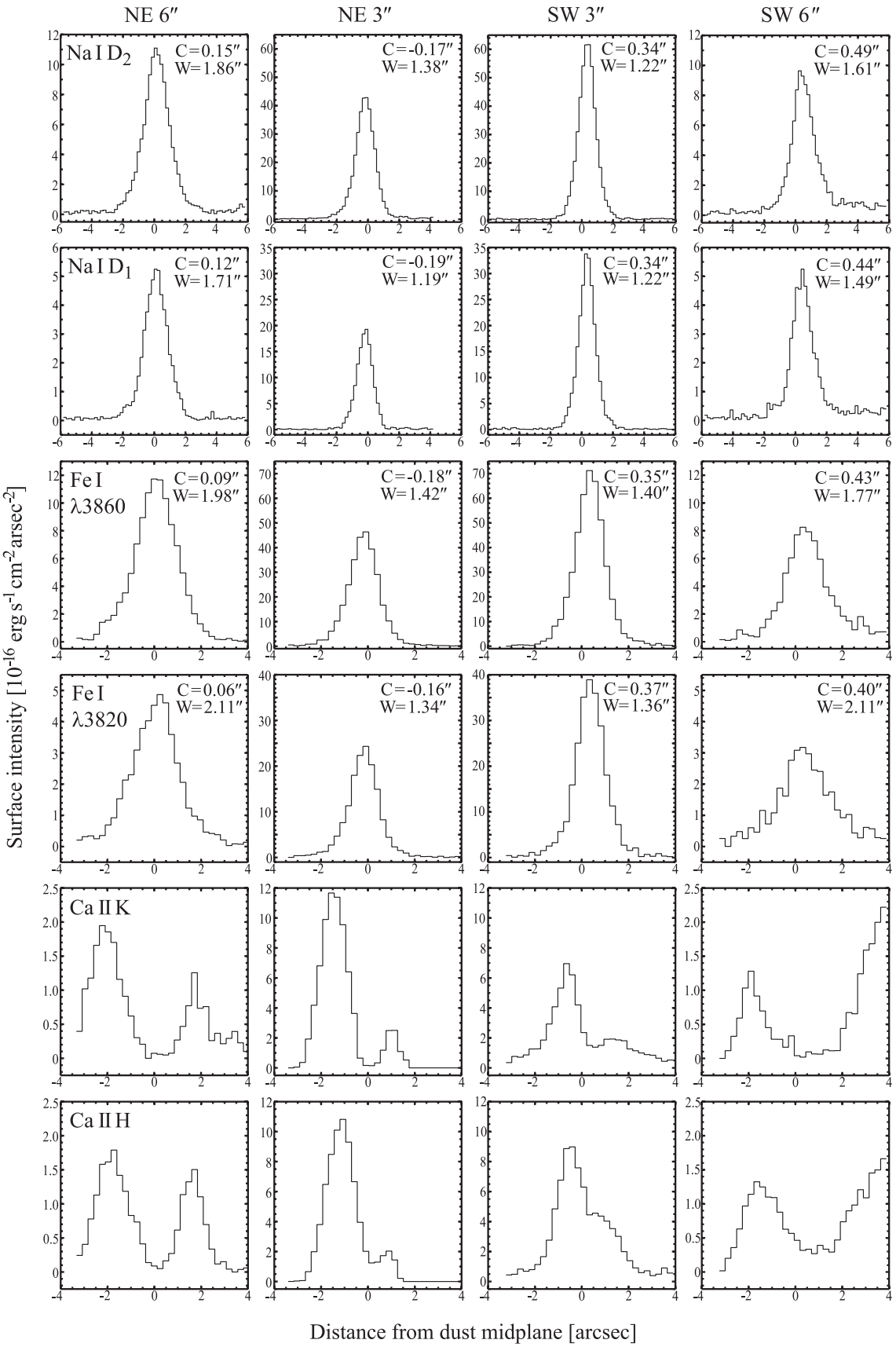

Fig. 5. The flux calibrated vertical profile of the disk gas emission at 3″ and 6″ NE and SW of the star for a few selected lines of Na I, Fe I and Ca II. Zero spatial offset refers to the dust disk midplane defined by the position angle 30.75 relative to the star, with the positive spatial direction to the north-west (NW). The centre and *FWHM* for Gaussian fits to the profiles are printed in the panels of Gaussian shaped profiles. The SW side dominates the emission at 3″, while the NE side slightly dominates at 6″.

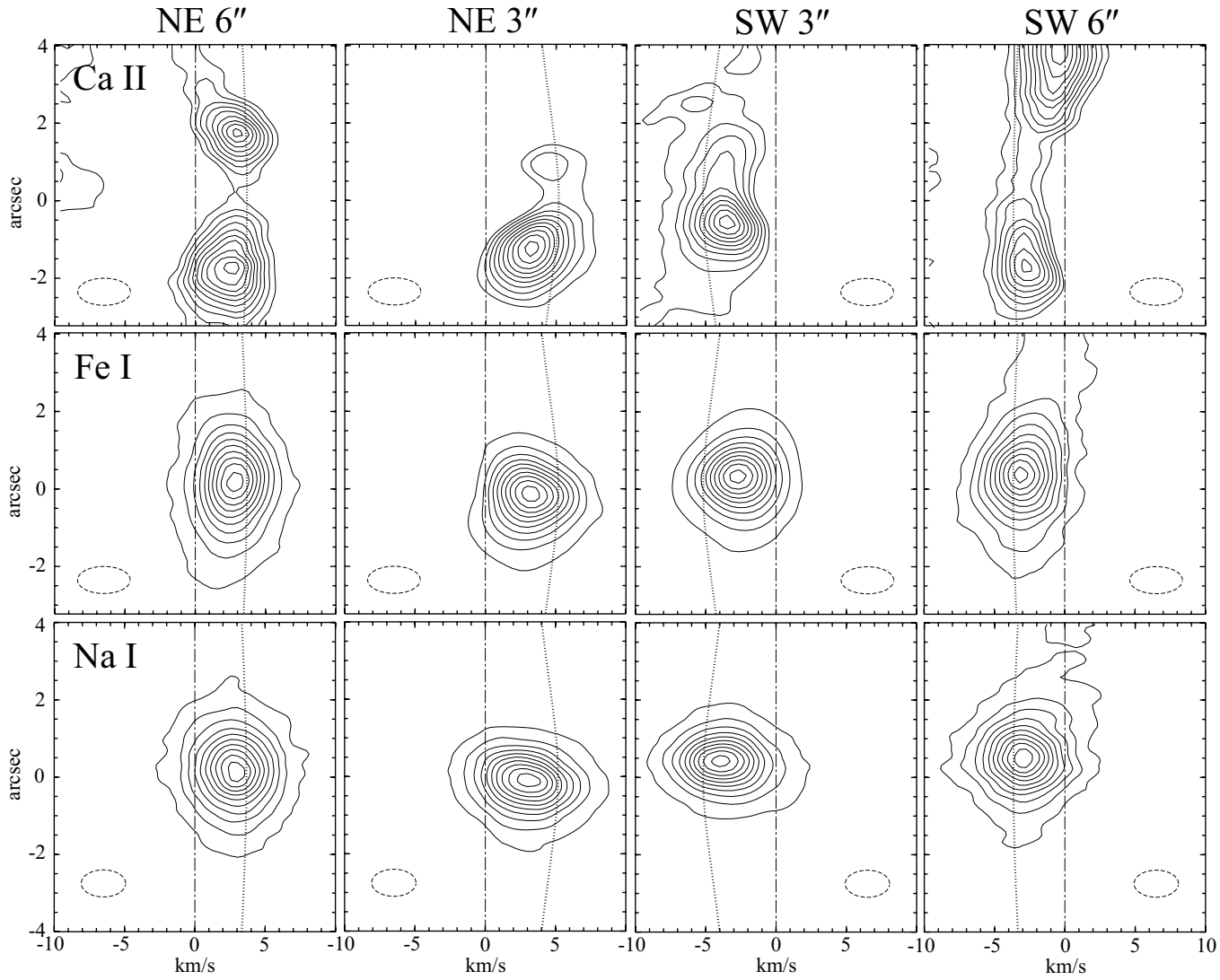

Fig. 6. The velocity distribution of the gas emission as observed by slits orthogonal to the disk at 3′ and 6″ NE and SW of the star for Ca II, Fe I and Na I. To improve the signal to noise, the H & K lines of Ca II, 10 of the brightest Fe I lines, and D_1 and D_2 of Na I were added for each species. The profiles were then normalised so that each level increases one tenth of the peak. The noise in the Fe I and Na I plots is below the lowest level curve, while the lowest level curve for Ca II still shows some noise. Velocities are referred to the system velocity 20.0 km s^{-1} of β Pic, with the positive direction being away from us. Positive offsets in the spatial direction are directed to the north-west (NW). The dash-dotted vertical lines correspond to the system velocity of β Pic, the dotted lines to the Kepler velocity at the projected distance from β Pic (assuming a stellar mass of $M = 1.75\,M_\odot$), while the dashed ellipse in each graph shows the spectral and spatial resolution attained. Note the complexity of the Ca II profile, and how the emission at 6′ SW (right-most panels) can be traced to the limit of the observations. The detected emission profiles from Ni I, Ni II, Ti I, Ti II, Cr I and Cr II are of much lower S/N, but similar to the profiles of Na I and Fe I.

by 40% to $N(\mathrm{Na\,I}) = 4.1 \times 10^{10}\,\mathrm{cm}^{-2}$. This can be compared to our observed column density $N(\mathrm{Na\,I}) = (3.4 \pm 0.4) \times 10^{10}\,\mathrm{cm}^{-2}$. We conclude that most, perhaps all, of the Na I gas seen in absorption is situated in the extended gas disk seen in emission. We have no reason to doubt that originators of other "stable" gas absorption components also belong to this extended disk.

5.2. Radiation pressure

Ions in the β Pic gas disk are subject to appreciable radiation pressure. To evaluate the significance, it is common to define the ratio between the forces of gravitation and radiation, $\beta \equiv F_{\mathrm{rad}}/F_{\mathrm{grav}}$. Since both the radiation and gravitational fields are inversely proportional to the square of the distance to the source, β is constant throughout the β Pic disk. For the observed atoms Na I and Fe I, $\beta \gg 1$, meaning that if left alone, gravity would be largely irrelevant and these atoms would rapidly accelerate out of the system at high velocities. This is not observed (Table 3 and Fig. 6). To investigate what the effects of a braking medium are, we solve the equation of motion for a gas particle,

$$m\frac{\mathrm{d}v}{\mathrm{d}t} = -F_{\mathrm{grav}} + F_{\mathrm{rad}} - F_{\mathrm{fric}}, \qquad (2)$$

where F_{fric} is the frictional force. Assuming $F_{\mathrm{fric}} = Cv$, where C is the friction coefficient (proportional to the density of the braking medium), and that the distance an atom travels

before reaching the terminal velocity is much shorter than the size of the disk, Eq. (2) may be solved to yield the terminal velocity (as $t \to \infty$)

$$v_\infty = \frac{\beta - 1}{C} F_{\rm grav}. \quad (3)$$

Equation (2) ignores magnetic forces, which should be of little importance for neutral atoms. If appreciable magnetic fields are present, however, ions with net charges may be significantly affected. We ignore this complication for the moment and assume that the magnetic fields are small enough to play a negligible role for the kinematics of the observed gas particles in the disk.

For β Pic we estimate $\beta_{\rm Na\,I} = 250$ and $\beta_{\rm Fe\,I} = 18$, while C depends on the detailed density and temperature structure. We calculated terminal velocities as a function of radius for the two models of Sects. 5.3.1 and 5.3.2. Details of the solution to Eq. (2), with estimates of C and β for several ions, are found in Liseau (2003).

5.3. Ionisation structure

To estimate the gas density of all Na atoms in the disk, and also get an idea of the total gas density, we need to address the ionisation structure of the disk. We employed the one-dimensional photoionisation/PDR code *Cloudy* (Ferland et al. 1998) for the task. Cloudy consistently maintains the ionization and thermal balance, and solves the radiative transfer by making use of the Sobolev approximation. For a detailed description of the code we used, see Liseau et al. (1999).

Several assumptions have to be made in order to compute the ionisation structure, perhaps the most important being that of the chemical abundances of the atomic gas. Since we have no detailed information, we confine ourselves to study two cases of chemical abundances: solar composition and a strongly metal depleted model. At first we also considered a case with typical interstellar medium abundances, but dismissed it due to the very high degree of Ca depletion compared to solar values, in contradiction with observations. We have no a priori reason to expect any of these assumed abundances to reflect reality, but we believe they still serve as valuable reference cases.

Another important assumption is that of the stellar spectral energy distribution (SED). We assume the atmosphere of β Pic to be well represented by an ATLAS 9 model (Kurucz 1992) with $T_{\rm eff} = 8000$ K, $\log g = 4.5$ (in cm s^{-2}) and $\log(Z/Z_\odot) = 0.0$, and the effective radius to be $R = 1.75\ R_\odot$, implying the luminosity $L = 11\ L_\odot$. Recent VLTI observations of β Pic estimate the stellar radius to be $(1.735 \pm 0.128)\ R_\odot$ (Di Folco et al. 2003), and comparing the ATLAS 9 SED of β Pic with observed data from the HST and FUSE archives, we find the agreement to be generally excellent (see Liseau 2003). Some deviations are found in the far-ultraviolet, where β Pic seems to be a slightly atypical A5V star with possible chromospheric activity (Bouret et al. 2002).

5.3.1. Solar composition disk

Assuming solar abundances throughout the disk, we can fit the radial Na I density of Sect. 5.1 to within 1% by setting the radial density profile of hydrogen nucleii to

$$n({\rm H}) = 2.25 \times 10^3 \left[\left(\frac{r}{r_0} \right)^{2.4} + \left(\frac{r}{r_0} \right)^{5.3} \right]^{-\frac{1}{2}} {\rm cm}^{-3}, \quad (4)$$

where r_0 is the same as in Sect. 5.1. The average fraction of neutral Na in the model is 10^{-3}, while hydrogen is entirely neutral. The hydrogen column densities are $N({\rm H\,I}) = 8 \times 10^{18}$ cm^{-2} and $N({\rm H_2}) = 3 \times 10^{18}$ cm^{-2}, consistent with the observational upper limits of $N({\rm H\,I}) \lesssim$ a few $\times 10^{19}$ cm^{-2} (Freudling et al. 1995) and $N({\rm H_2}) \lesssim 3 \times 10^{18}$ cm^{-2} (3σ, Lecavelier des Etangs et al. 2001). The gas temperature of the model disk is low, $T_{\rm gas}(100\,{\rm AU}) = 13$ K, while the dust is significantly warmer, $T_{\rm dust}(100\,{\rm AU}) = 50$ K. With a radial density as in Eq. (4) and a vertical profile similar to the Na I gas, the total gas disk mass out to 1000 AU becomes $\sim 0.1\ M_\oplus$.

Using the equations of motion of Sect. 5.2 to calculate the terminal velocity of elements subject to the gas drag of the hydrogen density law of Eq. (4) and temperature structure from Cloudy, we find that both Fe and Na, both with $\beta \gg 1$, would reach radial velocities on the order of hundreds to thousands km s^{-1}. That is in clear contradiction with the observed radial velocities reported in Table 3. The purported explanation of Paper I, that Na is ionised most of the time and therefore is subject to a small average radiation pressure, does not apply to Fe; indeed, both Fe I and Fe II experience a radiation pressure with $\beta \gg 1$. We know of only one remaining plausible explanation: there is a braking agent keeping the gas from reaching high velocities.

5.3.2. Metal depleted disk

To investigate the possibility of a more massive disk than implicated by solar abundances of Na I, we impose a radial density profile for hydrogen nucleii,

$$n({\rm H}) = 10^6 \left[\left(\frac{r}{r_0} \right)^{2.4} + \left(\frac{r}{r_0} \right)^{5.4} \right]^{-\frac{1}{2}} {\rm cm}^{-3}, \quad (5)$$

and tune the metal depletion to reproduce the Na I density profile. We found that an overall depletion factor of $\sim 10^{-3}$ (more precisely 8.5×10^{-4}) of the metals with respect to solar composition was required. Due to higher dust-gas interaction, the temperatures of the gas and the dust are similar over the disk, with $T_{\rm gas}(100\,{\rm AU}) = 36$ K and $T_{\rm dust}(100\,{\rm AU}) = 51$ K. The column densities of hydrogen are $N({\rm H\,I}) = 6 \times 10^{20}$ cm^{-2} and $N({\rm H_2}) = 3 \times 10^{21}$ cm^{-2}, significantly higher than the observed upper limits reported by Freudling et al. (1995) and Lecavelier des Etangs et al. (2001). With a radial density as in Eq. (5) and a vertical profile similar to the Na I gas, the total gas disk mass out to 1 000 AU becomes $\sim 40\ M_\oplus$, similar to the mass recently inferred from possible emission in the pure rotational transitions of H_2, $J = 2 \to 0$ (28 μm) and $J = 3 \to 1$ (17 μm), detected from β Pic in ISO/SWS data (Thi et al. 2001). Due to the low gas temperatures of our model, however, the predicted fluxes in

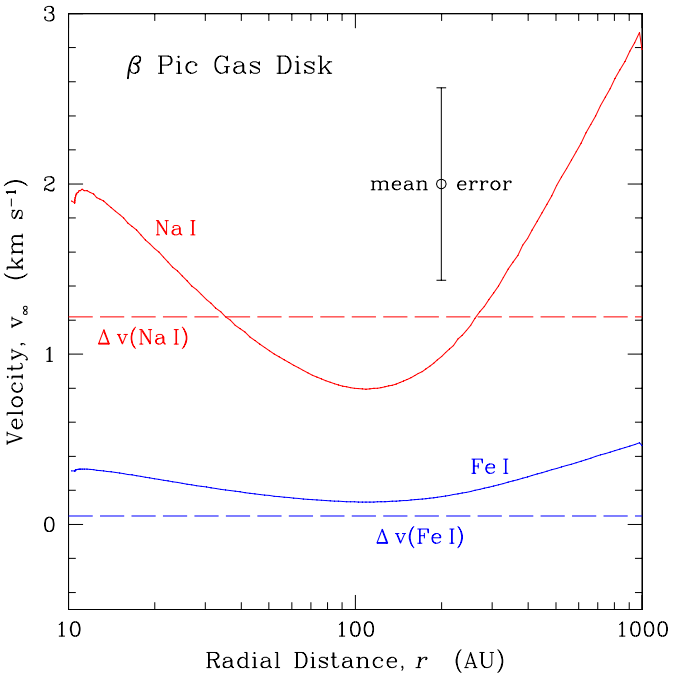

Fig. 7. The terminal velocities for Na I and Fe I in a metal depleted disk with the radial density of Eq. (5), as a function of radius. The horizontal dashed lines show the measured radial velocities, as determined from absorption lines (Table 3), with the estimated error shown by the vertical bar. The error is dominated by the wavelength calibration uncertainty of 0.5 km s^{-1}.

the 17 μm and 28 μm lines are only $F_{17} = 6{\times}10^{-15}$ erg s^{-1} cm^{-2} and $F_{28} = 2 \times 10^{-15}$ erg s^{-1} cm^{-2}, respectively, for ortho/para in thermal equilibrium. This is more than an order of magnitude lower than the fluxes $F_{17} = 7.7 \times 10^{-14}$ erg s^{-1} cm^{-2} and $F_{28} = 7.0 \times 10^{-14}$ erg s^{-1} cm^{-2} reported by Thi et al. (2001), and can be traced to their higher assumed gas temperature of 100 K.

Calculating the terminal velocities of the radiation pressure sensitive elements Fe and Na, we produce Fig. 7, where the terminal velocity is plotted against the radial distance. We find that the derived terminal velocities are consistent with observed radial velocities reported in Table 3.

5.4. Summary

We have found that in our thin disk, constructed by fitting a solar composition gas to the Na I observations, the predicted H I and H_2 column densities are consistent with the observed limits. With these low densities, however, the radiation pressure is predicted to accelerate, e.g., Na I to radial velocities inconsistent with observations.

On the other hand, in our thick disk, constructed by fixing the H density to be consistent as the braking agent for the metals, the predicted column densities of H I and H_2 are both above the observed upper limits, although the predicted H_2 *emission* is still far below the claimed detection.

The situation is puzzling, but a possible solution may be found if a main braking agent *different* from hydrogen is in action. If, e.g., the observed gas is replenished from dust collisions rather than being primordial, as seems suggested by the close spatial correlation between gas and dust, then a more natural candidate might be oxygen or oxygen bearing species (P. Artymowicz, private communication). More detailed models are in preparation, but hopefully the upcoming Space InfraRed Telescope Facility will solve the issue unambiguously by better observational constraints.

6. Conclusions

Our main observational results are:

1. We have observed 88 spatially resolved emission lines coming from Fe I, Na I, Ca II, Ni I, Ni II, Ti I, Ti II, Cr I and Cr II in the β Pictoris gas disk.
2. We trace the gas emission to the limits of our observations, from 0.″7 (13 AU) out to 17″ (323 AU) radially to the NE in Na I, and 4″ (77 AU) above the disk plane at radius 6″ (116 AU) in Ca II.
3. The scale height of the gas at 6″ from the star is twice as high as the equivalent dust scale height.
4. There is a brightness NE/SW asymmetry in the gas emission reminiscent of the dust asymmetry, although much stronger.
5. The inner gas disk is tilted by ∼5°, similarly to the dust disk.
6. The heliocentric radial velocity of β Pic is 20.0 ± 0.5 km s^{-1}.
7. The radial velocities of ions observed in absorption are close to or at the system velocity of β Pic (to a few km s^{-1}).
8. The estimated radial density from Na I in emission predicts a column density similar to the one observed in absorption, meaning that most, perhaps all, Na I is distributed in the observed disk. We have no reason to doubt that originators of other "stable" gas absorption components also belong to this extended disk.
9. Our disk models show that assuming hydrogen to be the braking agent for metals pushed out by radiation pressure in the β Pic disk leads to contradictions with observations.

A more detailed study of the chemical composition of the β Pic disk will be presented in a forthcoming paper.

Acknowledgements. We would like to thank the staff at the VLT and UVES for their outstanding contributions in performing these demanding service observations, in particular Fernando Comerón for kindly rescheduling an erroneous observation block, and Andrea Modigliani for addressing errors in the UVES pipeline. We acknowledge the interesting discussions we have had with Pawel Artymowicz, Doug Lin, and Philippe Thébault. We thank the referee Alain Lecavelier des Etangs for a rapid and detailed report. This research has made use of NASA's Astrophysics Data System Bibliographic Services, atomic line lists compiled by the National Institute for Standards and Technology, and the SIMBAD database.

References

Artymowicz, P. 2000, Space Sci. Rev., 92, 69
Augereau, J. C., Nelson, R. P., Lagrange, A. M., Papaloizou, J. C. B., & Mouillet, D. 2001, A&A, 370, 447
Aumann, H. H. 1985, PASP, 97, 885

Backman, D. E., & Paresce, F. 1993, in Protostars and Planets III, ed. E. H. Levy, & J. I. Lunine (Univ. Arizona Press, Tucson), 1253
Bouret, J.-C., Deleuil, M., Lanz, T., et al. 2002, A&A, 390, 1049
Di Folco, E., Kervella, P., Thévenin, F., et al. 2003, poster at IAU Symp., 221, Sydney, Australia
Ferland, G. J., Korista, K. T., & Verner, D. A. 1998, PASP, 110, 761
Freudling, W., Lagrange, A. M., Vidal-Madjar, A., Ferlet, R., & Forveille, T. 1995, A&A, 301, 231
Heap, S. R., Lindler, D. J., Lanz, T. M., et al. 2000, ApJ, 539, 435
Hobbs, L. M., Vidal-Madjar, A., Ferlet, R., Albert, C. E., & Gry, C. 1985, ApJ, 293, L29
Holland, W. S., Greaves, J. S., Zuckerman, B., et al. 1998, Nature, 392, 788
Kalas, P., & Jewitt, D. 1995, AJ, 110, 794
Kurucz, R. L. 1992, in IAU Symp., 149, The Stellar Populations of Galaxies, ed. B. Barbuy, & A. Renzini (Dordrecht: Kluwer), 225
Lagrange, A. M., Backman, D. E., & Artymowicz, P. 2000, in Protostars and Planets IV, ed. V. Mannings, A. P. Boss, & S. S. Russell (Tucson: Univ. Arizona Press), 639
Lagrange, A.-M., Beust, H., Mouillet, D., et al. 1998, A&A, 330, 1091
Lecavelier des Etangs, A., Vidal-Madjar, A., Roberge, A., et al. 2001, Nature, 412, 706
Liseau, R. 2003, ESA Special Publication SP-539, in press
Liseau, R., Brandeker, A., Fridlund, M., et al. 2003, A&A, 402, 183
Liseau, R., White, G. J., Larsson, B., et al. 1999, A&A, 344, 342
Mouillet, D., Larwood, J. D., Papaloizou, J. C. B., & Lagrange, A. M. 1997, MNRAS, 292, 896
Olofsson, G., Liseau, R., & Brandeker, A. 2001, ApJ, 563, L77 (Paper I)
Smith, B. A., & Terrile, R. J. 1984, Science, 226, 1421
Thi, W. F., Blake, G. A., van Dishoeck, E. F., et al. 2001, Nature, 409, 60
Weinberger, A. J., Becklin, E. E., & Zuckerman, B. 2003, ApJ, 584, L33
Zuckerman, B. 2001, ARA&A, 39, 549